2018

Optimal Control of Wave Energy Converters

Shangyan Zou
MICHIGAN TECHNOLOGICAL UNIVERSITY, szou2@mtu.edu

OPTIMAL CONTROL OF WAVE ENERGY CONVERTERS

By

Shangyan Zou

A DISSERTATION

Submitted in partial fulfillment of the requirements for the degree of

DOCTOR OF PHILOSOPHY

In Mechanical Engineering-Engineering Mechanics

MICHIGAN TECHNOLOGICAL UNIVERSITY

2018

This dissertation has been approved in partial fulfillment of the requirements for the Degree of DOCTOR OF PHILOSOPHY in Mechanical Engineering-Engineering Mechanics.

Department of Mechanical Engineering-Engineering Mechanics

Dissertation Advisor: *Dr. Ossama Abdelkhalik*

Committee Member: *Dr. Rush D. Robinett*

Committee Member: *Dr. Nina Mahmoudian*

Committee Member: *Dr. Wayne W. Weaver*

Department Chair: *Dr. William W. Predebon*

Dedication

To my mother, father, and wife

Without your love, support, and encouragement, I would neither be who I am nor would this work be what it is today.

To grandmother and grandfather

Who always believe me and expect me in completing this work.

To my advisor and teachers

Who guide, support and encourage me with your knowledge, patience, and quality.

To my colleagues and friends

Who help me and enrich my life.

Contents

List of Figures

List of Tables

Preface

Chapter 1 provides the introduction of this dissertation with a detailed survey of the literature. Chapter 2 presents the model of the interaction between the wave and the single body heaving device, the single body pitching device, the single body three degrees of freedoms device and the Wave Energy Converters array. Chapter 3 introduces the development of the unconstrained controller, which includes the Singular Arc control and the Simple Model Control. Chapter 4 proposes the constrained control development which includes the Pseudospectral optimal control, Linear Quadratic optimal control, and the Collective Control. The state and wave estimation are introduced in Chapter 5, which includes the Kalman Filter, Extended Kalman Filter, and the Kalman-consensus Filter. Chapter 6 presents the development of the hydraulic power take-off system. The materials of Chapter 2, 3, 4, 5 and 6 are published as references [1, 2, 3, 4, 5, 6, 7, 8, 9]. The contents of Chapter 1 include part of the literature review of those articles.

Acknowledgments

I would like to express my sincere gratitude to all those who have supported me, helped me, and inspired me during my doctoral program at Michigan Technological University.

First of all, I would like to thank my advisor, Dr. Ossama Abdelkhalik. Thank you for giving me the opportunity to join your research group and pursue a Ph.D. Your guidance, support, and encouragement played a significant role in completing this work. I learned not only the knowledge but also personal qualities from you.

Second, I am grateful to Dr. Bo Chen, Dr. Lyon B. King, Dr. Rush Robinett, Dr. Umesh Korde and all the instructors and professors who provided advice and supported me when I am struggled with some problem.

Third, my gratitude also goes to my parents and grandparents. Thank you for educating me since childhood and encouraging me to explore the unknowns. You have taught me to be confident, hard-working, and gave me the harbor that I can rely on.

Next, I would like to thank my wife Xin He. Thank you for your support and company. Thank you for your understanding of my interest in academia, and supporting me as I continue my career.

Finally, I would like to thank all my colleagues and friends who have helped me and enriched my life in my doctoral program.

Definitions

BEM	Boundary Element Method
CCC	Complex Conjugate Control
CWR	Capture Width Ratio
DDC	Discrete Displacement Cylinder
DoF	Degrees of Freedom
FK	Froude-Krylov
FSA	Force Shifting Algorithm
GA	Genetic Algorithm
JONSWAP	Joint North Sea Wave Observation Project
LQG	Linear Quadratic Gaussian
MPC	Model Predictive Control
NLP	Non Linear Programming
OWC	Oscillating Water Column
PD	Proportional-derivative control
PID	Proportional Integral Derivative
PM	Pierson-Moskowitz
PMP	Pontryagins Minimum Principle
PS	Pseudospectral

PTO	Power Take Off
RL	Resistive Loading control
SA	Singular Arc
SB	Shape-based
SMC	Simple Model Control
SPMG	Synchronous Permanent Magnet Generator
SUMT	Sequential Unconstrained Minimization Techniques
WEC	Wave Energy Converter

Nomenclature

The variables and parameters used in this dissertation are summarized in the Nomenclature. The scalars, vectors, and matrices are denoted as a different format. Additionally, the superscription c denotes the variables and parameters of the coupled (surge-pitch) motion, the h denotes the variables and parameters of the heave motion.

Nomenclature Chapter 1 - 5

A	Frequency dependent added mass (kg)
$\mathbf{A}_1$	Transformed state penalty matrix
$\mathbf{A}_e, \mathbf{B}_e, \mathbf{C}_e$	Excitation force matrices
Apz	Coupling force between different masses (N)
$\mathbf{A}_r, \mathbf{B}_r, \mathbf{C}_r, \mathbf{D}_r$	Radiation force matrices
A_s	Surface area (m^2)
B	Frequency dependent radiation damping ($N.s.m^{-1}$)
$\mathbf{B}_1$	Transformed control penalty matrix of the coupled motion
B_m	Damping coefficient of the resistive loading control ($N.s.m^{-1}$)
B_v	Viscous damping coefficient ($N.s.m^{-1}$)
c	Artificial damping coefficient ($N.s.m^{-1}$)
c_d	Vertical distance from the COG to sensor's cell (m)
c_{lin}	Linearized radiation damping coefficient ($N.s.m^{-1}$)

$\mathbf{C}_g$	Consensus gain
$\mathbf{C}$	External Force matrix of the coupled motion
D	Distance between the floater and the water surface (m)
D_{max}	Maximum allowable displacement (m)
$\mathbf{D}_\phi$	Derivative matrix
$\mathbf{D}_\phi^{-1}$	Integration matrix
E	Extracted wave energy
$\mathbf{F}$	System matrix
$\mathscr{F}$	System Jacobian matrix
$\mathbf{F}_1$	Transformed system matrix
F_d	Diffraction force (N)
F_e	Excitation force (N)
F_{ew}	Excitation force coefficient ($\mathrm{N.m^{-1}}$)
F_{FK}	Froude-Krylov force (N)
F_r	Radiation force (N)
F_s	Hydrostatic force (N)
F_T	Total wave force without infinity mass (N)
F_{Ts}	Surface integration of the total wave force (N)
$\tilde{F}_T$	Pseudo measurement of F_T (N)
$\tilde{F}_{Ts}$	Measurement of F_{Ts} (N)
g	Gravitational acceleration on earth ($\mathrm{m.s^{-2}}$)

$g(x)$	Inequality constraint function
$\mathbf{G}$	Weight matrix of the process noise
$\mathbf{G}_u$	Control force weight matrix
h	Water depth (m)
h_{cog}	Height of the center of gravity to the bottom of the cylinder (m)
h_{eq}	Vertical distance between the floater and the artificial mass (m)
h_{ex}	Excitation impulse response function
h_r	Radiation impulse response function
H	Hamiltonian
H_m	Output Jacobian matrix
H_p	Length of prediction horizon (s)
H_s	Significant wave height (m)
J	Objective function
J_r	Moment of inertia of the rigid body (kg.m^2)
J_∞	Added moment of inertia at infinity frequency (kg.m^2)
k	Artificial stiffness coefficient (N.m^{-1})
$\hat{k}$	Unit directional vector along z direction
$\mathbf{k}$	State of the auxiliary equation
K	Hydrostatic stiffness coefficient (N.m^{-1})
K_d	Derivative control gain
$\mathbf{K}_g$	Kalman gain

K_{moor}	Mooring stiffness (N.m^{-1})
K_{res}	Hydrostatic restoring stiffness coefficient (N.m.rad^{-1})
K_p	Proportional control gain
L	Horizontal distance between the floater and the artificial mass (m)
m	Total mass (kg)
m_r	Rigid body mass (kg)
m_∞	Added mass at infinity frequency (kg)
$\vec{n}$	Normal direction of the surface
N_{cw}	Integer number of control updates
N_f	Number of Fourier terms
N_H	Integer length of prediction horizon
p	Pressure measured by pressure sensors (Pa)
P_0	Power produced by individual floater (W)
P_{array}	Total power produced by the WEC array (W)
$\mathbf{P}$	Estimation error covariance matrix
q	Interaction factor
$\mathbf{Q}$	State penalty matrix
$\mathbf{Q}_p$	Process noise covariance matrix
r	Position of the floater in the WEC array (m)
r_g	Weight of external penalty function
R_c	Radius of a cylinder (m)

$\mathbf{R}$	Control penalty matrix
R_s	Radius of a sphere (m)
$S(\omega)$	Wave spectrum density ($m^2.s.rad^{-1}$)
$\mathbf{S}$	State of the Riccati equation
T_{end}	Total simulation time (s)
u	Control force (N)
u_{max}	Maximum control capacity (N)
$\mathbf{U}_1$	Transformed control force
$\mathbf{v}$	Measurement noise
v_e	Velocity of the excitation force ($m.s^{-1}$)
v_h	Heave velocity of the floater ($m.s^{-1}$)
v_p	Pitch velocity of the floater ($rad.s^{-1}$)
v_s	Surge velocity of the floater ($m.s^{-1}$)
V	Volume of the displaced water (m^3)
$\mathbf{W}$	Weight of objective matrix
x	Surge displacement (m)
x_{CB}	x coordinate of the center of buoyancy (m)
z	Heave displacement (m)
$\tilde{z}$	Measurement of the heave displacement (m)
z_{CB}	z coordinate of the center of buoyancy (m)
z_{max}	Maximum allowable heave displacement (m)

α_0	Initial angle between the connector/arm and the horizontal axis (rad)
β	Wave direction (^{o})
ϵ	instantaneous change of the angle α (rad)
$\eta(\omega)$	Wave elevation (m)
θ	Pitch rotation (rad)
ρ	Density of water (kg.m^{-3})
τ_e	Excitation torque (N.m)
τ_{ew}	Excitation torque coefficient (N)
τ_G	Torque due to the gravity (N.m)
τ_{PTO}	Power take off torque (N.m)
τ_r	Radiation torque (N.m)
τ_s	Hydrostatic restoring torque (N.m)
$\phi(\omega)$	Random phase shift (rad)
$\vec{\phi}$	Basis function vector
$\boldsymbol{\phi}$	Basis function matrix
χ	Wave number (rad.m^{-1})
$\Psi(\hat{x})$	Disagreement
ω_0	Fundamental frequency (rad.s^{-1})
ω_n	nth wave frequency (rad.s^{-1})
ω_p	Peak frequency of the wave (rad.s^{-1})

Nomenclature Chapter 6

A_{hose}	Area of the hose (m^2)
A_v	Instantaneous opening area of the valve (m^2)
A_0	Maximum opening area of the valve(m^2)
$A1$	Piston area of chamber 1 (m^2)
$A2$	Piston area of chamber 2 (m^2)
$A3$	Piston area of chamber 3 (m^2)
$A4$	Piston area of chamber 4 (m^2)
C_d	Valve discharge coefficient
C_{Q1}	Flow loss coefficient of the hydraulic motor ($m^3.s^{-1}.Pa^{-1}$)
C_v	Gas specific heat at constant volume ($J.(kg.K)^{-1}$)
d_{hose}	Diameter of the hose (m)
D_c	Characteristic dimension of the buoy (m)
D_M	Total hydraulic motor displacement (m^3)
D_w	Hydraulic motor displacement (m^3)
F_c	Force applied by the cylinder (N)
F_{fric}	Friction force of the cylinder (N)
F_{ref}	Reference control force (N)
k_{gen}	Number of generators
l_{hose}	Length of the hose (m)
p_{acc}	Pressure in the accumulator (Pa)

$p_{avg,exp}$	Expected average power output (W)
p_{A1}	Pressure in chamber 1 (Pa)
p_{A2}	Pressure in chamber 2 (Pa)
p_{A3}	Pressure in chamber 3 (Pa)
p_{A4}	Pressure in chamber 4 (Pa)
p_f	Pressure drop across the hose (Pa)
p_H	Pressure of the high pressure accumulator (Pa)
p_L	Pressure of the low pressure accumulator (Pa)
p_ζ	Pressure drop of the fitting (Pa)
p_λ	Pressure drop across a straight pipe/hose (Pa)
$P_{actuator}$	Actuator power extraction (W)
P_{ave}	Average extracted power (W)
P_{gen}	Generator power output (W)
P_M	Motor power output (W)
P_w	Wave energy transport ($W.m^{-1}$)
Q_{acc}	Inlet flow to the accumulator ($m^3.s^{-1}$)
Q_{A1}	Inlet flow to chamber 1 ($m^3.s^{-1}$)
Q_{A2}	Inlet flow to chamber 2 ($m^3.s^{-1}$)
Q_{A3}	Inlet flow to chamber 3 ($m^3.s^{-1}$)
Q_{A4}	Inlet flow to chamber 4 ($m^3.s^{-1}$)
Q_{in}	Inlet flow of the hose ($m^3.s^{-1}$)

Q_{out}	Outlet flow of the hose ($m^3.s^{-1}$)
R_{gas}	Ideal gas constant ($kg.m^2$)
Re	Reynold's number
t_v	Valve opening and closing time (s)
T_{gas}	Gas temperature (K)
T_w	Hydraulic accumulator wall temperature (K)
u_v	Valve opening and closing signal
v_c	Instantaneous piston velocity ($m.s^{-1}$)
v_{out}	Velocity of the outlet flow of the hose ($m.s^{-1}$)
V_{a0}	Accumulator size (m^3)
V_{ext}	Accumulator external volume of the pipeline (m^3)
V_g	Accumulator gas volume (m^3)
$V_{0,A1}$	External volume of the connecting hose to chamber 1 (m^3)
$V_{0,A2}$	External volume of the connecting hose to chamber 2 (m^3)
$V_{0,A3}$	External volume of the connecting hose to chamber 3 (m^3)
$V_{0,A4}$	External volume of the connecting hose to chamber 4 (m^3)
x_c	Instantaneous stroke of the cylinder (m)
$x_{c,max}$	Maximum stroke of the cylinder(m)
$\beta(p)$	Effective bulk modulus of the fluid(Pa)
ζ	Fitting loss coefficient
η_c	Cylinder efficiency

η_{out}	Electricity generation efficiency
ν	Kinematic viscosity of the fluid ($m^2.s^{-1}$)
τ_a	Accumulator thermal time constant (s)
ψ	Motor speed control coefficient
ω_M	Angular velocity of the hydraulic motor ($rad.s^{-1}$)

Abstract

In this dissertation, we address the optimal control of the Wave Energy Converters. The Wave Energy Converters introduced in this study can be categorized as the single body heaving device, the single body pitching device, the single body three degrees of freedoms device, and the Wave Energy Converters array. Different types of Wave Energy Converters are modeled mathematically, and different optimal controls are developed for them. The objective of the optimal controllers is to maximize the energy extraction with and without the motion and control constraints. The development of the unconstrained control is first introduced which includes the implementation of the Singular Arc control and the Simple Model Control. The constrained optimal control is then introduced which contains the Shape-based approach, Pseudospectral control, the Linear Quadratic Gaussian optimal control, and the Collective Control.

The wave estimation is also discussed since it is required by the controllers. Several estimators are implemented, such as the Kalman Filter, the Extended Kalman Filter, and the Kalman-Consensus Filter. They can be applied for estimating the system states and the wave excitation force/wave excitation force field. Last, the controllers are validated with the Discrete Displacement Hydraulic system which is the Power Take-off unit of the Wave Energy Converter.

The simulation results show that the proposed optimal controllers can maximize the energy absorption when the wave estimation is accurate. The performance of the unconstrained controllers is close to the theoretical maximum (Complex Conjugate Control). Furthermore, the energy extraction is optimized and the constraints are satisfied by applying the constrained controllers. However, when the proposed controllers are further validated with the hydraulic system, they extract less energy than a simple Proportional-derivative control. This indicates the dynamics of the Power take-off unit needs to be considered in designing the control to obtain the robustness.

Chapter 1

Introduction

1.1 Overview

Wave energy is one of the reliable renewable energy sources such as solar and wind energy. Different wave energy conversion concepts are proposed based on the different mechanism of energy absorbing, different water depth and different locations of the device (shoreline, near-shore, offshore) [10]. There are three main wave energy extraction concepts [10]: oscillating water column devices [11], oscillating body systems [12], and overtopping converters. In details, the single-body heaving buoys, two-body heaving systems, fully submerged heaving systems, and pitching devices can

be considered as the oscillating body systems. In a typical heaving buoy (point absorber) system, the energy extraction results from the oscillating movement of a single body reacting against a fixed frame of reference (the sea bottom or a bottom-fixed structure). In one typical configuration of these Wave Energy Converters (WECs), hydraulic cylinders are attached to the floating body. When the float moves due to heave the hydraulic cylinders drive hydraulic motors which in turn drive a generator [13]. This type of WECs extracts the wave heave energy. There are other types of WECs that extract surge energy [14]. Moreover, there are types of WECs extract wave energy from the pitch motion [15], for instance, the WaveStar buoy. The mechanisms that translate the motion of oscillating bodies in water into useful electrical energy are usually called Power take-off (PTO) systems.

1.2 Optimal control of single-degree-of-freedom WEC

The research of the wave energy conversion and optimal control starts from the middle of the 1970s [16, 17]. For the Single-Degree-Of-Freedom (S-DoF) WEC, the classical work about wave energy is to construct the wave model as a spring-mass-damper system.

$$m\ddot{x} + c_{lin}\dot{x} + Kx = F_e + u \tag{1.1}$$

There are many control strategies that already have been developed [18] [19] [20] for the single degree of freedom WEC. Reference [21] proposes a linear quadratic gaussian controller. The model predictive control method is addressed in reference [22]. In reference [23], pseudo-spectral (PS) method has been applied. In reference [5], a shape based method is developed. Reference [24] develops a multi-resonant feedback controller which is the time domain implementation of the Complex Conjugate Control [25]. In [26], the dynamic programming has was for maximizing energy capture. The optimal control can be analyzed using the Pontryagin minimum principle in time domain [27], or using resonant conditions in the frequency domain. The objective of the control is usually to maximize the extracted energy. The optimal solution computed within the context of the optimal control theory was developed in [2] for a S-DoF WEC.

Consider handling the constraints of the wave energy conversion problem specifically, there are several engineering implemented controllers applies discontinuous control for the wave energy conversion. The latching control is one example of a discontinuous control. Solving a continuous system with discontinuous control is known as the discontinuous system control [28]. In general, the discontinuity can happen in either the system or the control. Several controllers are developed which include the Bang-Bang control [29], the on-off control [30], the feedback controller [31] and the sliding mode control [32]. Although some of those controllers are not developed on a WEC problem, it is inspiring for exploring the advantage of the discontinuous control for

the WEC continuous system.

1.3 Optimal control of single body multi-degree-of-freedom WEC

Several references have motivated the use of a multiple degrees-of-freedom (multi-DoF) WEC as opposed to a single-mode WEC. Evans [33] extended the results of two-dimensional WECs to bodies in channels and accounts for the body orientation on the energy harvesting. In fact, reference [34] points out that the power that can be extracted from a mode that is antisymmetric to the wave (such as pitch and surge) is twice as much as that can be extracted from a mode that is symmetric (such as heave). One of the references that recently studied the pitchsurge power conversion is Reference [35]. Yavuz [35] models the pitchsurge motions assuming no heave motion; hence, there is no effect from the heave motion on the pitchsurge power conversion. The mathematical model used in reference [35] for the motions in these 2-DoF WECs is coupled through mass and damping only; there is no coupling in the stiffness. However, it has been observed that floating structures can be subject to parametric instability arising from variations of the pitch restoring coefficient [36]. The reference describes an experimental heaving buoy for which the parametric excitation causes the pitch motion to grow resulting in instability. A harmonic balance approach is

implemented to cancel this parametric resonance and results of tank experiments are presented. Reference [37] investigated experimentally the performance of a surge-heave-pitch WEC for the Edinburgh Duck, on a rig that allowed the duck to move in the 3-DoF. The controller in this experiment optimized the spring and damping coefficients in each of the three modes, in addition to the product of the nod angle and velocity, which is a nonlinear term that changes with the change of linear damping due to the duck rotation.

As will be detailed in this dissertation, the equations of motion for a 3-DoF WEC have a second-order term that causes the heave motion to parametrically excite the pitch mode; and the pitch and surge motions are coupled. For relatively large heave motions, which would be needed for higher energy harvesting, it is not possible to neglect this parametric excitation term. Rather, the controller should be designed to leverage this nonlinear phenomenon for optimum energy harvesting.

1.4 Optimal control of the WEC array

1.4.1 The WEC array modeling and layout optimization

The study of the dynamics of systems of interacting bodies also started in the 1970s' when people start to explore the wave energy conversion. Reference [38] applies the

linear wave theory to solve the interaction between multiple bodies which can be considered as the first investigation of the WEC array. The interaction factor q is defined in terms of the power generated by the WEC array (P_{array}) and the power generated by the isolated buoys (P_0).

$$q = \frac{P_{array}}{NP_0} \tag{1.2}$$

Later, as shown in references [39, 40], the configuration of the WEC array can significantly improve the power extraction. The subsequent study of the hydrodynamics of the WEC array is presented in references [41, 42, 43, 44]. Due to the complexity of solving the WEC array problem analytically, the semi-analytical approach is developed. There are four main semi-analytical approaches: the point absorber method [38, 45], the plane wave method [46, 47], the multiple scattering method [42, 48], the direct matrix method [49, 50, 51, 52]. Based on the research conducted on the hydrodynamics of the WEC array, the layout optimization is explored in terms of the energy extraction. There are three main approaches for the layout optimization. The first one is the selected optimization [53, 53, 54, 55, 56] which studies the performance of particular configuration of the WEC array. The second approach optimizes the spacing of the buoys by applying the local optimization method [57]. The last approach applies the global optimization to optimize the WEC array layout for maximizing the energy absorption [51, 58, 59].

1.4.2 The optimal control of the WEC array

Due to the complexity of the hydrodynamics of the WEC array, several references [56, 60, 61, 62, 63] applies the BEM resource to evaluate the performance of the controller which only applies a simple control law. Several controllers have been developed recently thanks to the numerical modeling of the WEC array and the improved capacity of the computer. The coordinated control (global control) is developed in reference [64]. The performance of the controller is compared with the independent control where a significant improvement is found. The global control is also studied in reference [65] which concludes we can obtain constructive interaction between buoys with proper control. Reference [66] introduces the decentralized model predictive control for a WEC array which has the triangular configuration. Reference [67] also studies the model predictive control by neglecting the cross interaction between floaters in the array. The control in-formed optimization is proposed in [68] for the array layout optimization. The reference concludes a 40% improvement of the energy extraction can be achieved with the knowledge of the control applied in the optimization.

1.5 The Power take-off units

1.5.1 General Review

Different classes of PTO units are reviewed in this section. The first research on the PTO unit is presented in reference [69] which tests the phase latching control with the hydraulic PTO experimentally. Later, the first theoretical model of the hydraulic system is developed in reference [70]. Although references [71, 72] points out that the hydraulic system is most suitable for wave energy conversion, different types of PTO units has their different advantages and disadvantages. There are four main categories of the PTO units: the air turbine, the water turbine, the direct drive system and the hydraulic system [73].

1.5.2 Air Turbines

The air turbine is usually applied in the oscillating water columns. There are three main categories of air turbines: the Wells turbine, the Impulse turbine, and the Denniss-Auld turbine. The Wells turbine is the most popular turbine due to its simplicity and economy which is most studied among different turbines [74, 75, 76, 77, 78, 79, 80, 81, 82, 83, 84]. It is later improved in terms of the efficiency, starting

characteristic and noise level [85, 86, 87, 88, 89, 90, 91]. The impulse turbine is studied in references [92, 93, 94] which is found to have a better performance than the Wells Turbine. Reference [85, 95, 96] study the other types of air turbines.

1.5.3 Hydro Turbines

The hydro turbine is applied for power generation for many decades. Although the hydro turbines have no water shortage problem, do not require a return pipe, and no damage to the environment [74], the energy extraction with hydro turbines require a sufficient head.

1.5.4 Direct Drive system

The direct drive system is also popular for the point absorber WEC. The direct drive system can also be categorized as the direct mechanical drive system and the direct electrical drive system. For the direct mechanical drive system, reference [97] introduces a direct driven rotary wave energy point absorber. Later reference [98] points out that the direct drive rotary system is more suitable for a high power level system, and the synchronous permanent magnetic linear generator (SPMG) is more suitable for a low power level system. A suboptimal controller is developed for a

slider-crank WEC in reference [99].

References [100, 101, 102] present the direct electrical drive PTO unit which has no requirement of the intermediate mechanical devices by combining the linear electrical generator with the WEC directly. The direct electrical drive PTO is found to have a good performance in terms of the energy conversion efficiency of a surge WEC in reference [103]. Additionally, as shown in reference [104], the global energy conversion efficiency can be improved by considering the electrical losses in designing the control. References [105, 106] develop the passive tunning control and the reactive control respectively with the direct drive system to maximize the energy extraction.

1.5.5 The hydraulic system

This section presents a review of hydraulic PTO units. Figure 1.1 is a general layout for a typical hydraulic PTO. The hydraulic system is composed of the actuator, the valve, the accumulators and the motor. The motion of the buoy will compress/decompress the chamber of the actuator and transfer the wave power to the hydraulic system. All the hydraulic systems can be categorized into three main groups: the constant-pressure, the variable-pressure, and the constantvariable pressure hydraulic systems [107, 108].

1.5.5.1 Constant pressure configuration

The first configuration is constructed with a low-pressure (LP) accumulator and a high-pressure (HP) accumulator. This type of hydraulic system can be achieved with a simple mechanism, and the control level is low.

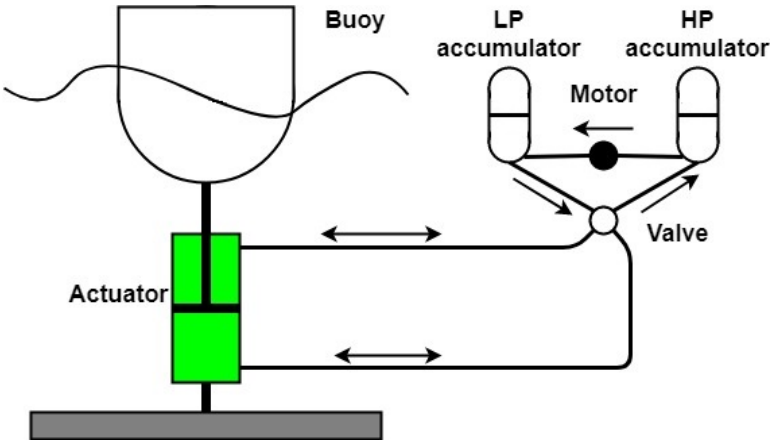

Figure 1.1: General layout for a hydraulic power take-off (PTO).

The typical configuration of a constant-pressure hydraulic system is presented in detail in [109, 110], using phase control. Control of the constant-pressure hydraulic system is achieved by implementing auxiliary accumulators in [111]. The latching and declutching controls are demonstrated in [112] using a constant-pressure hydraulic system. Additionally, a declutching control is presented in [113] for controlling a hydraulic PTO by switching on and off using a by-pass valve. The method is also tested with the SEAREV WEC with an even higher energy absorption. A detailed image of a single acting hydraulic PTO system with the phase control is presented in [70, 114].

The hydraulic system implemented in SEAREV is presented in [115]. In [116], a novel model of the hydraulic PTO of the Pelamis WEC is developed, with the ability to apply reactive power for impedance matching. In [117], a double-action WEC with an inverse pendulum is proposed. The authors of [117] report that a double-action PTO can supply the output power in each wave period without large instantaneous fluctuating power. A double-acting hydraulic cylinder array is developed in [118], where the model is found to be adaptive to different sea states to achieve higher energy extraction. The authors of [119] present the optimization of a hydraulic PTO of a WEC for an irregular wave where optimal damping is achieved by altering the displacement of the variable-displacement hydraulic motor. The authors of [120] present the design and testing of a hybrid WEC that obtains higher energy absorption than a single oscillating body with a hydraulic PTO. A discrete-displacement hydraulic PTO system is studied in [15] for the Wavestar WEC. An energy conversion efficiency of 70% is achieved. Additionally, adjustment of the force applied by the PTO is accomplished through implementing multiple chambers.

1.5.5.2 Variable pressure

A variable-pressure hydraulic system is suggested in [121, 122, 123]. In this situation, the piston is connected directly to a hydraulic motor. This system can achieve better

controllability, but the fluctuation of the output power is not negligible. Two hydraulic PTO systems are compared in [124], where constant-pressure hydraulic PTO and variable-pressure hydraulic PTO systems are compared. It was shown that a variable-pressure hydraulic PTO system would have a higher efficiency. The variable-pressure approach was also investigated in [125], where the hydraulic motor is used in order to remove the accumulator and control the output using the generator directly. A comparison between a constant-pressure system and a variable-pressure system was conducted in [126]; validation was conducted using AMEsim and demonstrated a good agreement. Power smoothing was achieved in [127] by means of energy storage.

1.5.5.3 Variable - Constant pressure

The variable–constant pressure hydraulic system is constructed with two parts: the variable pressure part and the constant pressure part. The variable pressure part is accomplished by a hydraulic transformer. A generic oil hydraulic PTO system, applied to different WECs, is introduced in [128]. The authors of [129] developed a PID controller, with the reactive power supplied by the hydraulic transformer (working as a pump). A suboptimal control is suggested in [129] for practical implementation in terms of the efficiency of the PTO.

Chapter 2

Modeling of the Wave Energy Converters

Energy can be extracted from the wave based on the interaction between the absorbers and the wave. Accordingly, it is essential to describe the interaction mathematically for the controller design. The model of the WEC varies for different configurations which include the freedom of motion, nonlinear effect, interaction with other absorbers and so on. Hence this chapter introduces the modeling of the WEC and focuses on discussing several configurations in details. The model of the ocean wave is first introduced in Section 2.1. Section 2.2 introduces the model of a single-degree-of-freedom heaving WEC which is the most classical configuration in the research of WEC. The model of the WaveStar, a pitching WEC, is developed in Section 2.3.

Further, the model of a three-degree-of-freedom WEC which includes the surge, heave, and pitch motion is discussed in Section 2.4. The following section (Section 2.5) extend the work to the study of the model of the WEC array.

2.1 Wave Model

Ocean waves can be viewed as the irregular wave. The irregular wave is the superposition of multiple regular waves with different amplitude, frequency and random phase shift. To describe the irregular wave, the wave spectrum is applied. There are several commonly used wave spectrum, for instance, the Joint North Sea Wave Observation Project (JONSWAP) spectrum, the Pierson-Moskowitz (PM) Spectrum, the Bretschneider spectrum and so on. In this dissertation, the Bretschneider spectrum is mostly applied. The spectral density of the Bretschneider spectrum can be expressed as:

$$S(\omega) = \frac{5}{16}\frac{\omega_p^4}{\omega^5}H_s^2 e^{-5\omega_p^4/(4\omega^4)} \tag{2.1}$$

where ω_p is the peak frequency, and H_s is the significant height of the wave. Those two quantities are the essential parameters of the ocean wave spectrum. Figure. 2.1 presents the frequency dependent wave elevation of a Bretschneider wave which has a significant height of 1m and a peak period of 9s.

The reason to select the Bretschneider spectrum is that it is a more conservative choice

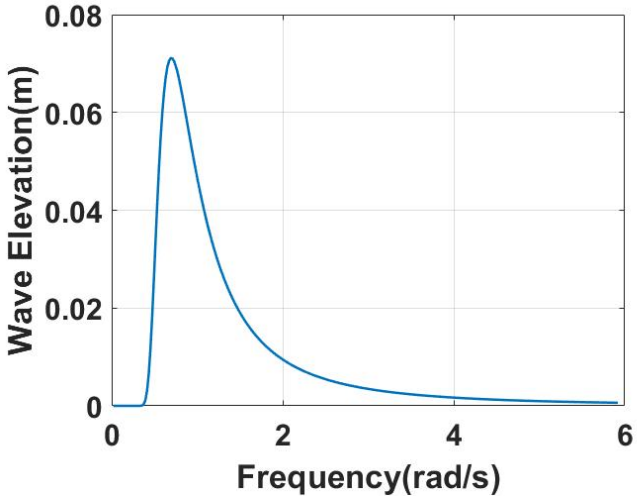

Figure 2.1: The wave elevation

by considering the power absorption estimation. The JONSWAP spectrum, which is frequently applied, has a narrow frequency band. However, the Bretschneider spectrum has a wider frequency band which makes the energy extraction more difficult. Consequently, the Bretschneider spectrum is applied to prevent the overestimation of the energy extraction.

2.2 Single Body Heaving Wave Energy Converter

The most studied WEC model is the single body heaving WEC. This section also introduces the modeling of a heaving point absorber. The geometry of the WEC is depicted in Figure. 2.2.

The x denotes the surge direction, z denotes the heave direction. The dynamics of

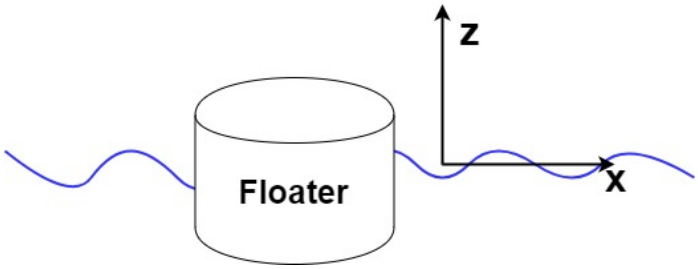

Figure 2.2: The geometry of a heaving point absorber

the wave and buoy interaction can be described as:

$$m_r \ddot{z} = F_e + F_r + F_s + u \tag{2.2}$$

where in the equation m_r represents the rigid body mass of the point absorber. F_e denotes the wave excitation force which comes from the incoming wave. The excitation force is the summation of the Froude-Krylov (FK) force and the diffraction force ($F_e = F_{FK} + F_d$). It can be precisely calculated by the surface integration of the pressure on the wet surface. F_r represents the radiation force which is generated by the radiated wave. F_s is the hydrostatic restoring force which results from the gravity and buoyancy. u is the control force. The equation can be further expanded which follows the Cummin's equation [130]:

$$m\ddot{z} = F_e + u - Kz - \int_0^t h_r(\tau)\dot{z}(t-\tau)d\tau \tag{2.3}$$

where in the equation $m = m_r + m_\infty$ indicates the total mass which is the summation of the rigid body mass and the added mass at the infinity frequency. K is the

hydrostatic stiffness coefficient. h_r is the radiation impulse response function. The energy extracted over the time interval $[0, T]$ from the wave energy converter can be computed as:

$$E = -\int_0^T \{u(t)\dot{z}(t)\}dt \tag{2.4}$$

2.2.1 The Wave Excitation Force

The excitation force is the force from the incoming wave acting on the floater which can be expressed by the summation of independent wave components:

$$F_e = \sum_{n=1}^{N} \Re(F_{ew}(\omega_n)\eta(\omega_n)e^{i(-\omega_n t+\phi(\omega_n))}) \tag{2.5}$$

where F_{ew} is the frequency dependent excitation force coefficients which can be computed by the Boundary Elements Method (BEM) softwares. For instance, WAMIT [131], Nemoh [132], Ansys AQWA [133]. $\eta(\omega_n)$ presents the frequency dependent wave elevation which is dependent on different wave spectrum. $\phi(\omega_n)$ is the random phase shift in the time domain of particular frequency ω_n. The excitation force also can be presented by the convolution:

$$F_e = \int_{-\infty}^{\infty} h_{ex}(t-\tau)\eta(\tau)d\tau \tag{2.6}$$

where $h_{ex}(t)$ is the excitation impulse response function, and $\eta(t)$ is the time domain wave elevation.

2.2.1.1 The Wave Excitation Force: Pressure Accumulation

To precisely compute the wave excitation force, the pressure accumulation can be applied. As mentioned before, the excitation force has two components: the Froude Krylov (FK) force and the diffraction force. However, for low frequencies, the diffraction forces are small compared to the Froude Krylov force [25]. In this section we will neglect the diffraction forces and hence the excitation force refers to the Froude Krylov force. The excitation force is modeled as the integration of the excitation pressure over the wet buoy surface. The excitation pressure distribution on the buoy surface is computed using the potential flow theory as follows. The surface is divided into a grid of cells, each cell is assumed to have uniform pressure over its area. Each cell is identified by two indices j and k; the index j determines the vertical position of a cell and k denotes the surface number in a certain vertical position j. The excitation force is then computed as [134]:

$$F_e = \sum_j \sum_k A_{s,jk} \vec{n}_{jk} \hat{k} \sum_{n=1}^{\aleph} \left(\rho g \eta(\omega_n) \frac{\cosh(\chi_n(z + z_{j,k} + h))}{\cosh(\chi_n h)} cos(\chi_n x_{j,k} - w_n t + \phi_n) \right) \tag{2.7}$$

where $A_{s,jk}$ is the surface area of the cell $\#jk$. η_n is the wave amplitude at frequency ω_n, χ_n is the wave number, $\chi_n = 2\pi/\lambda_n$ where λ_n is the wavelength associated with the frequency ω_n. The vector $\vec{n}_{jk}$ is the normal to the surface $\#jk$, $\hat{k}$ is the downward unit vector which is $[0; 0; -1]$, h is the mean water level height, $x_{j,k}$ and $z_{j,k}$ denotes the coordinate of the cell $\#jk$. χ_n has to satisfy the dispersion relation:

$$\omega_n^2 = g\chi_n \tanh(h\chi_n) \tag{2.8}$$

2.2.2 The Hydrostatic Restoring Force

The hydrostatic restoring force is a spring-like force which is composed by the gravity and buoyancy. When the buoy is partially submerged in the water, the hydrostatic force can be expressed as:

$$F_s = -Kz \tag{2.9}$$

where K is the hydrostatic stiffness coefficient. Normally, for a heaving cylindrical WEC, the hydrostatic coefficient can be approximated as:

$$K = \rho g \pi R_c^2 \tag{2.10}$$

where r is the radius of the surface at the bottom of the cylinder. Moreover the hydrostatic force also can be evaluated by the surface integration as:

$$F_s = \sum_j \sum_k A_{s,jk} \vec{n}_{jk} \hat{k} (-\rho g (z + z_{j,k})) \tag{2.11}$$

2.2.3 The Radiation Force

The radiation force, F_r, is due to the the radiated wave from the moving float. It can be modeled as [130]:

$$F_r(t) = -m_\infty \ddot{z}(t) - \int_0^t h_r(\tau) \dot{z}(t-\tau) d\tau \tag{2.12}$$

Instead of evaluating the convolution, a state space model can be applied to simplify the calculation of the radiation force [135]:

$$\begin{aligned} \dot{\vec{x}}_r &= \mathbf{A}_r \vec{x}_r + \mathbf{B}_r v \\ F_r &= \mathbf{C}_r \vec{x}_r \end{aligned} \tag{2.13}$$

where v is the heaving velocity of the WEC, $\vec{x}_r$ is the radiation state vector. The $\mathbf{A}_r$, $\mathbf{B}_r$ and $\mathbf{C}_r$ are the radiation matrices which can be obtained by approximating the

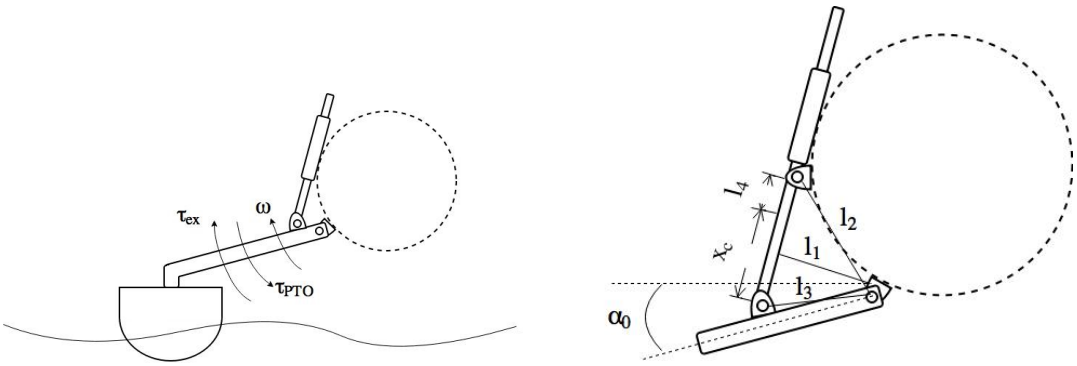

Figure 2.3: The geometry of the Wavestar absorber.

impulse response function $h_r(t)$ in the Laplace domain $H_r(s)$ as follows [136]:

$$H_r(s) = \frac{p_n s^n + p_{n-1} s^{n-1} + ...p_1 s + p_0}{q_m s^m + q_{m-1} s^{m-1} + ...q_1 s + q_0} \tag{2.14}$$

where $n < m$. The radiation matrices then can be identified based on the transfer function.

2.3 Single Body Pitching Wave Energy Converter

In this section, the dynamic model of the single body pitching WEC is introduced. The pitching WEC is referred to the WaveStar absorber [112]. The floater has a single degree of freedom motion which is the pitch rotation. The geometry of the proposed absorber is depicted in Figure 2.3.

The WEC dynamic model can be described based on linear wave theory by Equations (2.15) to (2.22):

$$J_r\ddot{\theta} = \tau_e + \tau_s + \tau_r - \tau_G - \tau_{PTO} \tag{2.15}$$

where J_r is the moment of inertia of the rigid body. θ is the pitch rotation of the floater. τ_e is the wave excitation torque acting on the buoy, τ_s is the restoring momentum, τ_r is the radiation torque, and τ_G is the torque caused by the gravity. τ_{PTO} is the PTO torque. The equation of motion can be further expanded as:

$$\ddot{\theta} = \frac{1}{J}(\tau_e - \tau_{PTO} - K_{res}\theta - h_r * \dot{\theta}) \tag{2.16}$$

where $J = J_r + J_\infty$ is the total moment of inertia and J_∞ is the moment of added mass at infinite frequency, K_{res} is the coefficient of the hydro-static restoring torque, and h_r is the radiation impulse response function. In Equation (2.16), the radiation torque is expanded as:

$$\tau_r = -J_\infty\ddot{\theta} - \tilde{\tau}_r \tag{2.17}$$

$$\tilde{\tau}_r = h_r * \dot{\theta} \tag{2.18}$$

The $*$ operation is the convolution between the impulse response function and the

angular velocity $\dot{\theta}$ which can be approximated by a state space model as:

$$\dot{\vec{x}}_r = \mathbf{A}_r \vec{x}_r + \mathbf{B}_r \dot{\theta} \tag{2.19}$$

$$\tilde{\tau}_r = \mathbf{C}_r \vec{x}_r + \mathbf{D}_r \dot{\theta} \tag{2.20}$$

Since the excitation torque can be expressed by the convolution between the impulse response function and the wave elevation ($\tau_e = h_{ex} * \eta$). The convolution can be approximated by a state space model as:

$$\dot{\vec{x}}_e = \mathbf{A}_e \vec{x}_e + \mathbf{B}_e \eta \tag{2.21}$$

$$\tau_e = \mathbf{C}_e \vec{x}_e \tag{2.22}$$

where $\mathbf{A}_e$, $\mathbf{B}_e$, and $\mathbf{C}_e$ are the excitation matrices which are identified from the excitation impulse response function. The parameters of the floater are listed in Table 2.1. The viscous damping is not considered in the proposed dynamic model because it is assumed to be negligible based on linear wave theory. In this designed study the extreme wave motion will not be achieved due to the limited capacity of the PTO unit. As a result, the small wave assumption can be held. The frequency response of the proposed WEC dynamic model without control is shown in Figure 2.4.

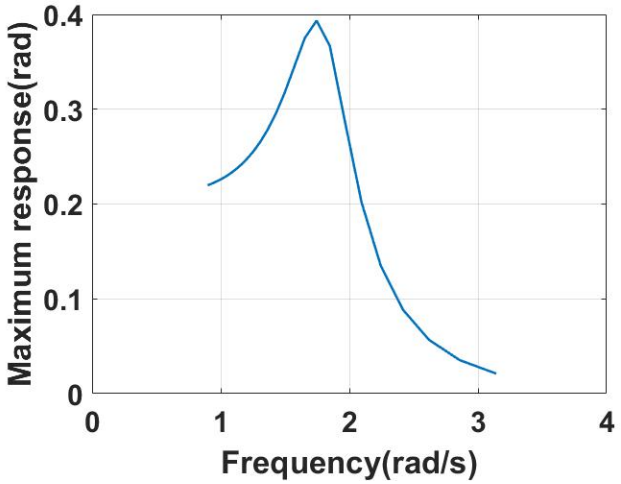

Figure 2.4: The frequency response of the dynamics of the Wavestar absorber.

Table 2.1
Model parameters for the Wavestar.

Symbol	Value	Unit
J	3.8×10^6	kg m^2
K_{res}	14×10^6	Nm/rad
The transfer function $H_r(s)$		
$(b_0, b_1, ..., b_5)$	$(0.01, 1.44, 62.4, 816, 1310, 144) \times 10^4$	
$(a_0, a_1, ..., a_5)$	$(0.001, 0.0906, 1.67, 6.31, 13.3, 9.18)$	
The transfer function $H_{ex}(s)$		
(b_0, b_1)	$(5.4, 270) \times 10^4$	
$(a_0, a_1, ..., a_4)$	$(0.036, 0.39, 1.5, 2.6, 1.6)$	

2.4 Single Body Three-Degree-of-Freedom WEC

Consider a cylindrical buoy has the heave, pitch and surge motion with base radius R_c, and a mass m_r. The geometry of the floater is plotted in Figure. 2.5.

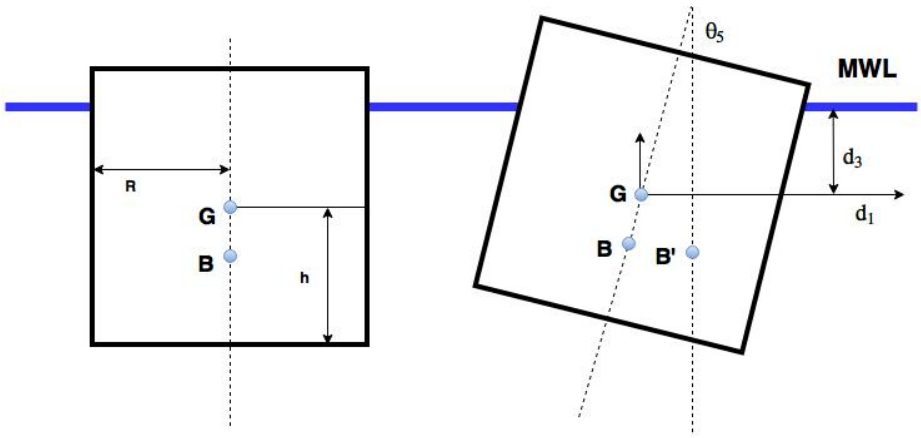

Figure 2.5: Geometry of a 3-DoF cylindrical Buoy; MWL is the mean water level[1]

where d_1, d_3, and θ_5 denotes the surge x, heave z and pitch θ motion respectively. h_{cog} is the height of the center of gravity from the base. G represents the center of gravity and B represents the center of buoyancy of the floater. Assuming a body fixed coordinate system located at the buoy's center of gravity. The pitch restoring moment is:

$$\tau_s = -\rho g V x_{CB} \tag{2.23}$$

where x_{CB} is the x-coordinate of the center of buoyancy, and V is the submerged

volume which can be computed as:

$$V = \pi R_c^2 \left(h_{cog} + \frac{z}{cos(\theta)} \right) \tag{2.24}$$

The coordinates of the center of buoyancy are:

$$x_{CB} = \frac{sin(\theta) \left(R_c^2 cos(\theta)^2 + R_c^2 + 4h_{cog}^2 cos(\theta)^2 + 8h_{cog} z cos(\theta) + 4z^2 \right)}{8cos(\theta) \left(z + h_{cog} cos(\theta) \right)} \tag{2.25}$$

$$z_{CB} = \frac{\left(R_c^2 cos(\theta)^2 - R_c^2 + 4h_{cog}^2 cos(\theta)^2 + 8h_{cog} z cos(\theta) + 4z^2 \right)}{8 \left(z + h_{cog} cos(\theta) \right)} \tag{2.26}$$

The resulting pitch restoring moment is:

$$\begin{aligned} \tau_s = -\pi \rho g R_c^2 sin(\theta) \left(h_{cog} + \frac{z}{cos(\theta)} \right) \\ \frac{\left(R_c^2 cos(\theta)^2 + R_c^2 + 4h_{cog}^2 cos(\theta)^2 + 8h_{cog} z cos(\theta) + 4z^2 \right)}{8cos(\theta) \left(z + h_{cog} cos(\theta) \right)} \end{aligned} \tag{2.27}$$

Linearizing Eq. (2.27) using Taylor expansion to a first order, we get:

$$\tau_s \approx \frac{-\pi \rho g R_c^2}{4} \left(R_c^2 + 2h_{cog}^2 + 4h_{cog} z + 2z^2 \right) \theta \tag{2.28}$$

The heave restoring force is:

$$\begin{aligned} F_s &= \rho g \pi R_c^2 \left(\frac{z}{cos(\theta)} - z_0 \right) \\ &\approx \rho g \pi R_c^2 \left(z \left(1 + \frac{\theta^2}{2} \right) - z_0 \right) \end{aligned} \tag{2.29}$$

where z_0 is the vertical position of the center of gravity at equilibrium, for $\theta = 0$. The system equations of motion are then:

$$\left(m_r + m_\infty^{11}\right)\ddot{x} + m_\infty^{15}\ddot{\theta} + B_{v1}\dot{x} + K_{moor}x = F_e^1 + F_r^1 + u_1 \tag{2.30}$$

$$\left(m_r + m_\infty^{33}\right)\ddot{z} + B_{v3}\dot{z} + \rho g \pi R_c^2 \left(z\left(1 + \frac{\theta^2}{2}\right) - z_0\right) = F_e^3 + F_r^3 + u_3 \tag{2.31}$$

$$\left(J_r + J_\infty^{55}\right)\ddot{\theta} + J_\infty^{51}\ddot{x} + B_{v5}\dot{\theta} + \frac{\pi\rho g R_c^2}{4}\left(R_c^2 + 2h_{cog}^2 + 4h_{cog}z + 2z^2\right)\theta = F_e^5 + F_r^5 + u_5 \tag{2.32}$$

The radiation forces can be expressed as:

$$F_r^1 = -h_{r,11} * \dot{x} - h_{r,15} * \dot{\theta}$$

$$F_r^3 = -h_{r,33} * \dot{z}$$

$$F_r^5 = -h_{r,51} * \dot{x} - h_{r,55} * \dot{\theta}$$

where $h_{r,ij}$ are the radiation impulse response functions. Eqs. (2.30)– (2.32) are coupled and nonlinear. If we linearize Eq. (2.31), the heave equation becomes linear and decoupled from the surge-pitch equations. If we linearize the surge-pitch equations assuming the higher order terms $z \times \theta$ and $z^2 \times \theta$ are small, we get a coupled system of equations of the form:

$$\mathbf{m}\ddot{\vec{x}} + \mathbf{C}\dot{\vec{x}} + \mathbf{K}\vec{x} = \vec{F}_e + \vec{F}_r + \vec{u} \tag{2.33}$$

where the excitation force vector $\vec{F}_e = [F_e^1\,, F_e^3\,, F_e^5]^T$, the control force vector $\vec{u} = [u_1\,, u_3\,, u_5]^T$, the matrix $\mathbf{m}$ is:

$$\mathbf{m} = \begin{bmatrix} m_r + m_\infty^{11} & m_\infty^{15} \\ J_\infty^{51} & J_r + J_\infty^{55} \end{bmatrix} \tag{2.34}$$

the matrix $\mathbf{C}$ is:

$$\mathbf{C} = \begin{bmatrix} B_{v1} & 0 \\ 0 & B_{v5} \end{bmatrix} \tag{2.35}$$

and the matrix $\mathbf{K}$ is:

$$\mathbf{K} = \begin{bmatrix} K_{moor} & 0 \\ 0 & K_{res} \end{bmatrix} \tag{2.36}$$

where K_{moor} is the mooring stiffness in surge direction. K_{res} is a time-varying stiffness in pitch direction which has a constant part and a time varying part: $K_{res} = K_c + K_p(t)$. The expression for K_c and $K_p(t)$ is:

$$K_c = \frac{\pi \rho g R_c^2}{4} \left(R_c^2 + 2h_{cog}^2\right) \tag{2.37}$$

$$K_p(t) = \pi \rho g R_c^2 h_{cog} z \tag{2.38}$$

Thus the pitch-surge system of equations are coupled linear time varying, and the

heave model is an uncoupled linear time invariant equation. The problem is more challenging than S-DoF WECs due to this coupled motion. The heave motion also influences the surge and pitch motion and it is independent of the other two modes itself. A similar problem is found in mechanical vibrations. The excitation from heave motion in coupled motion is called the parametric excitation. For the single degree of freedom, this parametric excitation phenomenon is modeled through Mathieu's equation. The analysis of the system with parametric exciting starts from the 1990s [137] [138]. Researchers work on the S-DoF WECs with single frequency parametric exciting term has found that the energy harvested from the parametrically excited system is much more than non-parametric excited [139] [140] and the stability is also discussed by [141] [142] [143]. Then the problem has been expanded to the single degree of freedom with the multi-frequency parametric exciting system recently. The analysis of the system excited by the multi-frequency parametric excitation terms has been done by [144] [145] [146], although there is no controller included for energy harvesting. In our problem, the coupled motion can be considered as a two-degree-of-freedom (2-DoF) motion with the multi-frequency parametrically excited system, and the main purpose of designing the controller is to maximize the energy capture.

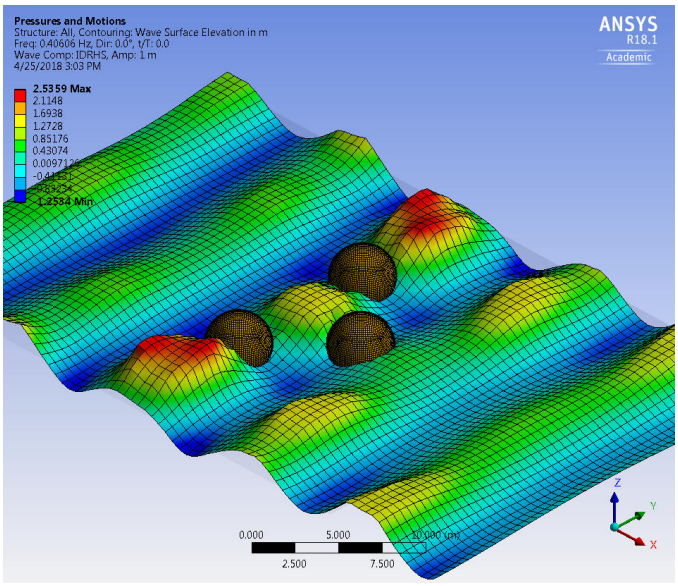

Figure 2.6: The layout of the WEC array

2.5 Wave Energy Converters Array

The dynamic model of the WEC array is presented in this section. The WEC array has three spherical Wave Energy Converters which has 2m radius. The three buoys have a triangular layout which is shown in Fig. 2.6.

The positions of those three bodies expressed in the global coordinates are (0, 5), (5, 0) and (0, −5) respectively. The wave direction of the wave farm is 0^o. The dynamics of the WEC array can be described as:

$$\ddot{\vec{z}} = \mathbf{m}^{-1}(\vec{F}_e + \vec{u} - \mathbf{K}\vec{z} - \mathbf{C}_r\vec{x}_r)$$

$$\dot{\vec{x}}_r = \mathbf{A}_r\vec{x}_r + \mathbf{B}_r\vec{v} \tag{2.39}$$

where the $\vec{z}$ is the heave displacement of the three bodies respectively. The total mass $\mathbf{m} = \mathbf{m}_r + \mathbf{m}_\infty$ can be expressed by the summation of the rigid body mass and the added mass. The rigid body mass and the added mass are written as:

$$\mathbf{m}_r = \begin{bmatrix} m_{r,11} & 0 & 0 \\ 0 & m_{r,22} & 0 \\ 0 & 0 & m_{r,33} \end{bmatrix} \tag{2.40}$$

$$\mathbf{m}_\infty = \begin{bmatrix} m_{\infty,11} & m_{\infty,12} & m_{\infty,13} \\ m_{\infty,21} & m_{\infty,22} & m_{\infty,23} \\ m_{\infty,31} & m_{\infty,32} & m_{\infty,33} \end{bmatrix} \tag{2.41}$$

Additionally, $\mathbf{K}$ represents the hydrostatic coefficients.

$$\mathbf{K} = \begin{bmatrix} K_{11} & 0 & 0 \\ 0 & K_{22} & 0 \\ 0 & 0 & K_{33} \end{bmatrix} \tag{2.42}$$

The $\vec{x}_r$ is the radiation state vector, and $\mathbf{A}_r$, $\mathbf{B}_r$ and $\mathbf{C}_r$ are the radiation matrices which can be identified from the radiation damping B_{ij} and the added mass A_{ij} of the ith body influenced by the motion of the jth body. The construction of the total radiation matrices is introduced in reference [147]. The $\vec{F}_e = [F_{e,1},\ F_{e,2},\ F_{e,3}]^T$ is the

vector of the incoming wave excitation force which can be expressed as:

$$F_{e,i}(t) = \sum_{n} \Re(F_{ew,i}(\omega_n)\eta(\omega_n)e^{i(-\omega_n t+\phi_n)}) \tag{2.43}$$

where $F_{ew,i}(\omega_n), i = 1, 2, 3$ is the frequency domain excitation force coefficient which takes the position of the floater in the array into consideration. The $\vec{u} = [u_1,\, u_2,\, u_3]^T$ is the control force vector.

2.5.1 The WEC array surrogate model

The hydrodynamics of the floaters in the WEC array are coupled. Hence, to avoid the evaluation of the complex hydrodynamics, the details of the surrogate model which is identical to the hydrodynamic model is proposed in reference [148]. The surrogate model applies mechanical elements which includes the spring, damper and masses to

approximate the hydrodynamics behavior. The model can be expressed as:

$$
\begin{aligned}
&\dot{x}_1 = x_4 \quad \dot{x}_2 = x_5 \quad \dot{x}_3 = x_6 \\
&\dot{x}_4 = \frac{1}{m_1}(F_{e,1} + Apz_1 - K_{11}x_1 + u_1) \\
&\dot{x}_5 = \frac{1}{m_2}(F_{e,2} + Apz_2 - K_{22}x_2 + u_2) \\
&\dot{x}_6 = \frac{1}{m_3}(F_{e,3} + Apz_3 - K_{33}x_3 + u_3) \\
&\dot{x}_7 = x_{10} \quad \dot{x}_8 = x_{11} \quad \dot{x}_9 = x_{12} \\
&\dot{x}_{10} = \frac{1}{m_4}(Apz_4 - m_{r,4}g) \\
&\dot{x}_{11} = \frac{1}{m_5}(Apz_5 - m_{r,5}g) \\
&\dot{x}_{12} = \frac{1}{m_6}(Apz_6 - m_{r,6}g)
\end{aligned}
\tag{2.44}
$$

where x_1, x_2 and x_3 represents the displacement of the three bodies respectively. x_4, x_5 and x_6 are the velocities of the three buoys. Further, x_7, x_8 and x_9 are the displacement of the three artificial masses. The x_{10}, x_{11} and x_{12} are the velocities of the three artificial masses. We can denote three floaters and artificial masses in the WEC array as shown in Fig. 2.7.

The $m_i = m_{r,i} + m_{\infty,i}, i = 1, 2..., 6$ represents the total mass of the ith body, where $m_{r,i}$ is the rigid body mass and $m_{\infty,i}$ is the added mass. The added mass of the three bodies can be obtained from WAMIT, while the added mass of the artificial masses can be computed by $m_{\infty,i} = \rho\frac{1}{3}\pi R_{s,i}^3, i = 4, 5, 6$. The $F_{e,i}$ is the excitation force of the

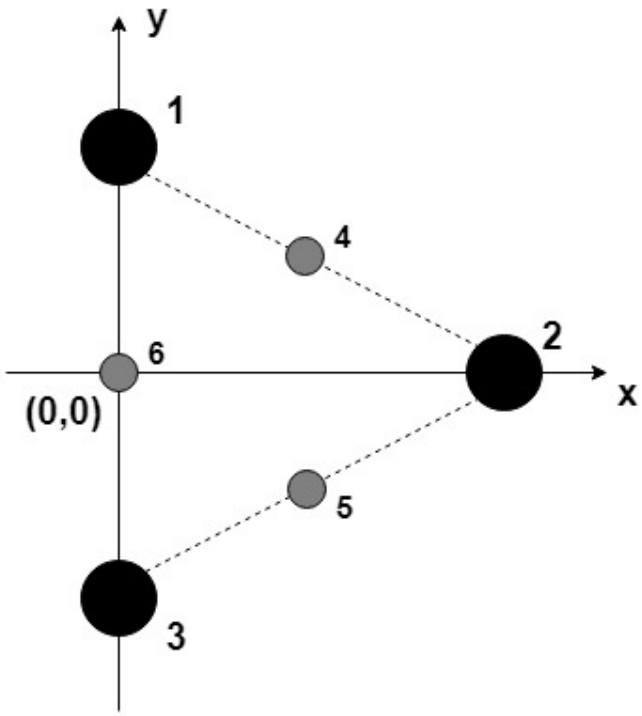

Figure 2.7: The layout of the WEC array surrogate model

ith body which is described in Eq. (2.43). The hydrodynamics coupling are described by the internal forces of the Surrogate model:

$$Apz_1 = -k_{14}(z_1 - z_4)\sin(\alpha 0 + \epsilon_{14}) - c_{14}(v_1 - v_4)\sin(\alpha 0 + \epsilon_{14})$$
$$- k_{16}(z_1 - z_6)\sin(\alpha 0 + \epsilon_{16}) - c_{16}(v_1 - v_6)\sin(\alpha 0 + \epsilon_{16}) \quad (2.45)$$

$$Apz_2 = -k_{24}(z_2 - z_4)\sin(\alpha 0 + \epsilon_{24}) - c_{24}(v_2 - v_4)\sin(\alpha 0 + \epsilon_{24})$$
$$- k_{25}(z_2 - z_5)\sin(\alpha 0 + \epsilon_{25}) - c_{25}(v_2 - v_5)\sin(\alpha 0 + \epsilon_{25}) \quad (2.46)$$

$$Apz_3 = -k_{35}(z_3 - z_5)\sin(\alpha 0 + \epsilon_{35}) - c_{35}(v_3 - v_5)\sin(\alpha 0 + \epsilon_{35})$$
$$- k_{36}(z_3 - z_6)\sin(\alpha 0 + \epsilon_{36}) - c_{36}(v_3 - v_6)\sin(\alpha 0 + \epsilon_{36}) \quad (2.47)$$

$$Apz_4 = k_{14}(z_1 - z_4)\sin(\alpha 0 + \epsilon_{14}) + c_{14}(v_1 - v_4)\sin(\alpha 0 + \epsilon_{14})$$
$$+ k_{24}(z_2 - z_4)\sin(\alpha 0 + \epsilon_{24}) + c_{24}(v_2 - v_4)\sin(\alpha 0 + \epsilon_{24}) \quad (2.48)$$

$$Apz_5 = k_{25}(z_2 - z_5)\sin(\alpha 0 + \epsilon_{25}) + c_{25}(v_2 - v_5)\sin(\alpha 0 + \epsilon_{25})$$
$$+ k_{35}(z_3 - z_5)\sin(\alpha 0 + \epsilon_{35}) + c_{35}(v_3 - v_5)\sin(\alpha 0 + \epsilon_{35}) \quad (2.49)$$

$$Apz_6 = k_{16}(z_1 - z_6)\sin(\alpha 0 + \epsilon_{16}) + c_{16}(v_1 - v_6)\sin(\alpha 0 + \epsilon_{16})$$
$$+ k_{36}(z_3 - z_6)\sin(\alpha 0 + \epsilon_{36}) + c_{36}(v_3 - v_6)\sin(\alpha 0 + \epsilon_{36}) \quad (2.50)$$

where

$$\epsilon_{ij} = \frac{z_i - z_j}{\sqrt{L^2 + h_{eq}^2}\cos(\alpha_0)} \quad (2.51)$$

where k_{ij} and c_{ij} represent the artificial stiffness and damping between the ith and

jth body. The $\alpha 0$ is the initial angle between the spring-damper connector and the horizontal axis. The ϵ_{ij} describes the instantaneous change of the angle α which is denoted in Fig. 2.8.

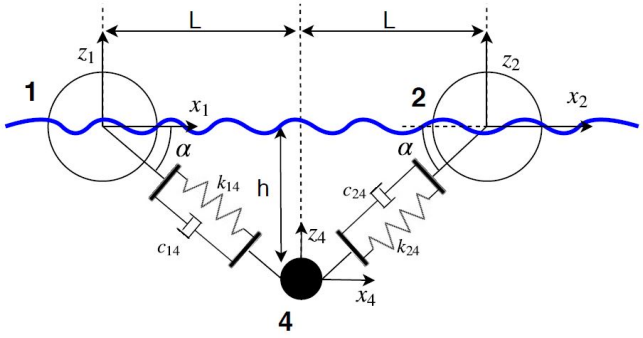

Figure 2.8: The connection between body 1 and body 2

The proposed surrogate model will replace the hydrodynamic model to simulate the hydrodynamic behavior and predict the energy absorption of the wave farm.

2.5.2 The model identification

To approximate the hydrodynamic model of the WEC array accurately, the parameters of the surrogate model need to be identified properly. The unknown parameters of the surrogate model of the three body WEC array are:

$$P = [k_{14},\ k_{16},\ k_{24},\ k_{25},\ k_{35},\ k_{36},\ c_{14},\ c_{16},\ c_{24},\ c_{25},\ c_{35},\ c_{36},$$
$$m_{r,4},\ m_{r,5},\ m_{r,6},\ R_{s,4},\ R_{s,5},\ R_{s,6}] \tag{2.52}$$

Since the wave direction in this paper is 0^o, the system response of the buoy 1 and buoy 3 are identical. The spring, damper and artificial masses are symmetric about the x axis. Hence, the variables need to be identified can be reduced to:

$$P = [k_{14},\, k_{24},\, k_{16},\, c_{14},\, c_{24},\, c_{16},\, m_{r,4},\, m_{r,6},\, R_{s,4},\, R_{s,6}] \tag{2.53}$$

The objective function of the system identification is set up as:

$$\text{Minimize}: \quad J = \sum_{i=1}^{3} e_i^T e_i \tag{2.54}$$

$$i = 1,\, 2,\, 3 \tag{2.55}$$

where e_i represents the approximation error of the displacement of the ith body:

$$e_i = \tilde{z}_i - z_i \tag{2.56}$$

where $\tilde{z}_i$ is the displacement propagated based on the surrogate model and $\vec{z}_i$ is the displacement of the ith body which is obtained from the AQWA simulation. The Genetic Algorithm [149] is applied for the system identification to identify the optimal parameters of the Surrogate model.

Chapter 3

Optimal Control of Wave Energy Converters: Unconstrained control

Based on the dynamic model of the buoy and wave interaction introduced in the last chapter, the controller needs to be designed for different WECs. The essential part of the wave energy conversion is the design of the controller since the control force is the external force that will extract energy from the ocean. There is a significant effort made by the researchers on developing the controllers to maximize the energy capture. In this dissertation, the proposed controllers also aim at absorbing the maximum energy. In this chapter, the proposed controllers only consider the energy extraction regardless of the constraint on the displacement, velocity, and control capacity. Section 3.1 introduces the Singular Arc controller which is developed based

on the optimal control theory. The Simple Model Control is introduced in Section 3.2 which is designed based on the knowledge of the total wave force. The total wave force combines all the wave force acting on the floater which provides the benefit that the people working with wave energy conversion do not require a background of each wave force.

3.1 Singular Arc Controller

The Singular Arc (SA) controller is developed based on the optimal control theory. The Singular Arc means when we solve optimal control of the wave energy conversion, the singularity will happen. However, the controller is still solvable.

3.1.1 Singular Arc Controller for the Simplified WEC Models

In this section, the SA controller is derived for a heaving point absorber with simplified WEC model. The simplified WEC model has a frequency-independent radiation force. Hence the model presented in Eq. (2.3) will be modified as:

$$m\ddot{z} = (F_e + u - Kz - c_{lin}\dot{z}) \tag{3.1}$$

The simplified WEC model can be presented in a state space format as:

$$\dot{x_1} = x_2 \, , \, \dot{x_3} = 1$$
$$\dot{x_2} = \frac{1}{m}(F_e(x_3) + u - Kz - c_{lin}x_2) \tag{3.2}$$

where c denotes the linearized radiation damping. The optimal control then can be solved for the simplified WEC model. Assuming no limits on the control value, the optimal control problem is then defined as:

$$Min : J((x(t), u(t)) = \int_0^{t_f} \{u(t)x_2(t)\}dt \tag{3.3}$$

$$Subject\ to : Equations\ (3.2)$$

The Hamiltonian [27] in this problem is defined as:

$$H(x_1, x_2, x_3, u, \lambda_1, \lambda_2, \lambda_3) = ux_2 + \lambda_1 x_2 + \frac{\lambda_2}{m}(F_e(x_3) + u - c_{lin}x_2 - Kx_1) + \lambda_3 \tag{3.4}$$

where $\vec{\lambda} = [\lambda_1, \lambda_2, \lambda_3]^T$ are Lagrange multipliers. The necessary conditions for optimality show that the optimal solution (x_1^*,x_2^*,x_3^*,u^*,λ_1^*,λ_2^*,λ_3^*) should satisfy the Euler-Langrange equations:

$$\begin{aligned} \frac{\partial H}{\partial \lambda} &= \dot{x} \\ \frac{\partial H}{\partial x} &= -\dot{\lambda} \\ \frac{\partial H}{\partial u} &= 0 \end{aligned} \tag{3.5}$$

Evaluating the Hamiltonian partial derivatives in Eq. (3.5), we find that the optimal trajectory should satisfy the motion constraints in (3.2) in addition to:

$$\dot{\lambda_1} = \frac{K}{m}\lambda_2 \, , \ , x_2 + \frac{\lambda_2}{m} = 0 \tag{3.6}$$

$$\dot{\lambda_2} = -\lambda_1 + \frac{c_{lin}}{m}\lambda_2 - u \tag{3.7}$$

$$\dot{\lambda_3} = -\frac{1}{m}\frac{\partial F_e(x_3)}{\partial x_3}\lambda_2 \tag{3.8}$$

Since the Hamiltonian H is linear in the control u, The optimality conditions (3.6)-(3.8) do not yield an expression for u, which means that the solution is a singular arc control. For this singular arc, it is possible to show that the optimal control is given by [150]:

$$u = \frac{m}{2c_{lin}}\frac{\partial F_e(x_3)}{\partial x_3} + c_{lin}x_2 + Kx_1 - F_e(x_3) \tag{3.9}$$

If we consider a limitation on the control force, the Pontryagin's Minimum Principal can be applied to determine the optimal switching condition between the SA controller and the saturation.

$$u = \begin{cases} u_{sa}, & \frac{\partial H}{\partial u} = 0; \\ \gamma, & \frac{\partial H}{\partial u} < 0; \\ -\gamma, & \frac{\partial H}{\partial u} > 0; \end{cases} \tag{3.10}$$

where γ is the maximum available control level, and u_{sa} is the SA control defined in Eq. (3.9).

3.1.2 Singular Arc Control for the WEC Models with Radiation States

Let us consider the dynamics described in Eq. (2.3) without simplification where the radiation force is dependent on the frequency which can be expressed by a state space model (Eq. (2.13)). The system model can then be represented by a state space

format as:

$$\dot{x}_1 = x_2 \tag{3.11}$$

$$\dot{x}_2 = \frac{1}{m}(F_e(x_3) - \mathbf{C}_r\vec{x}_r - Kx_1 + u) \tag{3.12}$$

$$\dot{x}_3 = 1 \tag{3.13}$$

$$\dot{\vec{x}}_r = \mathbf{A}_r\vec{x}_r + \mathbf{B}_r x_2 \tag{3.14}$$

Define $\vec{x} = [x_1, x_2, x_3, \vec{x}_r]$ as the state vector. The cost function is the same as that defined in Eq. (3.3). The Hamiltonian in this case is defined as:

$$H = ux_2 + \lambda_1 x_2 + \frac{\lambda_2}{m}(F_e(x_3) - \mathbf{C}_r\vec{x}_r - Kx_1 + u) + \lambda_3 + \vec{\lambda}_r(\mathbf{A}_r\vec{x}_r + \mathbf{B}_r x_2) \tag{3.15}$$

where $\vec{\lambda}_r \in \mathbb{R}^{1*n_r}$ are the costate associated with the radiation states. The optimality conditions are also derived from Eq. (3.5):

$$\dot{\lambda}_1 = \frac{K}{m}\lambda_2 \tag{3.16}$$

$$\dot{\lambda}_2 = -\lambda_1 - u - \vec{\lambda}_r\mathbf{B}_r \tag{3.17}$$

$$\dot{\lambda}_3 = -\frac{\lambda_2}{m}\frac{\partial F_{ext}(x_3)}{\partial x_3} \tag{3.18}$$

$$\dot{\vec{\lambda}}_r = \frac{\lambda_2}{m}\mathbf{C}_r - \vec{\lambda}_r\mathbf{A}_r \tag{3.19}$$

$$x_2 + \frac{\lambda_2}{m} = 0 \tag{3.20}$$

The optimality conditions in Eqs. (3.11)–(3.14) and (3.16)–(3.20) can be solved for the control $u(t)$. One way to solve these equations is to use Laplace transform to convert this system of differential equations to a system of algebraic equations in the S domain; this derivation is detailed in reference [2]. The obtained optimal control force in the S domain, $U(s)$, is of the form $U(s) = U_1(s) + U_2(s)$ where:

$$
\begin{aligned}
U_1(s) &= \frac{N_1(s)}{D_1(s)} \\
N_1(s) &= (ms^2 + (\mathbf{C}_r(s\mathbf{I} + \mathbf{A}_r)^{-1}\mathbf{B}_r - B_v)s + K)F_e(s) \\
D_1(s) &= s(\mathbf{C}_r(s\mathbf{I} - \mathbf{A}_r)^{-1}\mathbf{B}_r - \mathbf{C}_r(s\mathbf{I} + \mathbf{A}_r)^{-1}\mathbf{B}_r + 2B_v) \qquad (3.21) \\
U_2(s) &= \frac{N_2(s)}{D_2(s)} \\
N_2(s) &= \left(\left(\lambda_{20} + \vec{\lambda}_{r0}(s\mathbf{I} + \mathbf{A}_r)^{-1}\mathbf{B}_r\right)s - \lambda_{10}\right) \\
&\qquad \left(ms^2 + (\mathbf{C}_r(s\mathbf{I} - \mathbf{A}_r)^{-1}\mathbf{B}_r + B_v)s + K\right) \\
D_2(s) &= s^2(\mathbf{C}_r(s\mathbf{I} - \mathbf{A}_r)^{-1}\mathbf{B}_r - \mathbf{C}_r(s\mathbf{I} + \mathbf{A}_r)^{-1}\mathbf{B}_r + 2B_v) \qquad (3.22)
\end{aligned}
$$

The $U_2(s)$ is a transient term that depends only on the initial values of the co-states and is independent from the excitation force. So, for the steady state solution, the $U_2(s)$ term will be dropped, and $U(s) = U_1(s)$. The inverse Laplace of the $U_1(s)$ term depends on the size and values of the radiation matrices, which would vary depending on the desired level of accuracy. In general, the inverse Laplace transform of $U_1(s)$ will have harmonic terms and exponential terms. All exponential terms are dropped when considering the steady state solution.

3.2 Simple Model Control

Consider the system dynamics described in Eq. (2.3). The wave forces acting on the floater can be combined as a total force. This section, a Simple-Model-Control (SMC) is proposed for a heaving point absorber based on the total wave force. Since the total wave force is composed by the excitation force, hydrostatic force, radiation force (velocity dependent part). The system dynamics can be expressed based on the total force as:

$$(m_r + m_\infty)\ddot{z} = F_T(z, \dot{z}, t) + u \tag{3.23}$$

Note that the total force $F_T(z, \dot{z}, t)$ is assumed a function of time, buoy position, and buoy velocity. Although, the dependency of the total force is determined, the explicit format of the total force is assumed to be unknown. The dependence on time is intuitive since part of this force is due to the wave pressure on the buoy surface, and the wave pressure is time dependent. The buoy position determines the hydrostatic force, and hence the force F_T should be function of the position z. Also, the buoy velocity creates waves which affects the force on the buoy, and hence F_T is made also function of $\dot{z}$. Let the state vector $\vec{x} = [x_1,\, x_2,\, x_3]^T$ and $m = m_r + m_\infty$, the dynamic

model in Eq. (3.23) can be written in the state space form:

$$\begin{aligned}\dot{x}_1 &= x_2 \\ \dot{x}_2 &= \frac{1}{m}(F_T(x_1, x_2, x_3) + u) \\ \dot{x}_3 &= 1\end{aligned} \tag{3.24}$$

where the x_1 and x_2 represent the position and velocity of the buoy respectively, x_3 represents the time t. Since the objective is to maximize the harvested energy, the cost function is the same as defined in Eq. (3.3). The Hamiltonian can be written as:

$$H(x_1, x_2, x_3, F_T, \lambda_1, \lambda_2, \lambda_3) = ux_2 + \lambda_1 x_2 + \frac{\lambda_2}{m}(F_T + u) + \lambda_3 \tag{3.25}$$

The necessary conditions for optimality are shown in Eq. (3.5). By evaluating those partial derivatives, we find that the the optimal trajectory should satisfy the motion constraints in (3.24) in addition to:

$$\dot{\lambda}_1 = -\frac{\partial H}{\partial x_1} = -\frac{\lambda_2}{m}\frac{\partial F_T}{\partial x_1} \tag{3.26}$$

$$\dot{\lambda}_2 = -\frac{\partial H}{\partial x_2} = -u - \lambda_1 - \frac{\lambda_2}{m}\frac{\partial F_T}{\partial x_2} \tag{3.27}$$

$$\dot{\lambda}_3 = -\frac{1}{m}\frac{\partial F_T(x_3)}{\partial x_3}\lambda_2 \tag{3.28}$$

$$\frac{\partial H}{\partial u} = x_2 + \frac{\lambda_2}{m} = 0 \tag{3.29}$$

The optimal control force can be solved by solving the system dynamics and the optimality conditions simultaneously [3]:

$$u^* = m\frac{x_2\frac{\partial F_T}{\partial x_1} - \dot{F}_T - \frac{\partial F_T}{\partial x_2}F_T/m - x_2\frac{d}{dt}\frac{\partial F_T}{\partial x_2}}{\frac{\partial F_T}{\partial x_2}} \tag{3.30}$$

where u^* denotes the optimal control. To implement this control law in time domain, we need to compute F_T, $\dot{F}_T$, x_2, $\frac{\partial F_T}{\partial x_1}$ and $\frac{\partial F_T}{\partial x_2}$. These calculations are discussed in Section 5.1.1. The equation of the optimal controller also indicates the SMC is adaptive to different format of the total force which means it is adaptive to different dynamics or different nonlinearities.

Chapter 4

Optimal Control of Wave Energy Converters: Constrained control

In the last section, we discussed the optimal control without considering the constraint on the displacement, velocity, and control capacity. However, in the real ocean, those physical constraints usually existed. Hence, to develop a more realistic controller which takes the constraints into consideration is necessary. Section 4.1 presents the development of the Shape-Based controller. The proposed controller assumes the trajectory of the velocity and solves the control and energy by applying the system dynamics. The trajectory of the velocity will be adjusted to satisfy the constraint on the displacement and control. Section 4.2 presents the Pseudospectral optimal

control which approximates the dynamics with series expansion. The optimal control can then be solved numerically with the consideration of the constraints. The Linear Quadratic Gaussian Optimal Control is introduced in Section 4.3. The LQG controller implements the constraints by applying the penalty function to the state vector and the control force. Finally, the development of the controller is extended to the array of WECs. Section 4.4 derives the Collective Control for the WEC array. The controller applies the Proportional-Derivative control law where the control coefficients are optimized based on the overall performance of the WEC array by satisfying the constraints.

4.1 Shape-Based Approach

This Shape-Based (SB) controller is developed in this section. The velocity of the floater is approximated by series expansion. The position, acceleration, control forces are computed based on the system dynamics based on the knowledge of the excitation force. The velocity profile will then be optimized in terms of the energy extraction and constraints. The following Section 4.1.1 derives the SB controller with the simplified WEC model. The controller is further derived based on the higher-order WEC model in Section 4.1.2.

4.1.1 Shape-Based Approach for Simplified WEC Model

The equation of motion of a single body heaving point absorber is presented in Eq. (2.3). However, in this section, the SB concept is first explained here for the simplified dynamic model of a heaving point absorber which can be written as [26]:

$$\dot{\vec{x}} = \begin{bmatrix} \dot{x}_1 \\ \dot{x}_2 \end{bmatrix} = \begin{bmatrix} 0 & -K \\ \frac{1}{m} & \frac{-1}{m}(c_{lin} + B_v) \end{bmatrix} \begin{bmatrix} x_1 \\ x_2 \end{bmatrix} + \begin{bmatrix} K \\ \frac{c_{lin}}{m} \end{bmatrix} v_e + \begin{bmatrix} 0 \\ \frac{-1}{m} \end{bmatrix} u \tag{4.1}$$

where m is the total mass of the float including the radiation added mass. c_{lin} is the hydrodynamic damping of the float, B_v is the coefficient of the friction force acting on the float. K is the hydrostatic stiffness. x_1 and x_2 represent the spring force and the velocity of the float respectively. v_e is the vertical velocity of the wave and u is the control force. The distance between the floater and the water surface impacts the linearity of the model above. When the distance D exceeds the limitation, the buoyancy force gets smaller due to a smaller cross section of the buoy at the water level. Hence the spring force x_1 is constrained as:

$$x_1 = \begin{bmatrix} \frac{K}{k_{non}}(D_{max}(k_{non} - 1) + D) & if & D > D_{max} \\ KD & if & |D| \leq D_{max} \\ \frac{K}{k_{non}}(D_{max}(1 - k_{non}) + D) & if & D < -D_{max} \end{bmatrix} \tag{4.2}$$

where k_{non} is a nonlinearity coefficient, D_{max} is the maximum allowable displacement and is set as a given constraint, and D is computed as:

$$D(t) = \int_0^t (v_e(\tau) - v_h(\tau))\, d\tau \tag{4.3}$$

where v_h is the second state x_2. The Shape-Based (SB) approach assumes a Fourier series representation for the buoy velocity ($v_h \equiv x_2$) with unknown Fourier coefficients.

$$v_h(t, a_0, \cdots, a_N, b_1, \cdots, b_N) = \frac{a_0}{2} + \Sigma_{n=1}^{N_f} \left(a_n \cos\left(\frac{n\pi}{H_p} t\right) + b_n \sin\left(\frac{n\pi}{H_p} t\right) \right) \tag{4.4}$$

where H_p is the time interval over which the objective function will be optimized, and it is assumed that we have a model for the wave velocity over this horizon H_p, N_f is the number of Fourier terms and it is a design parameter. The SB approach seeks to optimize the Fourier coefficients so that the extracted energy of the horizon H_p is maximum. The frequencies in the Fourier expansion in Eq. (4.4) can be extracted from the predicted excitation force so that the frequencies in the velocity Fourier expansion match the frequencies in the predicted excitation force, ω_n, $n = 1, \cdots, N_f$. Hence the velocity can be written as:

$$v_h(t, a_0, \cdots, a_N, b_1, \cdots, b_N) = \frac{a_0}{2} + \Sigma_{n=1}^{N_f} \left(a_n \cos\left(\omega_n t\right) + b_n \sin\left(\omega_n t\right) \right) \tag{4.5}$$

For a given buoy velocity representation, the derivative of the velocity $\dot{v}_h(t)$ can be evaluated analytically. Given a model for the wave vertical velocity, $v_e(t)$, the vertical displacement between the float and the water surface is computed based on Eq. (4.3). The spring force x_1 then can be computed based on Eq. (4.2). Resultantly, the control force can be computed by applying Eq. (4.1):

$$u(t, a_0, \cdots, a_N, b_1, \cdots, b_N) = x_1(t) - (c_{lin} + B_v)v_h(t) + c_{lin}v_e(t) - m\dot{v}_h(t) \qquad (4.6)$$

The optimal control problem can then be formulated as follows:

Max $E(t) = -\int_0^T u(t)x_2(t)dt$, Subject to:

1. $|u| \leq u_{max}$,
2. $|D| \leq D_{max}$
3. The equations of motion defined in Eq. (4.1).

The design variables are the Fourier coefficients a_0, a_n, and b_n, $\forall\, n = 1 \cdots N_f$. The optimization algorithm used to solve this optimization problem is the interior point method [151]. The optimization process requires an initial guess for the coefficients. A good initial guess for the coefficients is one that is close to the optimal solution so that the computational cost of the optimization process is small. A good initial guess can be obtained using the available wave predication; the Fourier coefficients

are initialized such that the velocity matches the wave vertical velocity. To do that, the predicted wave velocity is expanded using Fourier series as follows:

$$v_e(t) = \frac{c_0}{2} + \Sigma_{n=1}^{N_f} \left(c_n \cos\left(\frac{n\pi}{T}t\right) + d_n \sin\left(\frac{n\pi}{T}t\right)\right) \tag{4.7}$$

In Eq. (4.7), the coefficients c_0, c_n, and d_n can be computed given the prediction for $v_e(t)$. These coefficients are used as initial guess for the coefficients a_0, a_n, and b_n, respectively, $\forall\, n = 1 \cdots N_f$.

4.1.2 Shape-Based Approach for Higher-Order Model WEC Optimal Control

For the performance model described in Eq. (2.3), the SB approach still approximates the buoy velocity using Fourier series as described in the last section. The optimization design variables are still the Fourier coefficients in the velocity Fourier expansion. For a given shape of the velocity (given a set of the design variables), the control force and the objective function (extracted energy) are evaluated as follows. The vector of radiation states $\vec{x}_r$ can be propagated in time over the Horizon H_p using the velocity profile, as described in Eq. (2.13). The history of the radiation states is then used along with the history of the velocity over H_p to compute the control force

using Eq. (2.3):

$$u = (m_r + m_\infty)\dot{x}_2 - F_e + \mathbf{C}_r\vec{x}_r + Kx_1 + B_v x_2 \tag{4.8}$$

where $\dot{x}_2$ is the derivative of the velocity which can be computed analytically by taking the derivative for the velocity Fourier expansion. Once the input control u is computed over the horizon H_p it is used to propagate the whole system over the horizon H_p using Eq. (2.3), and the corresponding extracted energy is computed using Eq. 2.4. This completes the evaluation of the control and the corresponding energy at any time step; this process is repeated as the simulation marches in time.

As a way to save on the computational cost, it is possible to take advantage of the fact that at each time a control command is needed we compute the control over a horizon H_p starting at that time. In other words, at a given time step, the SB approach computes the required control at each time step over H_p. This control history is stored and is used to save on the computational time. This control history is used at subsequent time steps without updating the control. This saving on the computational effort reduces the optimality of the solution since a control predicted at a previous time step is suboptimal. To implement this concept, we define the number of time steps in which new control calculations are not needed as the integer parameter $CtrlInteg$. The following parameters are also defined:

N_H : an integer that represents the Horizon length in units of wave period

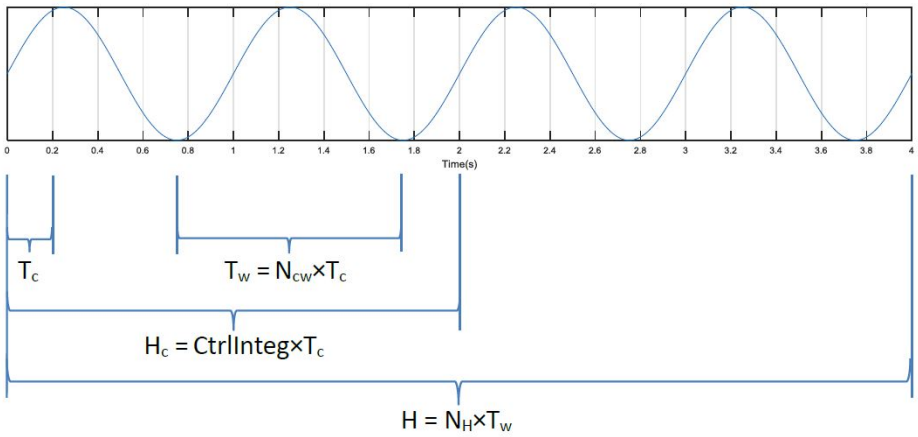

Figure 4.1: SB parameters definitions

N_{cw} : an integer that determines the number of control updates in one wave period

N_f : the number of Fourier terms

Figure 4.1 is an illustration that shows these parameters. Algorithm 1 shows an outline for the SB algorithm. The variable t is the time, $Tend$ is the end of simulation time. As can be seen from the above presentation, the SB method can be considered as a particular form of the model predictive control with a different parameterization than the standard piecewise constant input trajectory used in the literature [23].

Algorithm 1 Outline for the SB Algorithm

for all $t \in 0, ..., Tend$ **do**
  if $t < CtrlInteg$ steps of time **then**
    Use the wave perdition data to compute buoy velocity over the time horizon
    Optimize the Fourier coefficients for maximum energy extraction over the time horizon
    Save the computed control for the future $CtrlInteg$ time steps
  end if
  Apply control at current time t
end for

4.2 Pseudospectral Optimal Control

The Pseudospectral (PS) optimal control is introduced in this section. The proposed approach solves the control numerically by approximating the states and the control force with series expansion. The controller is derived for a single body 3-degree-of-freedom (surge, heave, pitch) WEC. Two cases will be investigated, the first case considers the linear dynamics without parametric excitation. The second case includes the parametric excitation.

4.2.1 System Approximation Using Fourier Series

The control forces and the states each is approximated by a linear combination of the basis functions, $\phi_k(t)$. For the WEC problem, and due to the periodicity nature of the wave, it is intuitive to select a Fourier series to be the basis functions. A truncated Fourier Series that has zero mean is used with N_f terms. Since we have both sine and cosine functions, N_f is an even number and is equal to twice the number of cosine (or sine) functions in the Fourier series. The vector of basis functions is:

$$\vec{\Phi}(t) = [\cos(w_0 t), \sin(w_0 t), ..., \cos(\frac{N_f}{2} w_0 t), \sin(\frac{N_f}{2} w_0 t)] \tag{4.9}$$

where $w_0 = 2\pi/T_{end}$ is the fundamental frequency, T_{end} represents the total simulation time. The states and the controller can be approximated using $\vec{\Phi}(t)$ as follows:

$$x_i(t) = \sum_{k=1}^{N/2} x_{ik}^c \cos(kw_0 t) + x_{ik}^s \sin(kw_0 t) = \vec{\Phi}(t)\hat{x}_i \tag{4.10}$$

$$u_j(t) = \sum_{k=1}^{N/2} u_{jk}^c \cos(kw_0 t) + u_{jk}^s \sin(kw_0 t) = \vec{\Phi}(t)\hat{u}_j \tag{4.11}$$

where in the above two equations, i is the state index, and j is the control index. In Eq. (4.10) x_{ik}^c/x_{ik}^s denotes the k_{th} coefficient of cosine/sine term of basis function for i_{th} state. In Eq. (4.11) u_{jk}^c/u_{jk}^s denotes the k_{th} coefficient of cosine/sine term of basis function for j_{th} control. The Fourier coefficients (or weight vectors) are grouped as follows:

$$\hat{x}_i(t) = [x_{i1}^c, x_{i1}^s, x_{i2}^c, x_{i2}^s, ..., x_{i\frac{N_f}{2}}^c, x_{i\frac{N_f}{2}}^s]^T \tag{4.12}$$

$$\hat{u}_j(t) = [u_{j1}^c, u_{j1}^s, u_{j2}^c, u_{j2}^s, ..., u_{j\frac{N_f}{2}}^c, u_{j\frac{N_f}{2}}^s]^T \tag{4.13}$$

In the problem the variables need to be optimized are the velocity of surge motion $v_s(t)$, the velocity of pitch rotation $v_p(t)$, the controller in surge direction $u_s(t)$ and

the controller in pitch direction $u_p(t)$. So we have $i = 1, 2$ $j = 1, 2$:

$$v_s(t) \approx x_1(t) = \vec{\Phi}(t)\hat{x}_1 \tag{4.14}$$

$$v_p(t) \approx x_2(t) = \vec{\Phi}(t)\hat{x}_2 \tag{4.15}$$

$$u_s(t) \approx u_1(t) = \vec{\Phi}(t)\hat{u}_1 \tag{4.16}$$

$$u_p(t) \approx u_2(t) = \vec{\Phi}(t)\hat{u}_2 \tag{4.17}$$

The main advantage of selecting the Fourier Series to be the basis function is that we can compute the derivative and integration of the approximation easier than the other orthogonal polynomials. The differentiation of the approximated states can be expressed as:

$$\dot{x}_i = \dot{\vec{\Phi}}(t)\hat{x}_i = \vec{\Phi}(t)\mathbf{D}_\phi\hat{x}_i \tag{4.18}$$

Because the basis function is the only time dependent term of the approximated states, and for a zero-mean Fourier Series, the derivative can be conveniently expressed as a matrix $\mathbf{D}_\phi \in R^{N\times N}$. The matrix is block diagonal, where each block $\mathbf{D}_\phi^k$ can be expressed as:

$$\mathbf{D}_\phi^k = \begin{bmatrix} 0 & k\omega_0 \\ -k\omega_0 & 0 \end{bmatrix} \tag{4.19}$$

where the matrix $\mathbf{D}_\phi$ is invertible, and its inverse is the matrix used to compute the integration of a state. The integration matrix is still block diagonal. Each block of

integration matrix can be written as:

$$\mathbf{D}_{\phi}^{-k} = \begin{bmatrix} 0 & -\frac{1}{k\omega_0} \\ \frac{1}{k\omega_0} & 0 \end{bmatrix} \tag{4.20}$$

This state approximation can be used to approximate all other quantities that are functions of the states. The viscous damping in the surge direction F_b^s can be expressed as:

$$F_b^s = B_{v,11} v_s = B_{v,11} \vec{\Phi}(t) \hat{x}_1 \tag{4.21}$$

The hydrostatic force F_s can be expressed as:

$$F_s = K_{11} z = K_{11} \vec{\Phi}(t) \hat{x}_z = K_{11} \vec{\Phi}(t) \mathbf{D}_{\phi}^{-1} \hat{x}_1 \tag{4.22}$$

The radiation forces can also be approximated using this Fourier series representation for the states eliminating the need for convolution integral evaluation. The radiation force in the surge mode can be written as:

$$\begin{aligned} F_r^1 &= \int_{-\infty}^{\infty} h_{r,11}(t-\tau) x_1^N(\tau) d\tau + \int_{-\infty}^{\infty} h_{r,15}(t-\tau) x_2^N(\tau) d\tau \\ &= F_r^{11} + F_r^{15} \end{aligned} \tag{4.23}$$

where each of the above two terms can be approximated as [152]:

$$F_r^{11} = (h_{r,11} * \vec{\Phi}(t))\hat{x}_1 = \vec{\Phi}(t)(\mathbf{G}_{r,11} - m_\infty^{11}\mathbf{D}_\phi)\hat{x}_1 \tag{4.24}$$

$$F_r^{15} = (h_{r,15} * \vec{\Phi}(t))\hat{x}_2 = \vec{\Phi}(t)(\mathbf{G}_{r,15} - m_\infty^{15}\mathbf{D}_\phi)\hat{x}_2 \tag{4.25}$$

where m_∞ denotes the added mass at infinite frequency. The matrix $\mathbf{G}_r \in R^{N\times N}$ is block diagonal, the k-th block is:

$$\mathbf{G}_{r,k} = \begin{bmatrix} B(k\omega_0) & k\omega_0 A(k\omega_0) \\ -k\omega_0 A(k\omega_0) & B(k\omega_0) \end{bmatrix} \tag{4.26}$$

The excitation force can also approximated by Fourier Series.

$$F_e^1 \approx \vec{\Phi}(t)\hat{e}_1 \tag{4.27}$$

$$F_e^5 \approx \vec{\Phi}(t)\hat{e}_2 \tag{4.28}$$

Substituting these approximated forces and states in the system's dynamics Eq. (2.33), we get:

$$r_1 = ((m_r + m_\infty^{11})\vec{\Phi}\mathbf{D}_\phi + B_{v,1}\vec{\Phi} + K_{11}\vec{\Phi}\mathbf{D}_\phi^{-1} + h_{r,11} * \vec{\Phi})\hat{x}_1$$
$$- \vec{\Phi}\hat{e}_1 - \vec{\Phi}\hat{\vec{u}}_1 + (m_\infty^{15}\vec{\Phi}\mathbf{D}_\phi + h_{r,15} * \vec{\Phi})\hat{x}_2 \quad (4.29)$$

$$r_2 = ((J_r + J_\infty^{55})\Phi\mathbf{D}_\phi + B_{v,5}\vec{\Phi} + K_{55}\vec{\Phi}\mathbf{D}_\phi^{-1} + h_{r,55} * \vec{\Phi})\hat{x}_2$$
$$- \vec{\Phi}\hat{e}_2 - \vec{\Phi}\hat{\vec{u}}_2 + (J_\infty^{51}\vec{\Phi}\mathbf{D}_\phi + h_{r,51} * \vec{\Phi})\hat{x}_1 \quad (4.30)$$

where r_1 and r_2 are residuals due to the approximation. In the Galerkin method, the residuals are orthogonal to the basis function. That is:

$$< r_1, \phi_j > = 0 \quad (4.31)$$

$$< r_2, \phi_j > = 0 \quad (4.32)$$

where $j = 1, ..., N$. This implies that the residuals vanish at all the collocation points.

4.2.2 Control Optimization for Linear Time-Invariant WECs

The objective of the proposed controller is to maximize the energy conversion of the surge and pitch mode. Hence the objective function can be expressed as:

$$J = \int_0^T \vec{u}^T \vec{v} dt = \frac{T}{2}(\hat{u}_1\hat{x}_1 + \hat{u}_2\hat{x}_2) \tag{4.33}$$

So the optimal control problem is to minimize Eq. (4.33) subject to Eqs. (4.29) (4.30). For the system dynamics described in Eq. (2.33) with constant pitch stiffness $K_{res} = Const$, the equation of motion can be written in matrix form as:

$$\begin{bmatrix} F_{d,11} & F_{d,12} \\ F_{d,21} & F_{d,22} \end{bmatrix} \begin{bmatrix} \hat{x}_1 \\ \hat{x}_2 \end{bmatrix} = \begin{bmatrix} \hat{u}_1 \\ \hat{u}_2 \end{bmatrix} + \begin{bmatrix} \hat{e}_1 \\ \hat{e}_2 \end{bmatrix} \tag{4.34}$$

where $\mathbf{F}_{d,ij}$ are given as a block diagonal matrix. The kth block is:

$$\mathbf{F}_{d,ij}^k = \begin{bmatrix} D_{ij}^k & M_{ij}^k \\ -M_{ij}^k & D_{ij}^k \end{bmatrix} \tag{4.35}$$

where $i, j = 1, 2$ and

$$D_{ij}^k = B_{ij}(k\omega_0) + B_{v,ij}$$

$$M_{ij}^k = k\omega_0(m_{r,ij} + A_{ij}(k\omega_0)) - K_{ij}/(k\omega_0)$$

where $A_{ij}(k\omega_0)$ denotes the added mass at kth frequency of ith mode due to jth mode. It is possible to solve for the optimal control analytically [23] by setting the partial derivative of $\tilde{J}$ with respect to the control to zero; that is $\frac{\partial \tilde{J}}{\partial u} = 0$. Hence, the expression of the optimal control is:

$$\hat{u}^* = -(\mathbf{F}_d^{-1} + \mathbf{F}_d^{-T})^{-1}\mathbf{F}_d^{-1}\hat{e} \tag{4.36}$$

4.2.3 Control Optimization for Linear Time-Varying WECs

When the pitch stiffness is a function of the heave amplitude, the pitch stiffness term K_{res} has a time-varying term $K_p(t)$. This is usually referred to as parametric excitation since the heave motion excites the pitch motion, which is coupled with the surge. Then the system becomes a time-varying system. This affects the second constraint Eq. (4.30) which becomes as follows in a Linear Time-Varying WEC:

$$\begin{aligned} r_2 = &((J_r + J_\infty^{55})\vec{\Phi}\mathbf{D}_\phi + B_{v,55}\vec{\Phi} + (K_c + K_p)\vec{\Phi}\mathbf{D}_\phi^{-1} + h_{r,55} * \vec{\Phi})\hat{x}_2 \\ &- \vec{\Phi}\hat{e}_2 - \vec{\Phi}\hat{u}_2 + (J_\infty^{51}\vec{\Phi}\mathbf{D}_\phi + h_{r,51} * \vec{\Phi})\hat{x}_1 \end{aligned} \tag{4.37}$$

The time-varying stiffness can be approximated as:

$$K_p(t) = \vec{\Phi}(t)\hat{s} \tag{4.38}$$

So the r_2 residual can be expressed as:

$$r_2 = ((J_r + J_\infty^{55})\vec{\Phi}\mathbf{D}_\phi + B_{v,55}\vec{\Phi} + K_c\vec{\Phi}\mathbf{D}_\phi^{-1} + \vec{\Phi}\hat{s}\vec{\Phi}\mathbf{D}_\phi^{-1} + h_{r,55} * \vec{\Phi})\hat{x}_2$$
$$- \vec{\Phi}\hat{e}_2 - \vec{\Phi}\hat{u}_2 + (J_\infty^{51}\vec{\Phi}\mathbf{D}_\phi + h_{r,51} * \vec{\Phi})\hat{x}_1 \tag{4.39}$$

The r_1 residual remains the same. The residuals can be discretized at collocation points:

$$r_1^j = ((m_r + m_\infty^{11})\vec{\Phi}_j\mathbf{D}_\phi + B_{v,11}\vec{\Phi}_j + K_{11}\vec{\Phi}_j\mathbf{D}_\phi^{-1} + h_{r,11} * \vec{\Phi}_j)\hat{x}_1$$
$$- \vec{\Phi}_j\hat{e}_1 - \vec{\Phi}_j\hat{u}_1 + (m_\infty^{15}\vec{\Phi}_j\mathbf{D}_\phi + h_{r,15} * \vec{\Phi}_j)\hat{x}_2 \tag{4.40}$$

$$r_2^j = ((J_r + J_\infty^{55})\vec{\Phi}_j\mathbf{D}_\phi + B_{v,55}\vec{\Phi}_j + K_c\vec{\Phi}_j\mathbf{D}_\phi^{-1} + \vec{\Phi}_j\hat{s}\vec{\Phi}_j\mathbf{D}_\phi^{-1} + h_{r,55} * \vec{\Phi}_j)\hat{x}_2$$
$$- \vec{\Phi}_j\hat{e}_2 - \vec{\Phi}_j\hat{u}_2 + (J_\infty^{51}\vec{\Phi}_j\mathbf{D}_\phi + h_{r,51} * \vec{\Phi}_j)\hat{x}_1 \tag{4.41}$$

where $\vec{\Phi}_j = \vec{\Phi}(t_j)$, the nodes t_j are uniformly spaced between 0 and T_{end}:

$$t_j = j\delta t \quad with\ \delta t = T_{end}/(N-1)\ and\ j = 0, ..., N-1 \tag{4.42}$$

The objective function will be the same as the time-invariant system in Eq. (4.33). To solve for the control, a Nonlinear Programming (NLP) approach will be implemented. The NLP is then to minimize Eq. (4.33), subject to Eqs. (4.40) and (4.41), which have a total of $2N$ equality constraints.

To further explain the logic of the controller, a framework diagram is included in Figure. 4.2. In the figure, the switch is on when we need to compute the control history over the prediction horizon. The switch is off when the time is between the beginning of the prediction horizon and the end. When the switch is off the controller will be extracted from the control history directly and feed to the dynamics system. When the time reaches the end of the prediction horizon, the switch is on again to compute the control history of the next prediction horizon.

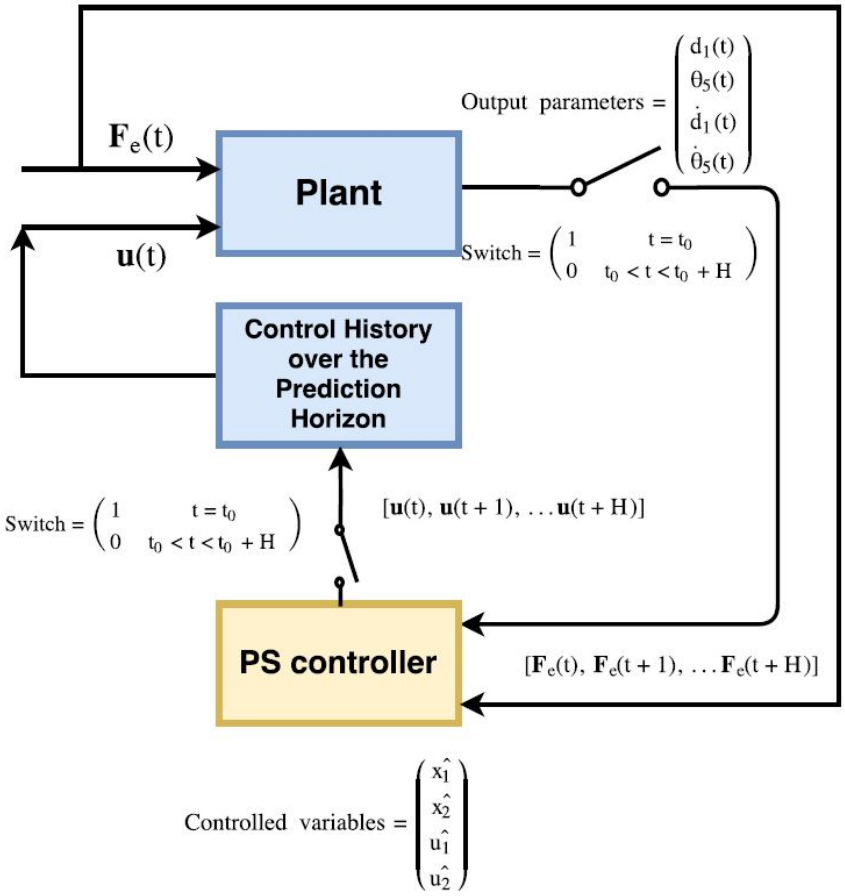

Figure 4.2: The framework diagram of the logic of the control [1]

4.3 Linear Quadratic Gaussian Optimal Control

Another classical control, the Linear Quadratic Gaussian (LQG) optimal control will be implemented here for a single body 3-degree-of-freedom WEC. The controller aims at absorbing the maximum energy within the constraints. The constraints are implemented in the cost function as penalty functions. Further, the optimal control problem is split into two parts. The first part is the LQ optimal controller which computes the control assuming the availability of the estimated states; this part requires, as input, the wave prediction and the estimation of the states. The second part is an LQ optimal estimator which generates the estimation and prediction. Only the control strategy will be discussed in this section. The estimator will be introduced in Section 5.2.2.

4.3.1 The LQ control law

As mentioned before, for a 3-dof WEC, the heave motion is uncoupled from the other two modes. Hence, the heave motion can be controlled by the SA controller [2]. The control for the coupled surge-pitch modes will be designed using a time-varying Linear Quadratic Gaussian optimal control approach. The objective is set to maximize the energy over the simulation time period within the state and control constraints; hence

we can write the objective function as:

$$\text{Minimize} \quad J = \int_0^{Tend} ((\mathbf{x}^c)^T \mathbf{Q}^c \mathbf{x}^c + (\mathbf{u}^c)^T \mathbf{W}^c \mathbf{x}^c + \frac{1}{2}(\mathbf{u}^c)^T \mathbf{R}^c \mathbf{u}^c) dt \tag{4.43}$$

The Lagrangian for surge-pitch motion then can be defined as:

$$L^c = (\mathbf{x}^c)^T \mathbf{Q}^c \mathbf{x}^c + (\mathbf{u}^c)^T \mathbf{W}^c \mathbf{x}^c + \frac{1}{2}(\mathbf{u}^c)^T \mathbf{R}^c \mathbf{u}^c \tag{4.44}$$

where $\mathbf{Q}^c$ and $\mathbf{R}^c$ are the state and control penalty matrix respectively. $\mathbf{x}^c$ is the state vector of the coupled system. $\mathbf{u}^c$ is the control vector of the coupled motion. Further, the matrices $\mathbf{W}^c$ and $\mathbf{R}^c$ are selected as:

$$\mathbf{W}^c = \begin{bmatrix} 0^{2\times 2} \\ I^{2\times 2} \\ \mathbf{0}^{n_r \times 2} \end{bmatrix} \tag{4.45}$$

$$\mathbf{R}^c = \begin{bmatrix} \epsilon_{r,1} & 0 \\ 0 & \epsilon_{r,5} \end{bmatrix} \tag{4.46}$$

The Lagrangian can be transformed to the following convex format:

$$\begin{aligned} L^c = &\frac{1}{2}(\mathbf{x}^c)^T (\mathbf{Q}^c - \mathbf{W}^c (\mathbf{R}^c)^{-1} (\mathbf{W}^c)^T) \mathbf{x}^c + \\ &\frac{1}{2}(\mathbf{u}^c + (\mathbf{R}^c)^{-1} (\mathbf{W}^c)^T \mathbf{x}^c)^T \mathbf{R}^c (\mathbf{u}^c + (\mathbf{R}^c)^{-1} (\mathbf{W}^c)^T \mathbf{x}^c) \end{aligned} \tag{4.47}$$

If we do not included any constraint for the states of surge and pitch, the state penalty matrix is set as $\mathbf{Q}^c = \mathbf{0}$. Let us define $\mathbf{A}_1^c = (\mathbf{Q}^c - \mathbf{W}^c(\mathbf{R}^c)^{-1}(\mathbf{W}^c)^T)$, $\mathbf{B}_1^c = \mathbf{R}^c$ and $\mathbf{U}_1^c = (\mathbf{u}^c + (\mathbf{R}^c)^{-1}(\mathbf{W}^c)^T\mathbf{x}^c)$. The system dynamics described in Eq. (2.33) can be compacted in a state space format as:

$$\dot{\mathbf{x}^c}(t) = \mathbf{F}^c(t)\mathbf{x}^c(t) + \mathbf{G}^c(t)\mathbf{u}^c(t) + \mathbf{c}^c(t) \tag{4.48}$$

where

$$\mathbf{F}^c(t) = \begin{bmatrix} 0^{2\times 2} & I^{2\times 2} & \mathbf{0}^{2\times n_r} \\ -\mathbf{m}^{-1}\mathbf{K} & -\mathbf{m}^{-1}\mathbf{C} & -\mathbf{m}^{-1}\mathbf{C}_r \\ \mathbf{0}^{n_r\times 2} & \mathbf{B}_r & \mathbf{A}_r \end{bmatrix} \tag{4.49}$$

$$\mathbf{G}^c = \begin{bmatrix} 0^{2\times 2} \\ \mathbf{m}^{-1} \\ \mathbf{0}^{n_r\times 2} \end{bmatrix} \tag{4.50}$$

$$\mathbf{c}^c(t) = \begin{bmatrix} 0^{2\times 2} \\ \mathbf{m}^{-1} \\ \mathbf{0}^{n_r\times 2} \end{bmatrix} \begin{bmatrix} \hat{F}_e^1 \\ \hat{F}_e^5 \end{bmatrix} \tag{4.51}$$

The dynamics can also be transformed to the format based on the new controller $\mathbf{U}_1^c$:

$$\dot{\mathbf{x}^c}(t) = \mathbf{F}_1^c(t)\mathbf{x}^c(t) + \mathbf{G}^c(t)\mathbf{U}_1^c(t) + \mathbf{c}^c(t) \tag{4.52}$$

where $\mathbf{F}_1^c(t) = \mathbf{F}^c(t) - \mathbf{G}^c(\mathbf{R}^c)^{-1}(\mathbf{W}^c)^T$. Hence the Hamiltonian can be defined as:

$$H = \frac{1}{2}(\mathbf{x}^c)^T\mathbf{A}_1^c\mathbf{x}^c + \frac{1}{2}(\mathbf{U}_1^c)^T\mathbf{B}_1^c\mathbf{U}_1^c + \boldsymbol{\lambda}^c(\mathbf{F}_1^c(t)\mathbf{x}^c(t) + \mathbf{G}^c(t)\mathbf{U}_1^c(t) + \mathbf{c}^c(t)) \tag{4.53}$$

Applying the necessary conditions for optimality, we get:

$$\dot{\boldsymbol{\lambda}}^c = -\frac{\partial H}{\partial \mathbf{x}^c} \equiv -\mathbf{A}_1^c\mathbf{x}^c - (\mathbf{F}_1^c(t))^T\boldsymbol{\lambda}^c \tag{4.54}$$

$$\frac{\partial H}{\partial \mathbf{U}_1^c} \equiv \mathbf{B}_1^c\mathbf{U}_1^c + \mathbf{G}^c\boldsymbol{\lambda}^c = \mathbf{0} \tag{4.55}$$

$$\frac{\partial H}{\partial \lambda_i^c} = \dot{x}_i^c \tag{4.56}$$

Hence, based on Eq. (4.55), the optimal control law is:

$$\mathbf{U}_1^{c*} = -(\mathbf{B}_1^c)^{-1}(\mathbf{G}^c)^T\boldsymbol{\lambda}^c \tag{4.57}$$

which requires evaluation of the costates. This system is inhomogeneous due to the excitation force ($\mathbf{c}^c(t)$ in Eq. (4.52)), then the costate is assumed in the form [153]:

$$\boldsymbol{\lambda}^c = \mathbf{S}^c\mathbf{x}^c + \mathbf{k}^c \tag{4.58}$$

where the term $\mathbf{k}^c$ is added due to the inhomogeneity of the system. Taking the derivative for Eq. (4.58) and solving Eq. (4.52), (4.54), (4.57) and (4.58) together, we

obtain the Riccati and the auxiliary equations as:

$$\dot{\mathbf{S}}^c + \mathbf{S}^c\mathbf{F}_1^c(t) + \mathbf{F}_1^c(t)^T\mathbf{S}^c - \mathbf{S}^c\mathbf{G}^c(\mathbf{B}_1^c)^{-1}(\mathbf{G}^c)^T\mathbf{S}^c + \mathbf{A}_1^c = \mathbf{0} \tag{4.59}$$

$$\dot{\mathbf{k}}^c + \mathbf{F}_1^c(t)^T\mathbf{k}^c - \mathbf{S}^c\mathbf{G}^c(\mathbf{B}_1^c)^{-1}(\mathbf{G}^c)^T\mathbf{k}^c + \mathbf{S}^c\mathbf{c}^c(t) = \mathbf{0} \tag{4.60}$$

Since there is no constraint on the final conditions, then the final conditions of the Riccati and Auxiliary equations are $\mathbf{S}^c(t_f) = \mathbf{0}$, $\mathbf{k}^c(t_f) = \mathbf{0}$. These two equations can be propagated backward to get the time history of the optimal feedback gain. Then the optimal control is:

$$\mathbf{U}_1^{c*} = -(\mathbf{B}_1^c)^{-1}(\mathbf{G}^c)^T(\mathbf{S}^c(t)\mathbf{x}^c(t) + \mathbf{k}^c(t)) \tag{4.61}$$

Finally the expression of the control force can be obtained after transforming back $\mathbf{U}_1^{c*}$ to get:

$$\mathbf{u}^{c*} = -((\mathbf{B}_1^c)^{-1}(\mathbf{G}^c)^T\mathbf{S}^c(t) + (\mathbf{B}_1^c)^{-1}(\mathbf{W}^c)^T)\mathbf{x}^c(t) - (\mathbf{B}_1^c)^{-1}(\mathbf{G}^c)^T\mathbf{k}^c(t) \tag{4.62}$$

A similar approach can be developed for the heave control to get:

$$u^{h*} = -((B_1^h)^{-1}(\mathbf{G}^h)^T\mathbf{S}^h(t) + (B_1^h)^{-1}(\mathbf{W}^h)^T)\mathbf{x}^h(t) - (B_1^h)^{-1}(\mathbf{G}^h)^T\mathbf{k}^h(t) \tag{4.63}$$

where

$$\mathbf{W}^h = \begin{bmatrix} 0 \\ 1 \\ \mathbf{0} \end{bmatrix} \tag{4.64}$$

$$B_1^h = R^h = \epsilon_{r,3} \tag{4.65}$$

4.4 Collective Control of WEC array

The control development is finally extended to the WEC array. To obtain a overall maximum energy extracted from the WEC array, the collective control is proposed in this section. The controller applies the PD feedback control law which can be expressed as:

$$\vec{u} = -\mathbf{K}_p \vec{z} - \mathbf{K}_d \vec{v}_h \tag{4.66}$$

where $\mathbf{K}_p$ and $\mathbf{K}_d$ are the feedback gains of the controller. The PD control gains matrices take the form of:

$$\mathbf{K}_p = \begin{bmatrix} K_{p,11} & 0 & 0 \\ 0 & K_{p,22} & 0 \\ 0 & 0 & K_{p,33} \end{bmatrix} \tag{4.67}$$

$$\mathbf{K}_d = \begin{bmatrix} K_{d,11} & K_{d,12} & K_{d,13} \\ K_{d,21} & K_{d,22} & K_{d,23} \\ K_{d,31} & K_{d,32} & K_{d,33} \end{bmatrix} \tag{4.68}$$

To have the maximum energy absorption and satisfy the constraints, the control feedback gains need to be optimized. The objective function can be expressed as:

$$\text{Minimize}: \quad J = \sum_i \int_0^T u_i v_{h,i} dt \tag{4.69}$$

$$\begin{aligned} Sub\ to: \quad & \mid z_i \mid - z_{max} \leqslant 0 \\ & \mid u_i \mid - u_{max} \leqslant 0 \\ & i = 1,\ 2,\ 3 \end{aligned} \tag{4.70}$$

where the variables of the optimization are:

$$\begin{aligned} \vec{x} = [&K_{p,11},\ K_{p,22},\ K_{p,33},\ K_{d,11},\ K_{d,12},\ K_{d,13} \\ &,\ K_{d,21},\ K_{d,22},\ K_{d,23},\ K_{d,31},\ K_{d,32},\ K_{d,33}] \end{aligned} \tag{4.71}$$

The u_i and v_i can be obtained by the propagation of the Surrogate model which is described in Eq. (2.44). The z_{max} is the maximum displacement of the floaters in the wave farm and u_{max} is the maximum control capacity. The constraint on the control force is dependent on the capacity of the device, it is a hard constraint. Hence, the control force is saturated by the control limitation in the simulation. The constraint on the displacement is implemented as an exterior penalty function in the cost function. The original cost function can be transformed as:

$$\text{Minimize}: \quad J = -E + \frac{1}{2} r_g \sum_{i=1}^{3} (max(0, g_i))^2 \tag{4.72}$$

$$i = 1,\ 2,\ 3 \tag{4.73}$$

where g_i represents the inequality constraints:

$$g_i = \mid z_i \mid - z_{max} \tag{4.74}$$

And the control force is saturated by the maximum control force u_{max}. The weight of the penalty function can be identified iteratively by applying the Sequential Unconstrained Minimization Techniques (SUMT) [154]. The details of the SUMT algorithm are summarized in Algorithm. 2.

The parameters of the SUMT need to be carefully selected to guarantee the optimality and the efficiency of the optimization.

Algorithm 2 The SUMT algorithm with the exterior penalty function

1: **Initialization:** Choose $\vec{x}_0$ (Initial guess of the optimization variable)
N_s (Number of SUMT iterations)
N_u (Number of Sequential Quadratic Programming iterations)
ϵ_i's (Stopping criteria)
r_g (Weight of the penalty function)
c_g (scaling multiplier for r_g)
2: **while** $q \leqslant N_s$ and $\Delta J^2 \geqslant \epsilon_1$ and $\Delta\vec{x}^T\Delta\vec{x} \geqslant \epsilon_2$ **do**
3: Call Sequential Quadratic Programming to minimize $J(\vec{x}^q, r_g^q)$
Output: $\vec{x}^{q*}$
4: Compute the stopping criteria
$\Delta J = J(\vec{x}^q, r_g^q) - J(\vec{x}^{q-1}, r_g^{q-1})$
$\Delta\vec{x} = \vec{x}^{q*} - \vec{x}^{(q-1)*}$
5: Update the states and parameters
$q = q + 1$
$r_g^q = c_g r_g^{q-1}$
$\vec{x}^q = \vec{x}^{(q-1)*}$
6: **end while**

Chapter 5

Wave Estimation for WEC control

The wave estimation and forecasting are required by the optimal controller. Hence it is necessary to provide the development of the estimator. There are several estimation techniques can be applied for wave estimation. Section 5.1 presents the Kalman Filter. The developed sequential estimator does not require a large data collection. The extended Kalman Filter (EKF) is introduced in Section 5.2 for a system has nonlinear dynamics. The EKF linearize the nonlinear system dynamics with the first order approximation. The last Section 5.3 presents the derivation and development of the consensus estimator for the estimation of the WEC array. The communication technology is applied to improve the wave estimation and forecasting.

5.1 Kalman Filter

The sequential estimator Kalman Filter is implemented for the wave estimation. In the wave energy conversion problem, the measurements (ex, position, velocity) collected is discrete, however, the system behaves continuously. Hence the continuous-discrete Kalman Filter is developed for different models. In this section, the details of the implementation of the Kalman Filter for the Simple Model Control is introduced.

5.1.1 Kalman Filter with the measurements of the total wave pressure

In this section, the Kalman Filter is designed for a heaving point absorber with the measurements of the total wave pressure acting on the floater. It is assumed that we measure the buoy position x_1, its velocity x_2, and also the total pressure using multiple pressure sensors on the buoy surface, as detailed in reference [4]. The surface pressure can then be used to compute the total force F_{Ts}. Let $\tilde{x}_i$ be the measurement of x_i and $\tilde{F}_{Ts}$ be the measurement of F_{Ts}. The measurement $\tilde{F}_{Ts}$ is then added to the quantity $m_\infty \dot{\tilde{x}}_2$ to obtain $\tilde{F}_T$ as a pseudo-measurement. These measurements will also be used to estimate the quantities $\dot{F}_T$, $\partial F_T/\partial x_1$ and $\partial F_T/\partial x_2$ which are required by the SMC controller.

Since we need to estimate the derivatives of the force F_T with respect to time and the states, it is convenient to approximate the force F_T using a series expansion. This way, it is possible to compute approximate expressions for the derivatives once the coefficients of the polynomial are determined. Moreover, it is possible to compute approximate expressions for the control force and the harvested energy analytically. Toward that end, it is assumed that the following series expansion approximates the force F_T:

$$\bar{F}_T = a_1 x_1 + a_2 x_2 + b_1 x_1^3 + b_2 sign(x_2) x_2^2 + \sum_{n=1}^{N} (c_n \cos(\omega_n t) + d_n \sin(\omega_n t)) \qquad (5.1)$$

The above series expansion is selected intuitively and in a general form. Higher order terms can be added to the polynomial terms if needed. While this series expansion is suitable for 1-DoF point absorbers, it is straightforward to write similar expansions for other types of WECs or extend it to account for multi-DoF WECs.

The coefficients in the Eq. (5.1) are estimated using a Kalman filter such that the square error between $\bar{F}_T$ and F_T is minimized. The frequencies $\omega_n, \forall n$, are assumed fixed and equally spaced in a particular range. This assumption enables the use of a linear Kalman filter. If desired, these frequencies could be appended to the Kalman filter state vector to be estimated; in such case, an extended Kalman filter would be needed for the resulting nonlinear system. If we use a sufficiently large number of frequencies, the assumption of fixed frequencies provides reasonable accuracy.

The Kalman filter uses the measurements to update the estimates of the coefficients in $\bar{F}_T$ sequentially in time. The state vector of the Kalman filter is selected as:

$$\hat{\vec{x}} = [\hat{a}_1,\, \hat{a}_2,\, \hat{b}_1, \hat{b}_2,\, \hat{c}_1, \cdots,\, \hat{c}_N,\, \hat{d}_1, \cdots,\, \hat{d}_N]^T \tag{5.2}$$

The dynamic equation of the Kalman filter is:

$$\dot{\hat{\vec{x}}} = \vec{0} \tag{5.3}$$

where $\vec{0}$ is a vector which components are all zeros. The coefficiensts $\hat{\vec{x}}$ are assumed to be constant in the dynamic model; yet they can be updated based on measurements in the Kalman update step. Each measurement is simulated as a zero mean white noise added to its true signal. The Kalman filter output equation is:

$$\hat{y} = \hat{F}_T = \hat{a}_1\tilde{x}_1 + \hat{a}_2\tilde{x}_2 + \hat{b}_1\tilde{x}_1^3 + \hat{b}_2 sign(\hat{x}_2)\tilde{x}_2^2 + \sum_{n=1}^{N}(\hat{c}_n \cos(\omega_n t) + \hat{d}_n \sin(\omega_n t)) \tag{5.4}$$

The process of implementing the Kalman filter in this dissertation is standard and is not presented; reference [155] presents the details on the process of linear Kalman filters. At each time step, the partial derivatives of F_T can be evaluated by taking

the derivatives of Eq. (5.1), and using the estimated states as follows:

$$\begin{aligned}
\frac{\partial F_T}{\partial t} &= \sum(-\hat{c}_n\omega_n \sin(\omega_n t) + \hat{d}_n\omega_n \cos(\omega_n t)) \\
\frac{\partial F_T}{\partial \tilde{x}_1} &= \hat{a}_1 + 3\hat{b}_1\tilde{x}_1^2 \\
\frac{\partial F_T}{\partial \tilde{x}_2} &= \hat{a}_2 + 2\hat{b}_2 sign(\tilde{x}_2)\tilde{x}_2\,, \; \frac{d}{dt}\frac{\partial F_T}{\partial \tilde{x}_2} = 2\hat{b}_2 sign(\tilde{x}_2)\dot{\tilde{x}}_2
\end{aligned} \tag{5.5}$$

These partial derivatives are substituted in Eq. (3.30) to compute the control force. As a result, the proposed control force only requires the current states which can be obtained from the state estimation by using Kalman Filter. The wave prediction is not required for the SMC controller.

5.1.1.1 Initialization of The Kalman Filter States

The initial conditions of the state vector $\hat{\vec{x}}_0$ dictate the effectiveness of the Kalman filter in estimating the coefficients. In this problem, in particular, there are multiple local solutions that the Kalman filter can converge to that are not the true values of the coefficients. Hence, it is critical to have a good initial guess for the coefficients. In this study, the initial guess values are obtained via an optimization process that is here described. First, measurements are collected over some period, called the initialization period T_0. In the simulations conducted in Section 5.1.1.2, $T_0 = 100$ seconds and measurements are collected every $\Delta t = 0.05$ seconds. The optimization

problem is to find the vector $\hat{\vec{x}}_0$ that minimizes the function:

$$J = \sum_{i=1}^{N_D} \|\bar{F}_T\left(\hat{\vec{x}}_0, \tilde{x}_1(i\Delta t), \tilde{x}_2(i\Delta t), i\Delta t\right) - \tilde{F}_T(i\Delta t)\|^2 \tag{5.6}$$

where N_D is the number of data points. A sequential quadratic programming algorithm was used to solve this optimization problem. It is noted here that this process works even when sea state changes over time. This is because data are collected continuously and used to update the estimate of the coefficients $\hat{\vec{x}}$ via the Kalman update step. In the simulations conducted, data collected over 100 s are used for this update step. Hence the introduced initialization of the Kalman Filter is adaptive to the changing environment using the collected data.

5.1.1.2 Simulation results

The simulation results are presented in this section. The performance of the SMC controller with Kalman Filter is shown. The numerical testing was conducted using the buoy shown in Figure 5.1. The dynamic model applied in the WEC plant in the simulation is the Cummins' equation (Eq. (2.3)), although the controller is derived based on the simple model by defining a total force. A Bretschneider wave is realized using 200 frequencies equally spaced in the range $0 - 4$ rad/s. The significant wave height is 0.3 m, and the peak period is 7 s. The hydrodynamic and hydrostatic forces

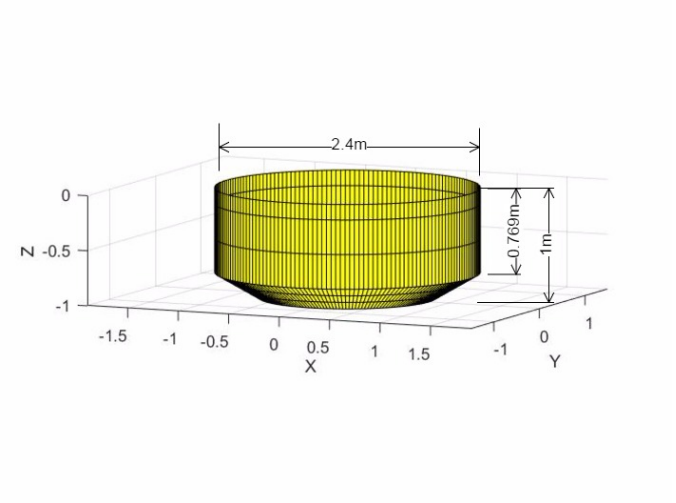

Figure 5.1: Geometry of the buoy used in the numerical simulations in this paper.

on the buoy are simulated using force coefficients that are computed using Nemoh [132]. These forces, in addition to the viscous damping force, are considered as data that simulates the force measurements $\tilde{F}_{Ts}$. These forces are also used to propagate the buoy motion and generate simulated measurements for the buoy position and velocity. The derivative of the measured velocity is computed at each time step and is used to compute the force $\tilde{F}_T$. The numerical parameters used to generate the data are as follows: the mass of the buoy is 4.637×10^3 kg, the stiffness of hydrostatic force is 4.437×10^4 N/m, and the viscous damping coefficient is 6.1525 Nm/s. The effectiveness of the proposed control system is assessed by comparing the harvested energy obtained using the proposed SMC to the optimal harvested energy as computed by the singular arc control (SA) [2]. The SA is computed assuming perfect measurements (noise free measurements) so that we can use the harvested energy from SA as a reference. Figure 5.2 shows the harvested energy over 10 minutes. In the

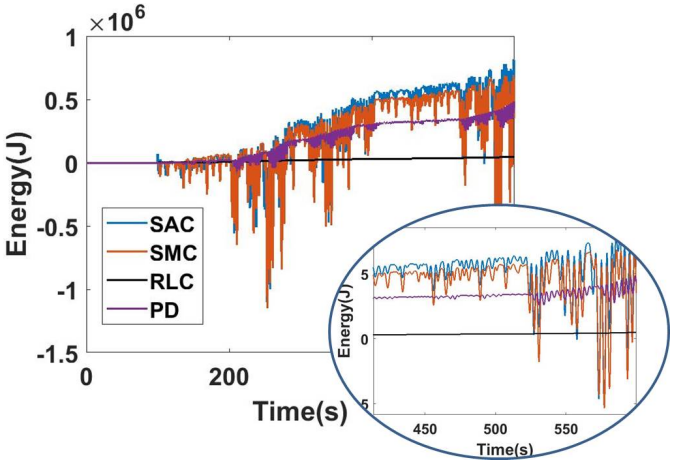

Figure 5.2: Comparison between the SMC, the SA, the RL and the PD in terms of harvested energy. The SMC performance is close to the ideal SA.

first 100 seconds, no control was applied; rather only measurements were collected and used to initialize the Kalman filter. Three different controls are presented in Figure 5.2. The SA is the maximum energy curve computed using the singular arc control. The SMC line is the energy harvested using SMC. The RL line is the energy harvested using the resistive loading control: $u = -B_m x_2$. Finally, the PD line is the energy extracted using the Proportional Derivative control $u = -K_p x_1 - K_d x_2$. The feedback gain of the RL and PD controllers are optimized in terms of energy extraction. As can be seen in Figure 5.2, the harvested energy using the SMC is very close to the optimal one, and it is significantly larger than the RL harvested energy. The control force produced using the SMC is shown in Figure 5.3, and the displacement of the buoy over time is shown in the same figure. To emphasize the accuracy of the assumed force series expansion in Eq. (5.1) when the actual forces on the buoy are linear, Figure 5.4 shows both the true and the approximate forces on the buoy surface.

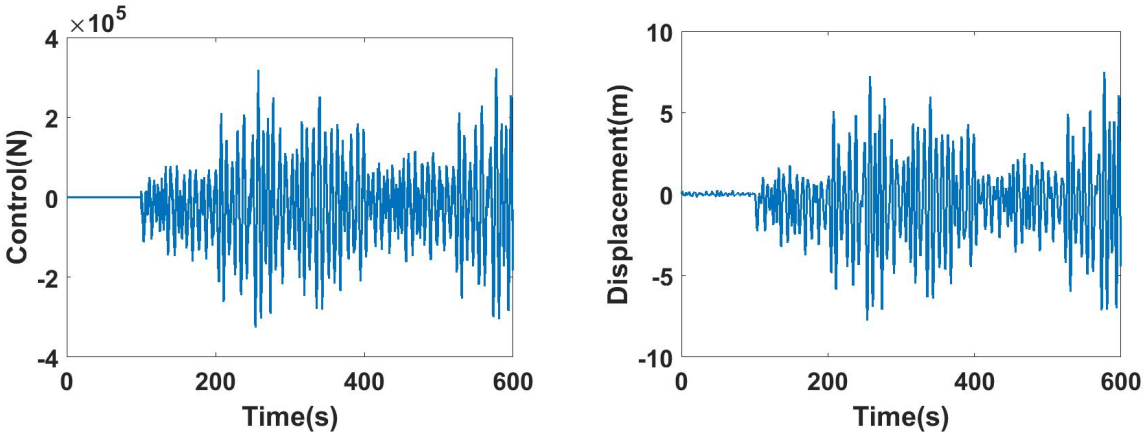

Figure 5.3: The Control force using SMC and the displacement of the buoy. No constraints on the control and the displacement are assumed.

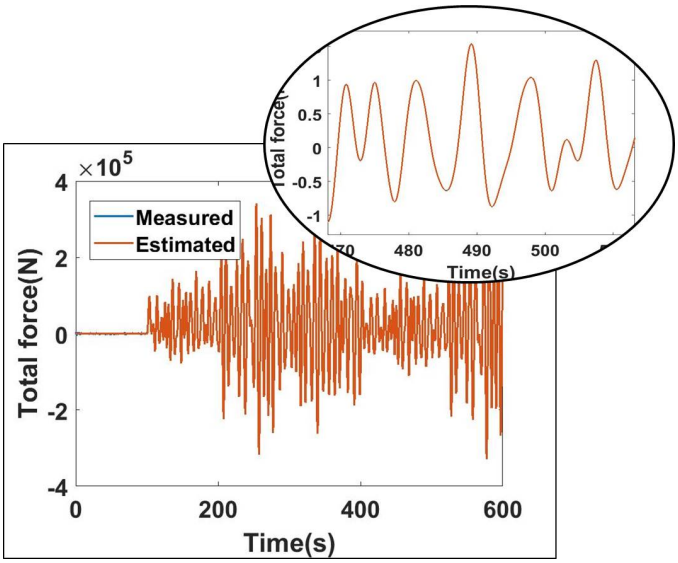

Figure 5.4: The series expansion for the force F on the buoy is a good approximation for the true force for the linear force test case

5.2 Extended Kalman Filter

The Extended Kalman Filter is introduced in this section. The EKF is usually applied for a nonlinear system and applies the first order approximation. The details of implementing the EKF for the SA controller and the LQG controller will be introduced in the following sections.

5.2.1 Extended Kalman Filter for Singular Arc Controller

The EKF will be first combined with the SA controller for wave and state estimation of a heaving point absorber. The nonlinearity happened in computing the excitation force when the surface integration is applied. In this case, the pressure will be measured by the pressure sensors.

5.2.1.1 Dynamic model of the Extended Kalman Filter

Define the state vector $\vec{x}$ of the estimation as:

$$\vec{x} = [x_1,\, x_2,\, \vec{x}_r,\, \vec{\eta},\, \vec{\omega},\, \vec{\phi}]^T \tag{5.7}$$

where η_i is the wave amplitude at frequency ω_i, and ϕ_i is the phase associated with ω_i. Further, η_i, ω_i, ϕ_i are the elements of the $\vec{\eta}$, $\vec{\omega}$ and $\vec{\phi}$. The EKF estimates the most N dominating frequencies in the wave, where N is a design variable. The heave dynamic equations in terms of the state vector $\vec{x}$ can be written as:

$$\dot{x}_1 = x_2 \tag{5.8}$$

$$(m_r + m_\infty)\dot{x}_2 = F_T + u \tag{5.9}$$

$$\dot{\vec{\eta}} = \vec{0} \tag{5.10}$$

$$\dot{\vec{\omega}} = \vec{0} \tag{5.11}$$

$$\dot{\vec{\phi}} = \vec{0} \tag{5.12}$$

where Eq. (5.9) is similar to Eq. (2.3), except Eq. (5.9) considers the viscous damping force. The F_T is the total wave force including the excitation force, radiation force, hydrostatic force and the viscous damping force. The excitation force is computed based on Eq. (2.7). The radiation force can be evaluated by the state space model (Eq. (2.13)). The hydrostatic force is computed based on Eq. (2.11). The viscous damping can be expressed by a linear damping force:

$$F_v = -B_v x_2 \tag{5.13}$$

5.2.1.2 WEC measurements model

The radiation force on the buoy is mainly a function of the buoy motion and hence it can be computed in real time. The hydrostatic force is also a function of the buoy position and hence it can be computed as a function of the buoy state. The excitation force, on the other hand, is a function of the buoy motion as well as the wave potential field. That means we need to know the wave and its potential field in order to compute the excitation force so that we can compute the control force $u(t)$. Hence, measurements are collected to estimate the excitation force. Typically, buoy position is measured. The buoy position, however, is a result of the interaction of the wave with the buoy body and hence it is not a direct measurement of the excitation force. Sensing the pressure at a few points on the buoy surface provides measurements that are more direct to the excitation force.

In this analysis, it is assumed that the measurements are: the position of the buoy, the pressure values at N points distributed on the buoy surface. The pressure is measured using pressure sensors which locations are known. Hence the output model for this system is constructed as follows:

$$\vec{y} \equiv [x_1, p_1, p_2, \cdots, p_N]^T = [h_{m,1}(\vec{x}), h_{m,2}(\vec{x}), \cdots, h_{m,N+1}(\vec{x})]^T \tag{5.14}$$

where the pressure at a cell of vertical distance $c_{d,j}$ from the center of gravity is:

$$p_j = \sum_{n=1}^{\aleph} \rho g \eta_n \frac{\cosh(\chi_n(x_1 + c_{d,j} + h))}{\cosh(\chi_n h)} cos(-\omega_n t + \phi_n) - \rho g(x_1 + c_{d,j}) - \frac{B_v x_2}{A_s} - \frac{\mathbf{C}_r \vec{x}_r}{A_s} \tag{5.15}$$

where A_s is the total surface area of the buoy. The first term in Eq (5.15) is the excitation pressure; the last term is the radiation pressure; the second term is the hydrostatic pressure, and the third term is the viscous damping pressure. The measurements are related to the output model through Eq. (5.16).

$$\tilde{y} = \vec{y} + \vec{v}(t) \tag{5.16}$$

where $\vec{v}(t)$ is the vector of sensors noises.

5.2.1.3 The Jacobian Matrices

To implement the EKF, we need to compute the partial derivatives of the functions in the dynamic model (from Eq. (5.8) to Eq. (5.12)) with respect to the state vector defined in Eq. (5.7). These derivatives are collected in the Jacobian matrix $\mathscr{F}$. Note that the pressure on a vertical surface does not contribute to the heave motion. In this analysis where we focus on the heave motion, the cells on non-vertical surfaces will be referred to as heave-effective cells. Assuming that the pressure sensors that are

on heave-effective cells are always submerged in the water then $\mathscr{F}$ can be computed as shown in Eq. (5.17), where:

$$\mathscr{F} = \begin{bmatrix} 0 & 1 & \mathbf{0} & \mathbf{0} & \mathbf{0} & \mathbf{0} \\ \frac{\partial F_T}{\partial x_1} & \frac{\partial F_T}{\partial x_2} & \frac{\partial F_T}{\partial \vec{x}_r} & \frac{\partial F_T}{\partial \vec{\eta}} & \frac{\partial F_T}{\partial \vec{\omega}} & \frac{\partial F_T}{\partial \vec{\phi}} \\ \mathbf{0} & \frac{\partial F_r}{\partial x_2} & \frac{\partial F_r}{\partial \vec{x}_r} & \mathbf{0} & \mathbf{0} & \mathbf{0} \\ \mathbf{0} & \mathbf{0} & \mathbf{0} & \mathbf{0} & \mathbf{0} & \mathbf{0} \\ \mathbf{0} & \mathbf{0} & \mathbf{0} & \mathbf{0} & \mathbf{0} & \mathbf{0} \\ \mathbf{0} & \mathbf{0} & \mathbf{0} & \mathbf{0} & \mathbf{0} & \mathbf{0} \end{bmatrix} \tag{5.17}$$

where

$$\frac{\partial F_T}{\partial x_1} = \frac{1}{m} \sum_j \sum_k A_{s,jk} \vec{n}_{jk} \hat{k} \left\{ \sum_n \left[\rho g \eta_n \frac{\sinh(\chi_n(x_1 + z_{j,k} + h))\chi_n}{\cosh(\chi_n h)} \cos(\chi_n x_{j,k} - \omega_n t + \phi_n) \right] - \rho g \right\} \tag{5.18}$$

$$\frac{\partial F_T}{\partial x_2} = -\frac{1}{m} Bvisc \tag{5.19}$$

$$\frac{\partial F_T}{\partial \vec{x}_r} = -\frac{1}{m} \mathbf{C}_r{}^T \tag{5.20}$$

$$\frac{\partial F_T}{\partial \eta_n} = \frac{1}{m} \sum_j \sum_k A_{s,jk} \vec{n}_{jk} \hat{k} \rho g \frac{\cosh(\chi_n(x_1 + z_{j,k} + h))}{\cosh(\chi_n h)} \cos(\chi_n x_{j,k} - \omega_n t + \phi_n) \tag{5.21}$$

$$\frac{\partial F_T}{\partial \omega_n} = \frac{1}{m} \sum_j \sum_k t A_{s,jk} \vec{n}_{jk} \hat{k} \rho g \eta_n \frac{\cosh(\chi_n(x_1 + z_{j,k} + h))}{\cosh(\chi_n h)} \sin(\chi_n x_{j,k} - \omega_n t + \phi_n) \tag{5.22}$$

$$\frac{\partial F_T}{\partial \phi_n} = -\frac{1}{m}\sum_j \sum_k A_{s,jk}\vec{n}_{jk}\hat{k}\rho g \eta_n \frac{\cosh(\chi_n(x_1 + z_{j,k} + h))}{\cosh(\chi_n h)} \sin(\chi_n x_{j,k} - \omega_n t + \phi_n) \tag{5.23}$$

$$\forall n = 1 \cdots N$$

The Jacobian matrix, $\mathbf{H}_m$, of the output equations is evaluated as follows.

$$\mathbf{H}_m(j,i) = \frac{\partial h_{m,j}}{\partial \vec{x}(i)} \tag{5.24}$$

where for $j = 1$:

$$\frac{\partial h_{m,1}}{\partial \vec{x}(1)} = 1, \quad \frac{\partial h_{m,1}}{\partial \vec{x}(l)} = 0, \forall l = 2, ..., N+1 \tag{5.25}$$

where for $j = 2, 3, \cdots, N+1$, we can write the following gradient functions for each frequency $n \in \{1, \cdots, N\}$:

$$\frac{\partial h_{m,j}}{\partial \eta_n} = \rho g \frac{\cosh(\chi_n(x_1 + z_{j,k} + h))}{\cosh(\chi_n h)} \cos(-\omega_n t + \phi_n) \tag{5.26}$$

$$\frac{\partial h_{m,j}}{\partial \omega_n} = \rho g \eta_n \frac{\cosh(\chi_n(x_1 + z_{j,k} + h))}{\cosh(\chi_n h)} t \sin(-\omega_n t + \phi_n) \tag{5.27}$$

$$\frac{\partial h_{m,j}}{\partial \phi_n} = -\rho g \eta_n \frac{\cosh(\chi_n(x_1 + z_{j,k} + h))}{\cosh(\chi_n h)} \sin(-\omega_n t + \phi_n) \tag{5.28}$$

For $j = 2, 3, \cdots, N+1$, we can write the following gradient functions with respect to the heave position:

$$\frac{\partial h_{m,j}}{\partial x_1} = \sum_n \rho g \eta_n \frac{\sinh(\chi_n(x_1 + z_{j,k} + h))\chi_n}{\cosh(\chi_n h)} \cos(-\omega_n t + \phi_n) - \rho g \tag{5.29}$$

$$\frac{\partial h_{m,j}}{\partial x_2} = -\frac{Bvisc}{A_s} \tag{5.30}$$

$$\frac{\partial h_{m,j}}{\partial \vec{x}_r} = -\frac{\mathbf{C}_r}{A_s} \tag{5.31}$$

5.2.1.4 The EKF Process

The WEC system under consideration is a continuous system while the measurements are collected at discrete points. Hence a continuous-discrete Extended Kalman Filter will be implemented [155]. Associated with the estimated state vector $\hat{\vec{x}}(t)$ is the matrix $\mathbf{P}(t)$ which is the covariance of the state error vector. The covariance matrix propagates in time according to the Riccati equation:

$$\dot{\mathbf{P}}(t) = \mathscr{F}(\hat{\vec{x}}(t), t)\mathbf{P}(t) + \mathbf{P}(t)\mathscr{F}^T(\hat{\vec{x}}(t), t) + \mathbf{G}(t)\mathbf{Q}_p(t)\mathbf{G}^T(t) \tag{5.32}$$

At each measurement time a Kalman gain is computed using Eq. (5.33).

$$\mathbf{K}_{g,k} = \mathbf{P}_k^- \mathbf{H}_{m,k}^T(\hat{\vec{x}}_k^-) \left[\mathbf{H}_{m,k}(\hat{\vec{x}}_k^-)\mathbf{P}_k^- \mathbf{H}_{m,k}^T(\hat{x}_k^-) + \mathbf{R}_k\right]^{-1} \tag{5.33}$$

The process of the continuous-discrete EKF implemented on the WEC system is here briefed:

1. Propagate the current state using Eqs. (5.8) to (5.12) to the next measurement time k; the resulting state is $\vec{x}_k^{\,-}$

2. Propagate the covariance matrix to the next measurement time k using the Riccati equation (5.32). The resulting covariance is $\mathbf{P}_k^-$

3. Compute the Kalman Gain using Eq. (5.33).

4. Update the state $\hat{\vec{x}}_k^{\,-}$ using: $\hat{\vec{x}}_k^{\,+} = \hat{\vec{x}}_k^{\,-} + \mathbf{K}_{g,k}[\vec{y}_{m,k} - \vec{y}(\hat{\vec{x}}_k^{\,-})]$

5. Update the covariance $\mathbf{P}_k^-$ using: $\mathbf{P}_k^+ = [\mathbf{I} - \mathbf{K}_{g,k}\mathbf{H}_{m,k}(\hat{\vec{x}}_k^{\,-})]\mathbf{P}_k^-$

6. The current state is $\hat{\vec{x}}_k^{\,+}$ and the current covariance is $\mathbf{P}_k^+$. Go to step 1).

The EKF needs to be initialized with initial guesses for the state vector and the covariance, $\hat{\vec{x}}(0)$ and $\mathbf{P}_0$, respectively. This EKF generates an estimate for the state vector $\hat{\vec{x}}$ at each time step k. Using the estimated state vector, $\hat{\vec{x}}$, an estimate for the excitation force $\hat{F}_e$ can be computed using Eq. (2.7), where the states x_1, ω_n, ϕ_n, and η_n are replaced by their estimates.

5.2.1.5 Pseudo Measurement

The velocity is not being measured in the problem. Preliminary simulation results show that the estimated excitation force converges to the true excitation force with reasonable accuracy after a transient period. In this transient period, the estimates of the amplitudes, frequencies, and phases deviate away before they converge to their true signals. Aiming at eliminating this deviation in the initial phase and improving the estimation accuracy, a pseudo-velocity measurement is added. The pseudo velocity measurement is generated by taking the derivative of the position, capitalizing on the available very accurate position sensors. This pseudo measurement is appended to the measurements vector and is handled as other measurements. The new output model is:

$$\vec{y} \equiv [x_1, x_2, p_1, p_2, \cdots, p_N]^T = [h_{m,1}(\vec{x}), h_{m,2}(\vec{x}), \cdots, h_{m,N+2}(\vec{x})]^T \tag{5.34}$$

5.2.1.6 Simulation results

The simulation results are presented in this section. Figure. 5.5 presents the floater (Sandia experimental buoy) applied in the simulation and the location of the pressure sensors. The device has a mass of 858.4kg, a volume of 0.8578m^3, and a diagonal inertia matrix of [83.9320, 83.9320, 137.5252]kg.m^2. The wave applied has a Bretschneider wave spectrum with totally 32 frequencies. It is assumed that there are 8 pressure sensors on one quadrant of the buoy surface at different heights.

Figure. 5.6 shows the energy absorbed using a complex conjugate control assuming perfect knowledge of the excitation force (ideal CCC in Figure. 5.6), the energy absorbed using a SA control assuming perfect knowledge of the excitation force (ideal SA in Figure. 5.6), and the energy absorbed using SA control assuming noisy measurements and using the EKF to estimate the excitation force (Real SA in Figure. 5.6). The energy harvested using the baseline resistive loading control based on the estimated buoy states (Real RL) is also shown in Figure. 5.6. The energy of the ideal CCC matches that of the ideal SA, which highlights the effectiveness of the SA control. As expected, the real SA produces lower energy harvesting due to the presence of measurements noises and model uncertainties, which result in errors in estimating the excitation force. Yet, the energy harvested using the real SA is high compared to the energy harvested using the real RL control.

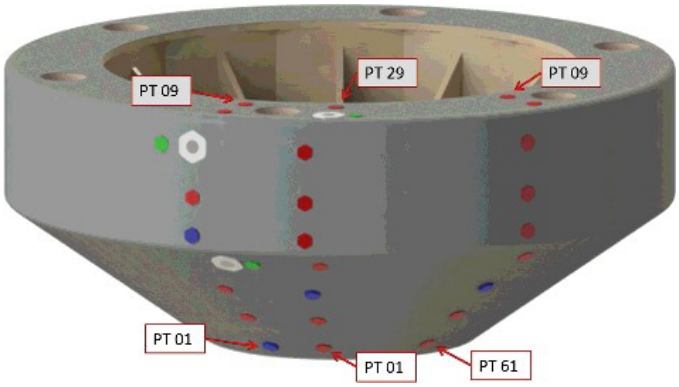

Figure 5.5: Schematic of the Sandia experimental WEC with locations of pressure transducers

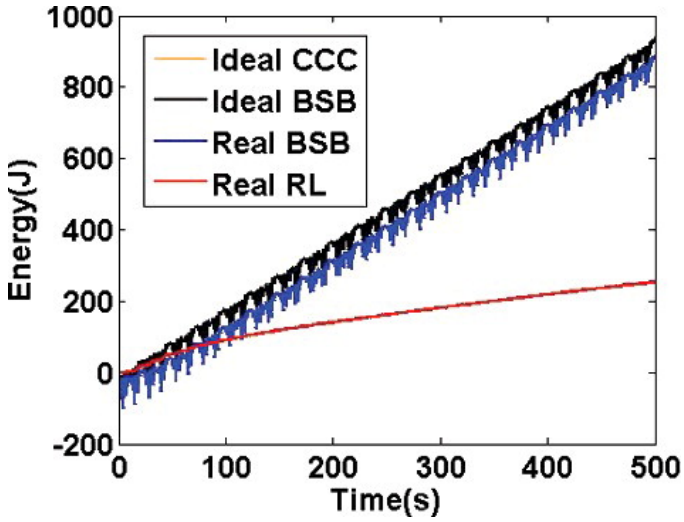

Figure 5.6: The extracted energy using SA control and EKF

The corresponding system response (ex, position, velocity), the control force and the excitation force are shown in Figure. 5.7. From the figures, we can tell that the estimated position matches the true one. The error in velocity estimation is also very small. The estimation of the excitation force is accurate. Figure. 5.8 shows the convergence of the estimated states, the wave frequency, and the wave amplitude respectively.

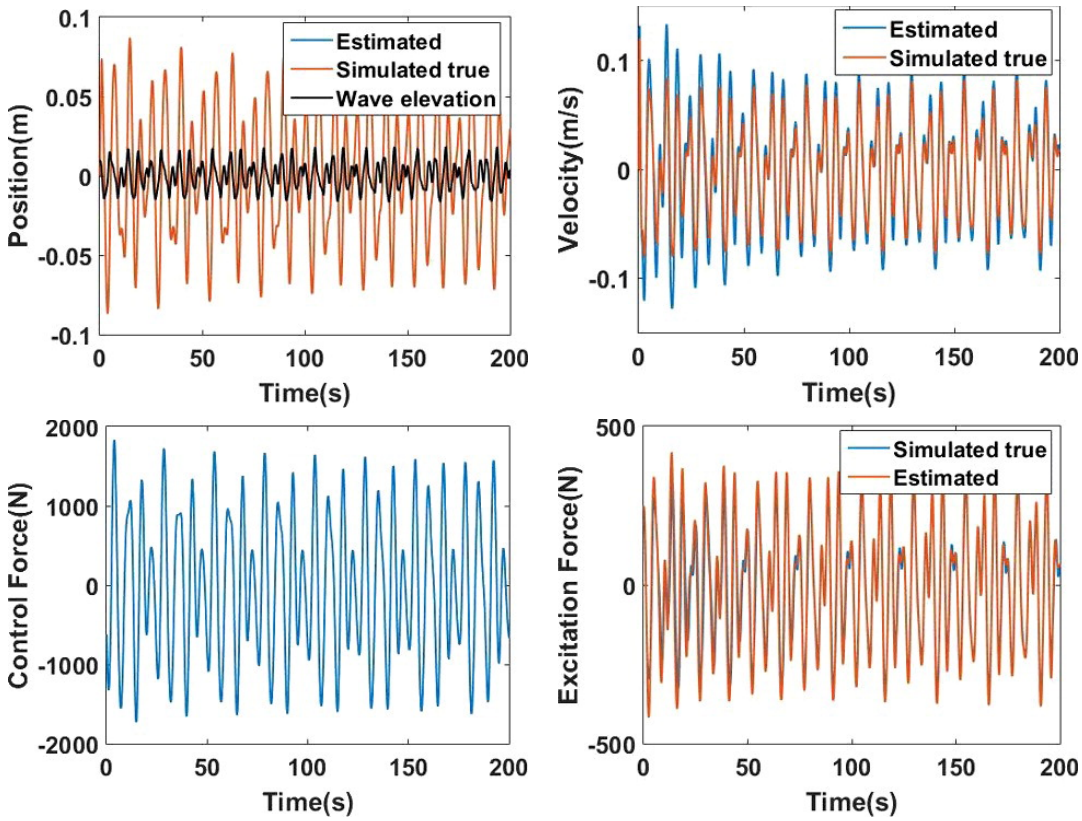

Figure 5.7: The estimation of the system responses, the control effort and the estimation of the excitation force

5.2.2 Extended Kalman Filter for Linear Quadratic Gaussian Controller

In this section, the wave estimation for the LQG controller by applying EKF is introduced. The EKF is designed for a single body 3-DoF WEC. The wave excitation force can be approximated by Fourier Series:

$$\hat{F}_e = \sum_{n=1}^{N_f} (a_n \cos(\omega_n t) + b_n \sin(\omega_n t)) \tag{5.35}$$

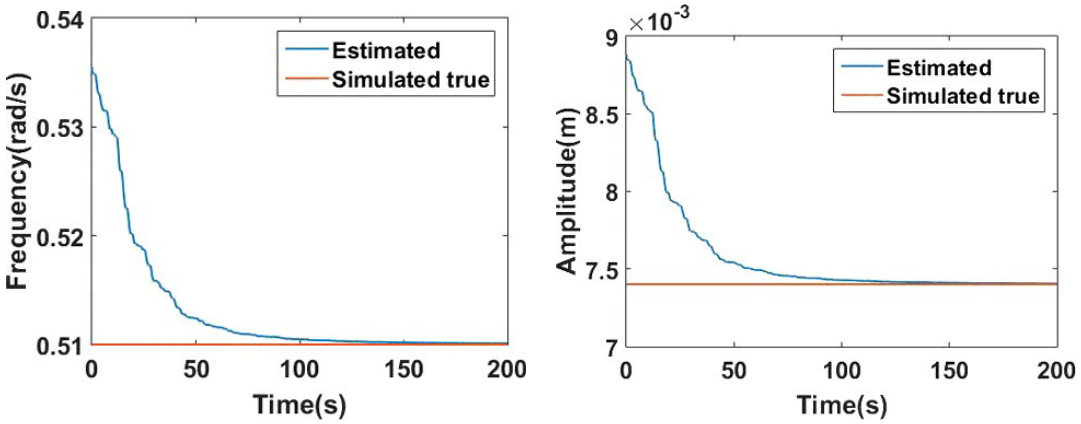

Figure 5.8: The convergence of the estimated states.

where N_f represents the number of Fourier terms used to approximate the excitation force. Since in this problem the surge-pitch motion is excited by heave motion, two Kalman filters are built to estimate the states: one for the coupled motion (surge and pitch), and one for the heave motion. Although we can combine those two Kalman filters into one, separating them reduces the computational cost. They are still coupled because the heave motion excites the surge and pitch motion. The current estimate of heave displacement is fed into a Kalman filter to estimate the states of surge and pitch motions.

In Fig. 5.9, the Kalman Filter 1 estimates the states of heave motion. The state vectors for Kalman Filter 1 and Kalman Filter 2 are:

$$\hat{\vec{x}}^h = [z,\ \dot{z},\ \vec{x}_r^3,\ \vec{a}^3,\ \vec{b}^3,\ \vec{\omega}^3]^T \tag{5.36}$$

$$\hat{\vec{x}}^c = [x,\ \theta,\ \dot{x},\ \dot{\theta},\ \vec{x}_r^c,\ \vec{a}^1,\ \vec{b}^1,\ \vec{a}^5,\ \vec{b}^5,\ \vec{\omega}^1,\ \vec{\omega}^5]^T \tag{5.37}$$

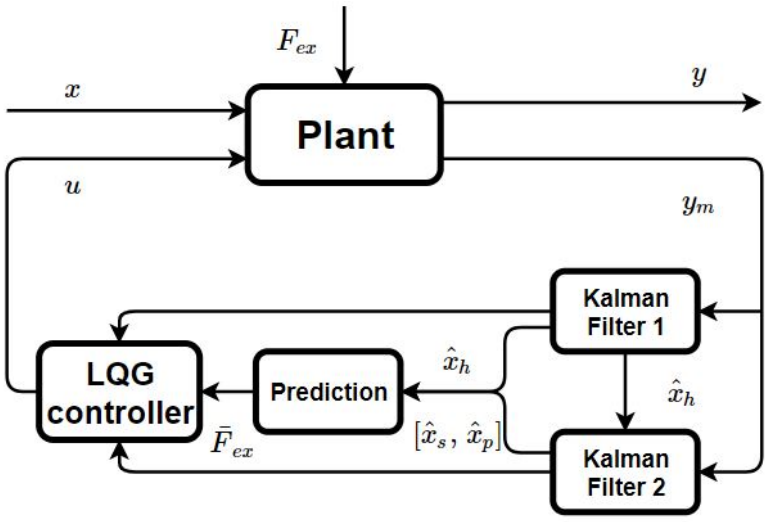

Figure 5.9: The flow chart of LQG optimal controller

where $\vec{a}^j$, $\vec{b}^j$, and $\vec{\omega}^j$ represent the coefficients and frequencies of cosine and sine functions, respectively, in the excitation force Fourier expansion. The superscript of those parameters j can be 1, 3 and 5 which denotes the surge, heave and pitch motions respectively. The subscript h denotes the states of the heave motion, and the subscript c denotes the states of the coupled motion.

The equations of motion of the dynamic system described in Eq. (2.33) and Eq. (2.31) can be written as a state space model. The detailed state space representation of Eq. (2.33) is presented in Section 4.3. Hence, in this section, we will mainly introduce the state space expression of Eq. (2.31). Let the first part of the states of Kalman Filter 1 be $\vec{x}_h = [d_3, \dot{d}_3, \vec{x}_r^3]^T$. Hence the equation of motion of the heave motion can

be written as:

$$\dot{\vec{x}}^h(t) = \mathbf{F}^h(t)\vec{x}^h(t) + \mathbf{G}^h(t)u_3(t) + \mathbf{c}^h(t) \tag{5.38}$$

where

$$\mathbf{F}^h(t) = \begin{bmatrix} 0 & 1 & \mathbf{0} \\ -\frac{1}{m^3}K_{33} & -\frac{1}{m^3}B_{v,3} & -\frac{1}{m^3}\mathbf{C}_r^3 \\ \mathbf{0} & \mathbf{B}_r^3 & \mathbf{A}_r^3 \end{bmatrix} \tag{5.39}$$

$$\mathbf{G}^h = \begin{bmatrix} 0 \\ \frac{1}{m^3} \\ \mathbf{0} \end{bmatrix} \tag{5.40}$$

$$\mathbf{c}^h(t) = \begin{bmatrix} 0 \\ \frac{1}{m^3} \\ \mathbf{0} \end{bmatrix} \hat{F}_e^3 \tag{5.41}$$

The $\hat{F}_e$ represents the estimation of excitation force. In this dissertation, a short-term prediction for excitation force will be needed to compute the control. The sea states are assumed to be steady within this short prediction period. Hence, the dynamics

of the states for estimating the excitation force are:

$$\dot{\vec{a}} = \vec{0} \tag{5.42}$$

$$\dot{\vec{b}} = \vec{0} \tag{5.43}$$

$$\dot{\vec{\omega}} = \vec{0} \tag{5.44}$$

where $\vec{a} = [\vec{a}^1, \vec{a}^3, \vec{a}^5]^T$, $\vec{b} = [\vec{b}^1, \vec{b}^3, \vec{b}^5]^T$, $\vec{\omega} = [\vec{\omega}^1, \vec{\omega}^3, \vec{\omega}^5]^T$.

5.2.2.1 The Jacobian Matrices

To implement the Extended Kalman Filter, we need to construct the Jacobian matrices from the nonlinear system. The partial derivatives are computed for Eq. (5.38), Eq. (4.48) and Eqs. (5.42) to (5.44). To write the partial derivatives in matrix format, the following matrices are defined:

$$\boldsymbol{\phi}^c = \begin{bmatrix} \boldsymbol{\phi}_c^1 & \boldsymbol{\phi}_s^1 & \mathbf{0} & \mathbf{0} \\ \mathbf{0} & \mathbf{0} & \boldsymbol{\phi}_c^5 & \boldsymbol{\phi}_s^5 \end{bmatrix} \tag{5.45}$$

$$\boldsymbol{\phi}^h = \begin{bmatrix} \boldsymbol{\phi}_c^3 & \boldsymbol{\phi}_s^3 \end{bmatrix} \tag{5.46}$$

$$\mathbf{D}_\phi^c = \begin{bmatrix} \mathbf{D}^1 & \mathbf{0} \\ \mathbf{0} & \mathbf{D}^5 \end{bmatrix} \tag{5.47}$$

$$\mathbf{D}_\phi^h = \mathbf{D}^3 \tag{5.48}$$

where

$$\boldsymbol{\phi}_c^j = \left[\cos(\omega_1^j t) \ldots \cos(\omega_n^j t)\right]$$
$$\boldsymbol{\phi}_s^j = \left[\sin(\omega_1^j t) \ldots \sin(\omega_n^j t)\right] \quad j = 1,\ 3,\ 5 \tag{5.49}$$

where D^1, D^3 and D^5 are row vectors of size n. The k^{th} component of the D^j vector can be expressed as:

$$D_k^j = -a_k^j \sin(\omega_k^j t)t + b_k^j \cos(\omega_k^j t)t \tag{5.50}$$

where $j = 1,\ 3,\ 5$ and $k = 1, \ldots, n$. The Jacobian matrix can then be written in the form:

$$\mathscr{F}^c(t) = \begin{bmatrix} & \begin{bmatrix} \mathbf{0} & \mathbf{0} & \mathbf{0} & \mathbf{0} & \mathbf{0} & \mathbf{0} \\ & \mathbf{m}^{-1}\boldsymbol{\phi}^c & & & \mathbf{m}^{-1}\mathbf{D}_{\phi}^c & \\ \mathbf{0} & \mathbf{0} & \mathbf{0} & \mathbf{0} & \mathbf{0} & \mathbf{0} \end{bmatrix} \\ \mathbf{F}^c(t) & \\ \mathbf{0} & \mathbf{0} \\ \vdots & \\ \mathbf{0} & \mathbf{0} \end{bmatrix} \tag{5.51}$$

In this study, it is assumed that the displacement and velocity will be measured for each of the surge, pitch and heave motions. For the coupled motion we can write the

measurements vector as:

$$\mathbf{y}_m^c = \left[x,\, \theta,\, \dot{x},\, \dot{\theta}\right]^T + \mathbf{v}^c(t) \tag{5.52}$$

where $\mathbf{v}^c(t) \sim N(\mathbf{0}, \mathbf{Q}_p^c(t))$ which is assumed to be white noise with normal distribution. So the Jacobian matrix of the output model of the surge-pitch motion is:

$$\mathbf{H}_m^c(t) = \begin{bmatrix} 1 & 0 & 0 & 0 & \mathbf{0} \\ 0 & 1 & 0 & 0 & \mathbf{0} \\ 0 & 0 & 1 & 0 & \mathbf{0} \\ 0 & 0 & 0 & 1 & \mathbf{0} \end{bmatrix} \tag{5.53}$$

In a similar way, the Jacobian matrices of heave motion can be derived to get:

$$\mathscr{F}^h(t) = \begin{bmatrix} & \begin{bmatrix} \mathbf{0} & \mathbf{0} & \mathbf{0} \\ & \frac{1}{M^3}\boldsymbol{\phi}^h & \frac{1}{M^3}\mathbf{D}_\phi^h \\ \mathbf{0} & \mathbf{0} & \mathbf{0} \end{bmatrix} \\ \mathbf{F}^h(t) & \\ \mathbf{0} & \mathbf{0} \\ \vdots & \\ \mathbf{0} & \mathbf{0} \end{bmatrix} \tag{5.54}$$

$$\mathbf{H}_m^h(t) = \begin{bmatrix} 1 & 0 & 0 & 0 & \mathbf{0} \\ 0 & 1 & 0 & 0 & \mathbf{0} \end{bmatrix} \tag{5.55}$$

where, the output model of the heave motion is:

$$\mathbf{y}_m^h = [z,\ \dot{z}]^T + \mathbf{v}^h(t), \tag{5.56}$$

and the $\mathbf{v}^h(t) \sim N(\mathbf{0}, \mathbf{Q}_p^h(t))$ is the measurement noise of heave motion which is also assumed to be white noise.

As indicated in Fig. 5.9, two Kalman Filters are implemented to generate estimation. The procedure of updating the estimation is the same as introduced in Section 5.2.1.4. Once the estimation of the states at a current time is available, Eq. (5.35) can be used for predicting the excitation force for a future short period.

5.2.2.2 Simulation results

In this section, the performance of the LQG controller is presented. The total simulation time is 200s. The motion is constrained; the constraint for the surge is 1m, for the heave is 0.2m, and for the pitch is 1rad. The wave applied in the simulation has a Bretschneider wave spectrum. The absorbed energy is shown in Figure. 5.10. The first figure compares between the energy absorption using the LQG controller and energy absorption using the LQ controller. The latter represents the ideal situation when we assume we have perfect knowledge of the wave. As can be seen in Fig. 5.10, the energy captured by the LQG controller is around 61.6% of the energy captured

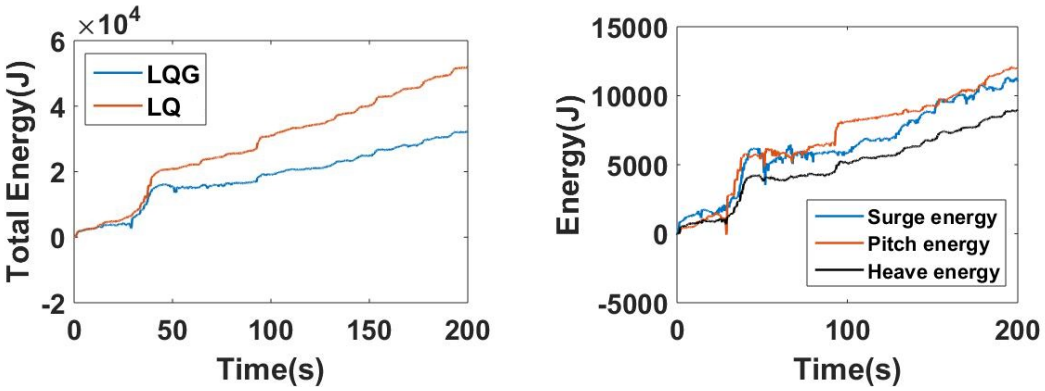

Figure 5.10: The energy extracted by the LQG controller.

by the LQ controller. The second figure shows the energy extracted from the surge, heave, and pitch mode respectively. From the figure, we can tell the total energy is 3.56 times the energy captured by heave motion only. Note that it can be shown that the maximum ratio between the total energy and heave energy is 3 when the system is linear (without parametric excitation) and in the absence of viscous damping. The control force is presented in Fig. 5.11; the maximum control force is around 20kN. Fig. 5.12 shows the pitch rotation and the pitch velocity. As can be seen in Fig. 5.12, the pitch rotation is within the specified constraints.

5.3 Consensus estimation for the WEC array

The consensus estimation is implemented in this section for the estimation of the wave field in the WEC array. The consensus estimation applies the communication technology to improve the performance of the estimation. The developed estimator

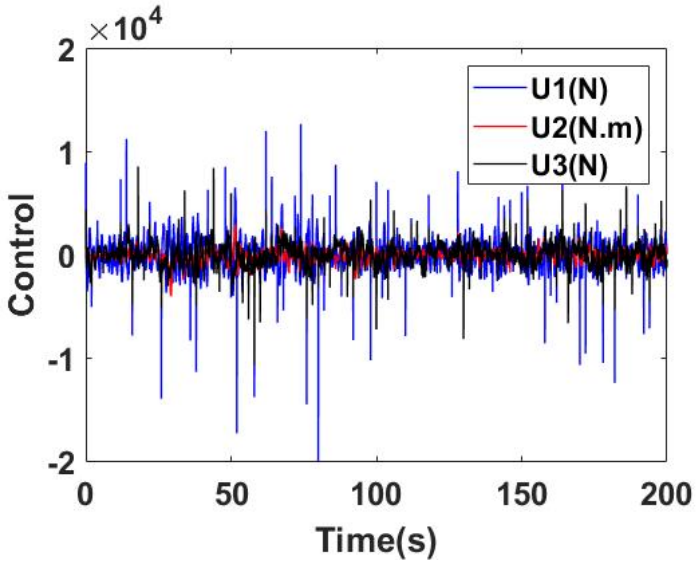

Figure 5.11: The control force

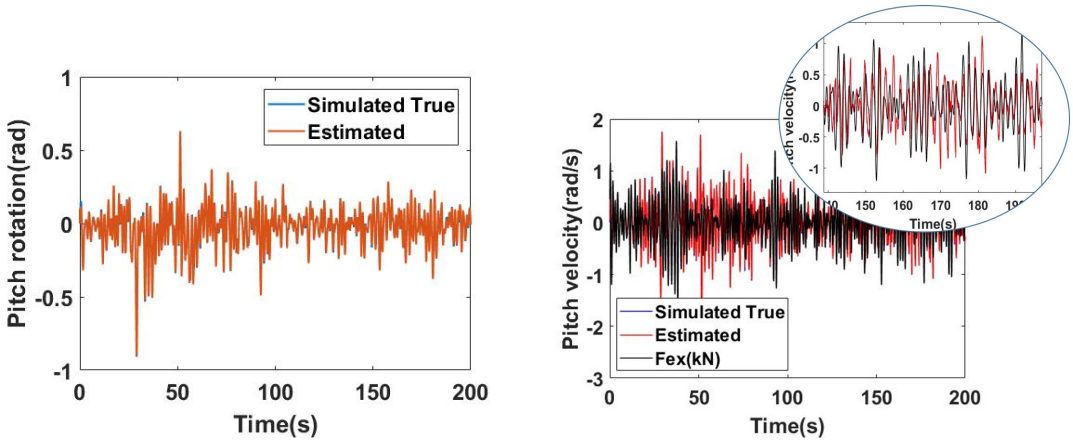

Figure 5.12: The pitch rotation and pitch velocity.

is extended from the discrete KCF developed in [156]. Then the derivation of the proposed Continuous-Discrete KCF is presented. Since most of the variables in the mathematical derivations and models are in the vector or matrix format, the different denotations for the scalar, vector, and matrix are neglected except a real number is included.

5.3.1 The Continuous-Discrete Kalman-Consensus Filter

When we have a continuous dynamic system and discrete measurements, a Continuous-Discrete Kalman-Consensus Filter becomes necessary. The continuous dynamics of each agent of the WEC array is described in Eq. (2.3), since the coupling between different agents is neglected. The dynamics can be presented in a state space format as:

$$\dot{\vec{x}}_i = \mathbf{F}\vec{x}_i + \mathbf{G}_u u_i + \mathbf{G}w_i \tag{5.57}$$

$$\vec{y}_{m,i} = \mathbf{H}_{m,i}\vec{x}_i + \vec{v}_i \tag{5.58}$$

where $\vec{x}_i$ is the state of the ith agent, u_i is the control input and $\vec{y}_{m,i}$ is the measurement output. The w_i and $\vec{v}_i$ are the process noise and measurement noise of ith agent, respectively. The $\mathbf{F}$ is the system matrix, $\mathbf{G}_u$ is the control matrix, $\mathbf{G}$ is the process noise gain matrix and $\mathbf{H}_{m,i}$ is the output matrix. The proposed CD-KCF

model can be summarized as:

$$
\begin{aligned}
\dot{\hat{\vec{x}}}_i &= \mathbf{F}\hat{\vec{x}}_i + \mathbf{G}_u u_i \\
\dot{\mathbf{P}}_i(t) &= \mathbf{F}(t)\mathbf{P}_i(t) + \mathbf{P}_i(t)\mathbf{F}^T(t) + \mathbf{G}(t)\mathbf{Q}_p(t)\mathbf{G}^T(t) \\
\hat{\vec{x}}_{k,i}^{+} &= \hat{\vec{x}}_{k,i}^{-} + \mathbf{K}_{g,k,i}(\vec{y}_{m,k,i} - \mathbf{H}_{m,k,i}\hat{\vec{x}}_{k,i}^{-}) + \mathbf{C}_{g,k,i}\sum_{N_i}(\hat{\vec{x}}_{k,j}^{-} - \hat{\vec{x}}_{k,i}^{-}) \\
\mathbf{P}_{k,i}^{+} &= (\mathbf{I} - \mathbf{K}_{g,k,i}\mathbf{H}_{m,k,i})\mathbf{P}_{k,i}^{-} \\
\mathbf{K}_{g,k,i} &= \mathbf{P}_{k,i}^{-}\mathbf{H}_{m,k,i}^{T}(\mathbf{R}_{k,i} + \mathbf{H}_{m,k,i}\mathbf{P}_{k,i}^{-}\mathbf{H}_{m,k,i}^{T})^{-1}
\end{aligned}
\tag{5.59}
$$

where $\hat{\vec{x}}_i$ is the states of the estimation of the ith agent. $\vec{y}_{m,k,i}$ is the measurements of the kth stage of the ith agent. $\mathbf{P}$ is the error covariance matrix of the state estimation, $\mathbf{Q}_p$ is the process noise covariance matrix, $\mathbf{R}$ is the measurement noise covariance matrix. $\mathbf{K}_{g,k,i}$ is the Kalman gain and $\mathbf{C}_{g,k,i}$ is the consensus gain. Algorithm. 3 shows the process of the CD-KCF. Furthermore, the stability of the proposed CD-KCF is shown in Appendix. A.

Algorithm 3 Continuous-Discrete Kalman-Consensus Filter: a Continuous-Discrete observer with a consensus term.

1: **Initialization:** $\mathbf{P}_i = \mathbf{P}_{i,0}, \hat{\vec{x}}_i = \hat{\vec{x}}_{i,0}$
2: **while** new data exists **do**
3: Compute the Kalman Gain
$\mathbf{K}_{g,k,i} = \mathbf{P}_{k,i}^{-}\mathbf{H}_{m,k,i}^{T}(\mathbf{R}_{k,i} + \mathbf{H}_{m,k,i}\mathbf{P}_{k,i}^{-}\mathbf{H}_{m,k,i}^{T})^{-1}$
4: Update the current estimation based on consensus law
$\hat{\vec{x}}_{k,i}^{+} = \hat{\vec{x}}_{k,i}^{-} + \mathbf{K}_{g,k,i}(\vec{y}_{m,k,i} - \mathbf{H}_{m,k,i}\hat{\vec{x}}_{k,i}^{-}) + \mathbf{C}_{g,k,i}\sum_{N_i}(\hat{\vec{x}}_{k,j}^{-} - \hat{\vec{x}}_{k,i}^{-})$
$\mathbf{P}_{k,i}^{+} = (\mathbf{I} - \mathbf{K}_{g,k,i}\mathbf{H}_{m,k,i})\mathbf{P}_{k,i}^{-}$
5: Propagate the estimation
$\dot{\hat{\vec{x}}}_i = \mathbf{F}\hat{\vec{x}}_i + \mathbf{G}_u u_i$
$\dot{\mathbf{P}}_i(t) = \mathbf{F}(t)\mathbf{P}_i(t) + \mathbf{P}_i(t)\mathbf{F}^T(t) + \mathbf{G}(t)\mathbf{Q}_p(t)\mathbf{G}^T(t)$
6: **end while**

5.3.2 Simulation results

In this section, the simulation results are presented to validate the performance of the proposed estimator for different cases. The measured states are only subset of the estimated states. The first case is designed to test the proposed CD-KCF for the WEC array interacts with regular wave. The second test case apply the CD-KCF for the WEC array interacts with the irregular wave. The performance of the regular Kalman Filter (KF) is also presented to compare it to the performance of the CD-KCF. To analyze the performance of the CD-KCF and KF, the following quantities are defined. The disagreement among the array is defined as:

$$\Psi(\hat{\vec{x}}) = (\sum_{i=1}^{N} \vec{\delta}_i^2)^{\frac{1}{2}} \tag{5.60}$$

The above equation can be further expanded to be: $\Psi(\hat{\vec{x}}) = (\sum_{i=1}^{N}\sum_{j=1}^{M} \vec{\delta}_{i,j}^2)^{\frac{1}{2}}$, if the basis vectors are orthogonal, where M is the number of elements in the $\vec{\delta}_i$ vector. Additionally, $\vec{\delta}_i = \hat{\vec{x}}_i - \bar{\hat{\vec{x}}}$, where $\bar{\hat{\vec{x}}}$ represents the average estimation which is computed as $\bar{\hat{\vec{x}}} = \frac{1}{N}\sum_i \hat{\vec{x}}_i$.

5.3.2.1 Test Case 1

The first test case is the estimation of the position and velocity of each buoy in a wave farm, in addition to the excitation force field using the CD-KCF. Practically, the estimated quantities are required by the controller. By applying the proposed estimator, a better energy extraction is expected if the more precise information is provided. Additionally, since the CD-KCF estimates in a distributed fashion, the wave farm will have a more stable performance even if the data collection and communication of some agents collapse. In this case, the wave farm has 16 buoys; only the heave motion is considered for each of them. The interaction between buoys is neglected in this section. The direction of the incoming wave β is 20^o, where β represents the angle between the wave propagation direction and the x axis. The distribution of the buoys is shown in Fig. 5.13.

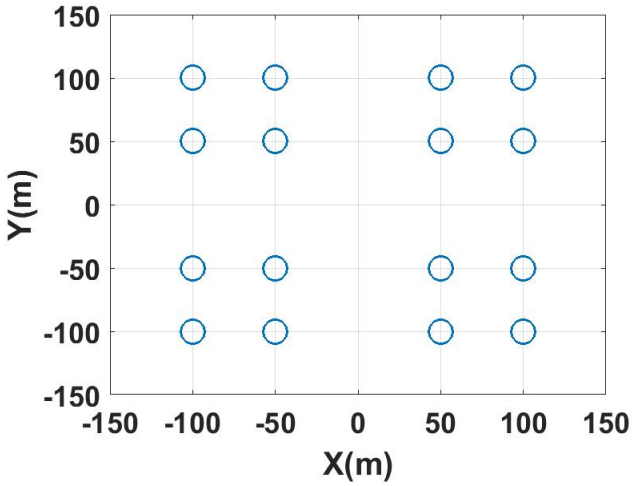

Figure 5.13: The distribution of the buoys in the wave farm

For observing the excitation force field, we need to introduce the expression of the excitation force field. The excitation force is function of the wave elevation; the wave elevation field can be expressed as [157, 158]:

$$\eta(t) = \sum_{j=1}^{N_w} \Re(\eta(\omega_j) e^{i(\chi_j r - \omega_j t + \phi_j)}) \tag{5.61}$$

where N_w is the total number of frequencies, $\eta(\omega_j)$ is the wave elevation at frequency ω_j, ϕ_j is the random time domain phase shift of particular frequency ω_j, k_j is the wave number which can be computed as $\chi = \omega^2/g$, where the deep water assumption is applied. The position r is expressed as:

$$r = x\cos(\beta) + y\sin(\beta) \tag{5.62}$$

The excitation force field can be expressed as:

$$F_e(t) = \sum_{j} \Re(F_{ew}(\omega_j)\eta(\omega_j) e^{i(\chi_j r - \omega_j t + \phi_j)}) \tag{5.63}$$

where $F_e(\omega_j)$ is the frequency domain excitation force coefficient. The system dynamics of each agent is described in Eq. (2.3). However, the radiation damping is approximated with a linear damping force as:

$$F_r = c_{lin}\dot{z}_i \tag{5.64}$$

where z_i is the heave displacement of each agent. There is no control force included in the simulation ($u = 0$), only free motion is considered. Additionally:

$$F_{e,i}(t) = \sum_j \Re(F_{ew}(\omega_j)\eta(\omega_j)e^{i(\chi_j r_i - \omega_j t + \phi_j)}) \tag{5.65}$$

Consequently, the state space model of the unforced and uncoupled wave farm can be expressed as:

$$\dot{x}_{1,i} = x_{2,i} \tag{5.66}$$

$$\dot{x}_{2,i} = \frac{1}{m}(F_{e,i}(t) - Kx_{1,i} - c_{lin}x_{2,i}) \tag{5.67}$$

To estimate the excitation force, a Fourier Series approximation for the excitation force is used:

$$F_{e,i}(t) \approx \sum_{j=1}^{N_f} a_j \cos(\chi_j r_i - \omega_j t) + b_j \sin(\chi_j r_i - \omega_j t) \tag{5.68}$$

$$\approx \boldsymbol{\phi}(r_i, t)[\vec{a}, \vec{b}]^T \tag{5.69}$$

where N_f is the number of Fourier terms in the approximation, $\boldsymbol{\phi}(r_i, t) = [\cos(\vec{\theta_i}), \sin(\vec{\theta_i})]$ and $\vec{\theta_i} = \vec{\chi} r_i - \vec{\omega} t$. Hence, the dynamics of the estimator can be

expressed as:

$$\dot{\hat{x}}_{1,i} = \hat{x}_{2,i} \tag{5.70}$$

$$\dot{\hat{x}}_{2,i} = \frac{1}{m}(\boldsymbol{\phi}(r_i, t)[\hat{\vec{a}},\ \hat{\vec{b}}]^T - K\hat{x}_{1,i} - c_{lin}\hat{x}_{2,i}) \tag{5.71}$$

$$\dot{\hat{\vec{a}}} = 0^{N_f \times 1} \tag{5.72}$$

$$\dot{\hat{\vec{b}}} = 0^{N_f \times 1} \tag{5.73}$$

The differential equations can be written in a state space form as $\dot{\hat{\vec{x}}} = \mathbf{F}_i\hat{\vec{x}}$, where $\hat{\vec{x}} = [\hat{x}_{1,i},\ \hat{x}_{2,i},\ \hat{\vec{a}},\ \hat{\vec{b}}]^T$and:

$$\mathbf{F}_i = \begin{bmatrix} 0 & 1 & 0^{1\times N_f} & 0^{1\times N_f} \\ -\frac{K}{m} & -\frac{c}{m} & \frac{\cos(\vec{\theta}_i)}{m} & \frac{\sin(\vec{\theta}_i)}{m} \\ 0^{N_f\times 1} & 0^{N_f\times 1} & 0^{N_f\times N_f} & 0^{N_f\times N_f} \\ 0^{N_f\times 1} & 0^{N_f\times 1} & 0^{N_f\times N_f} & 0^{N_f\times N_f} \end{bmatrix} \tag{5.74}$$

where the estimated quantities are the position, velocity of each agent and the unknown coefficients of the wave field which are generally required by the controller. Although the unknown coefficients are unmeasurable, the position and velocity are measurable. Additionally, for more realistic case, the WEC system becomes more stochastic (ex, nonlinear effect). Consequently, it is appropriate to select Kalman filter to develop consensus estimation of the wave field. The dynamics of the coefficients $\hat{\vec{a}}$ and $\hat{\vec{b}}$ are 0 which means they are not propagated. However, they are not fixed

during the estimation. The coefficients will be adjusted based on the new collected measurements which accounts for the stochastic wave condition. In this model, it is desired to have a consensus among the agents in the WEC array only on the coefficients of the excitation force $\hat{\vec{a}}$ and $\hat{\vec{b}}$. The position and the velocity of each agent are not required to have a consensus. As a result, the algorithm of the CD-KCF is modified to be suitable for this WEC array problem, by multiplying the consensus update term by a matrix that eliminates the unnecessary states from the consensus update, as shown in Algorithm. 4, step 4 where $\mathbf{P}^{-}_{k,i,22}$ represents the covariance matrix of the states which requires consensus update.

Algorithm 4 Continuous-Discrete Kalman-Consensus Filter: the consensus update term accounts only for a partial state vector.

1: **Initialization:** $\mathbf{P}_i = \mathbf{P}_{i,0}, \hat{\vec{x}}_i = \hat{\vec{x}}_{i,0}$
2: **while** new data exists **do**
3: Compute the Kalman Gain
$\mathbf{K}_{g,k,i} = \mathbf{P}^{-}_{k,i}\mathbf{H}^{T}_{m,k,i}(\mathbf{R}_{k,i} + \mathbf{H}_{m,k,i}\mathbf{P}^{-}_{k,i}\mathbf{H}^{T}_{m,k,i})^{-1}$
4: Update the current estimation based on consensus law
$\hat{\vec{x}}^{+}_{k,i} = \hat{\vec{x}}^{-}_{k,i} + \mathbf{K}_{g,k,i}(\vec{y}_{m,k,i} - \mathbf{H}_{m,k,i}\hat{\vec{x}}^{-}_{k,i}) + \gamma \begin{bmatrix} 0^{size(\mathbf{P}^{-}_{k,i,11})} & 0^{size(\mathbf{P}^{-}_{k,i,12})} \\ 0^{size(\mathbf{P}^{-}_{k,i,21})} & \mathbf{P}^{-}_{k,i,22} \end{bmatrix} \sum_{N_i}(\hat{\vec{x}}^{-}_{k,j} - \hat{\vec{x}}^{-}_{k,i})$
$\mathbf{P}^{+}_{k,i} = (\mathbf{I} - \mathbf{K}_{g,k,i}\mathbf{H}_{m,k,i})\mathbf{P}^{-}_{k,i}$
5: Propagate the estimation
$\dot{\hat{\vec{x}}}_i = \mathbf{F}\hat{\vec{x}}_i + \mathbf{G}_u u_i$
$\dot{\mathbf{P}}_i(t) = \mathbf{F}(t)\mathbf{P}_i(t) + \mathbf{P}_i(t)\mathbf{F}^{T}(t) + \mathbf{G}(t)\mathbf{Q}_p(t)\mathbf{G}^{T}(t)$
6: **end while**

The performance of this CD-KCF is tested numerically. The wave farm interacts with a regular wave which has a significant height of 0.3 m and a peak period of 7 s. The rigid body mass of the buoy is 4637 kg, the added mass at infinity frequency is

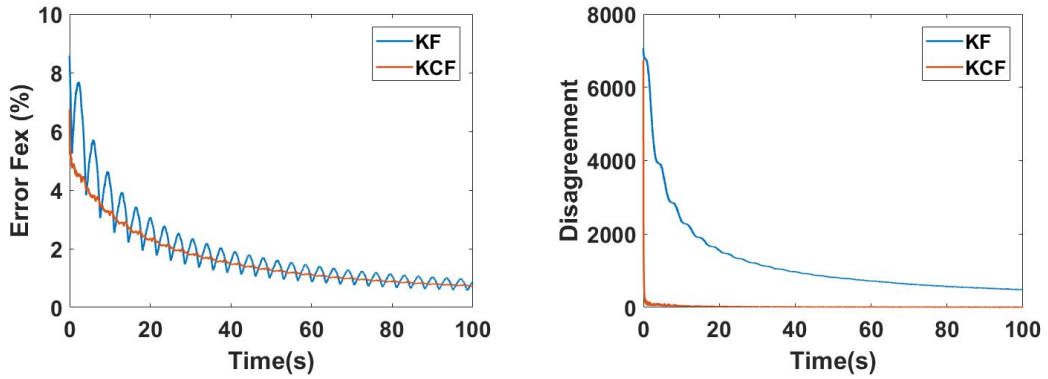

Figure 5.14: The average percent estimation error and the disagreement of the excitation force

2702kg, the hydrostatic stiffness is 4.44×10^4 N.m^{-1} and the linear damping is 1064 N.s.m^{-1}. Fig. 5.14 shows the average percent estimation error of the excitation force of all the agents, which is defined as

$$\bar{e}_e = (\sum_i \frac{\mid \hat{F}_{e,i} - F_{e,i} \mid}{\max \mid F_{e,i} \mid})/N \tag{5.75}$$

As shown in Fig. 5.14, the estimation error of the CD-KCF has slightly better convergence compared to the standard KF. The disagreement of the estimation is also shown in the figure. The states of the estimation for the WEC array contains the position, velocity and the coefficients $\hat{a}$ and $\hat{b}$. Since the agents in the WEC array only have consensus on the coefficients which represents the wave field. The disagreement is computed only based on the coefficients. The disagreement of the CD-KCF converges significantly faster than the KF which means all the agents reach a consensus quickly in this case. The computational cost of the CD-KCF is 263.37s which is less than the standard KF which takes 268.38s.

5.3.2.2 Test Case 2

The second test case presents the estimation of the position, velocity, and the excitation force field in a wave array that is subject to an irregular wave. The irregular wave has the Bretschneider wave spectrum. The significant height of the wave is 0.3 m and the peak period is 7 s. The total number of frequencies of the wave field is assumed 200 ranging from 0.1 rad.s^{-1} to 4 rad.s^{-1}. The initial guess for the coefficients is assumed of the form:

$$\vec{a}_i = \alpha_i(\vec{a}_e \cos(\phi) - \vec{b}_e \sin(\phi)) \tag{5.76}$$

$$\vec{b}_i = \alpha_i(-\vec{a}_e \sin(\phi) - \vec{b}_e \cos(\phi)) \tag{5.77}$$

where α_i is a random weight on the initial guess for different agents, $\vec{a}_e = \Re(F_e(\omega)\eta(\omega))$ and $\vec{b}_e = \Im(F_e(\omega)\eta(\omega))$. Two different simulations are presented in this section. The first simulation assumes less number of frequencies in the estimator while the true model is simulated using 200 frequencies. Specifically, 30 different frequencies are assumed in the CD-KCF model, which means the state vector includes 30 a and b coefficients. The main reason for using fewer frequencies in the estimation model is the computational cost. The computational cost of the CD-KCF is 1493.13s compared to 1560.40s of the standard KF. The CD-KCF is slightly faster than the standard KF. The average percent estimation error of the excitation force is shown

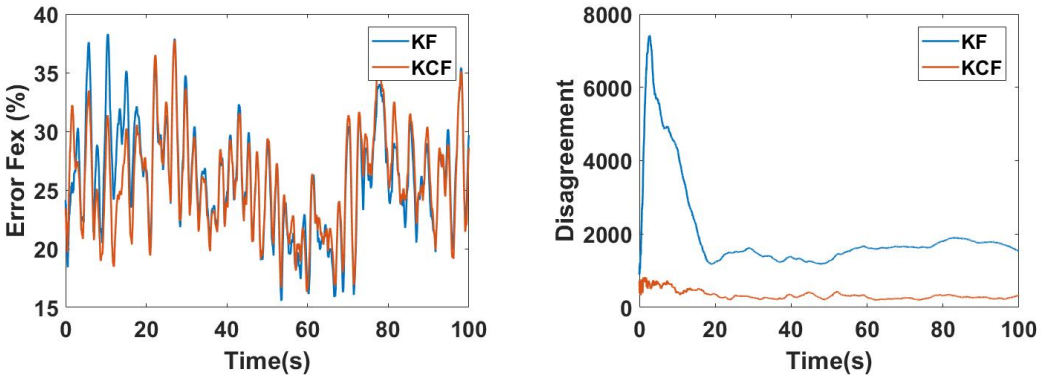

Figure 5.15: The average percent estimation error and the disagreement of the excitation force using 30 frequencies

in Fig. 5.15. The CD-KCF converges slightly faster than the KF; the performance of both filters is nearly the same in terms of the estimation error. The second figure in Fig. 5.15 shows the disagreement in the estimation of the two filters on the coefficients. The CD-KCF has a significantly better agreement than the KF.

To study the impact of the number of frequencies in the estimator model on the results, the simulation is extended to estimate the true excitation force using 200 frequencies in the estimator model. The estimation error of CD-KCF and KF is shown in the first figure in Fig. 5.16. The CD-KCF has a better performance both in terms of the convergence speed and estimation error. As shown in the second figure in Fig. 5.16, the disagreement of the estimation on the coefficients converges significantly faster in the case of the CD-KCF.

The percent estimation error converges to about 25% as shown in Fig. 5.15 when using only 30 frequencies in the estimator model, whereas it converges to about 0% when

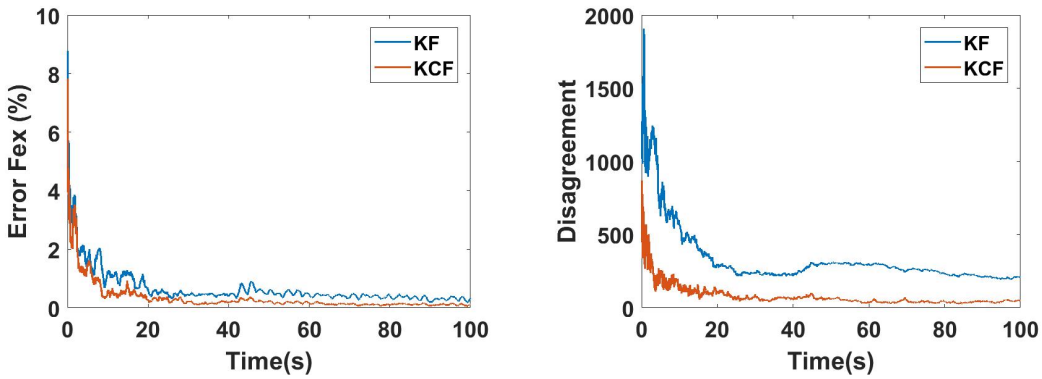

Figure 5.16: The average percent estimation error and the disagreement of the excitation force using 200 frequencies

using 200 frequencies, as shown in Fig. 5.16. This is expected since the estimation with less number of frequencies cannot fully capture the true wave spectrum. To highlight the impact of the number of frequencies on the estimation performance, Fig. 5.17 show simulations using 30, 100, and 200 frequencies in the estimator model of the CD-KCF. Both the estimation error and the disagreement significantly improved by increasing the number of frequencies. Moreover, from the figures regarding the estimation error, we can tell that the required time to obtain reasonable low-level error is less than 40s. Typically, the sample time of the ocean observation is around 15-30mins within which the sea state is reasonably described [159]. Apparently, the converging time of the developed estimator is significantly less than the sample time. Additionally, based on the wave conditions applied in references [160, 161], we can consider an even faster wave dynamics where the sea state changes around 120s. It is still much larger than 40s. Hence, the proposed estimator is able to catch the constantly changing wave.

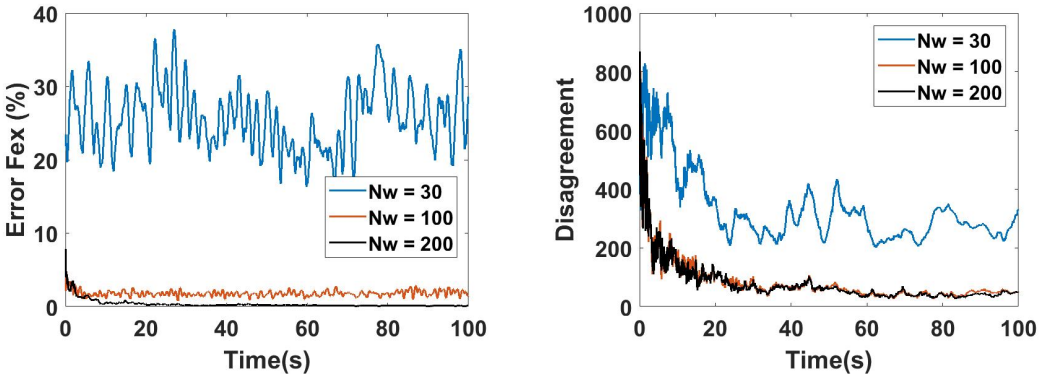

Figure 5.17: Estimation error and Disagreement obtained with different number of frequencies using the CD-KCF

Chapter 6

Power Take Off Constraints

This Chapter introduces the Power take-off constraints of the WEC. In previous chapters, the optimal control and the optimal estimation are proposed for the WEC. Although some of them consider the constraint on the displacement and the control force. The realistic performance of the controller with the Power take-off (PTO) unit implemented is not validated. Among the different categories of PTO units, the hydraulic system and direct drive system are mainly applied for WEC control. Section 6.1 introduces the modeling of the discrete displacement hydraulic PTO. The details of the dynamics of the hydraulic cylinder, hoses, directional valves, pressure accumulators and the hydraulic motor are presented in this section. Section 6.2 presents the numerical validation on the proposed system. The control algorithms that will be applied to the hydraulic system and the simulation tool are introduced

first. The simulation results are then presented.

6.1 Modeling of The Discrete Displacement Hydraulic Power Take-Off unit

In this dissertation, the Discrete Displacement Cylinder (DDC) hydraulic system is used to apply the PTO torque. A simplified illustration for this system is shown in Figure 6.1. More details about the DDC hydraulic system can be found in [15]. As shown in Figure 6.1, the DDC hydraulic system is mainly composed of the actuator/cylinder, the manifold valves, the manifold accumulators, and the generator. The PTO torque is computed in the Equation (6.1) as the product of the cylinder force and the moment arm:

$$\tau_{PTO} = F_c l_1 \tag{6.1}$$

where the moment arm can be expressed by Equation (6.2):

$$l_1 = \frac{l_2 l_3 \sin(\theta - \alpha_0)}{x_c + l_4} \tag{6.2}$$

$$x_c = -l_4 + \sqrt{-2 l_2 l_3 \cos(\theta - \alpha_0) + (l_2^2 + l_3^2)} \tag{6.3}$$

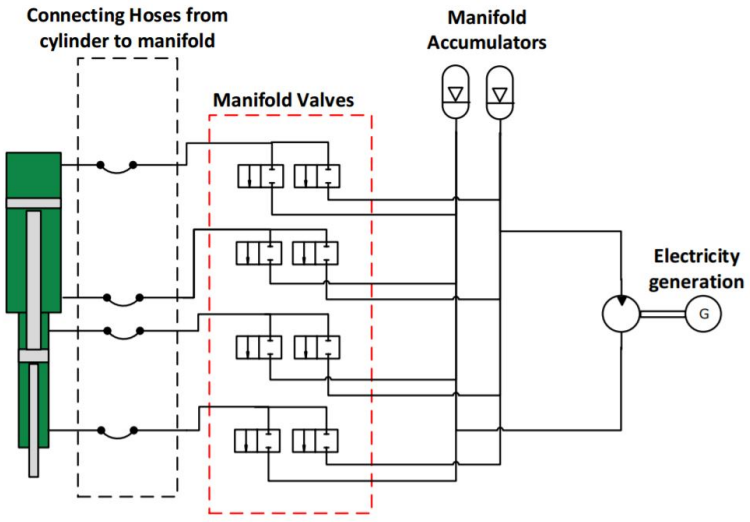

Figure 6.1: The layout of the Discrete Displacement Cylinder (DDC) hydraulic system.

6.1.1 The Hydraulic Cylinder

The actuator force F_c is generated by the hydraulic cylinder and can be computed by Equations (6.4) and (6.5):

$$\tilde{F}_c = -p_{A1}A1 + p_{A2}A2 - p_{A3}A3 + p_{A4}A4 \tag{6.4}$$

$$F_c = \tilde{F}_c - F_{fric} \tag{6.5}$$

where p_{Ai} is the pressure of the ith chamber and Ai is the area of the piston. F_{fric} is the cylinder friction force. The dynamics of the chamber pressure can be described

by flow continuity Equations (6.6) to (6.9):

$$\dot{p}_{A1} = \frac{\beta(p_{A1})}{A1(x_{c,max} - x_c) + V_{0,A1}}(Q_{A1} - v_c A1) \tag{6.6}$$

$$\dot{p}_{A2} = \frac{\beta(p_{A2})}{A2x_c + V_{0,A2}}(Q_{A2} + v_c A2) \tag{6.7}$$

$$\dot{p}_{A3} = \frac{\beta(p_{A3})}{A3(x_{c,max} - x_c) + V_{0,A3}}(Q_{A3} - v_c A3) \tag{6.8}$$

$$\dot{p}_{A4} = \frac{\beta(p_{A4})}{A4x_c + V_{0,A4}}(Q_{A4} + v_c A4) \tag{6.9}$$

where $V_{0,A1}$, $V_{0,A2}$, $V_{0,A3}$, and $V_{0,A4}$ are the volumes of the connecting hoses of different chambers. $x_{c,max}$ is the maximum stroke of the cylinder. x_c and v_c are the position and velocity of the piston, respectively, which are defined positive down. $\beta(p_{Ai})$ is the effective bulk modulus of the fluid based on different pressures, and is assumed to be constant in this study. Additionally, Q_{Ai} is the flow from the connecting hose to the ith chamber. The cylinder friction is expressed by Equation (6.10):

$$F_{fric} = \begin{cases} \tanh(a_f v_c) \mid \tilde{F}_c \mid (1 - \eta_c), & \text{if } F_c v_c > 0 \\ \tanh(a_f v_c) \mid \tilde{F}_c \mid (\frac{1}{\eta_c} - 1) & \text{otherwise} \end{cases} \tag{6.10}$$

where a is the coefficient used to smooth the friction curve versus velocity. η_c is a constant efficiency of the cylinder.

6.1.2 The Hoses

The hoses connected between the cylinder and the manifold valves are modeled by Equations (6.11) and (6.12) which refer to [15]:

$$\dot{Q}_{out} = \frac{(p_1 - p_2)A_{hose} - p_f(Q_{out})A_{hose}}{\rho l_{hose}} \tag{6.11}$$

$$\dot{p}_1 = \frac{(Q_{in} - Q_{out})\beta}{A_{hose} l_{hose}} \tag{6.12}$$

where Q_{in} and Q_{out} are the fluid flows in and out of the hose, and p_1 and p_2 are the pressures of the inlet and outlet of the hose, respectively. A_{hose} is the area of the hose, l_{hose} is the length of the hose, ρ is the fluid density, and $p_f(Q_{out})$ is the pressure drop across the hose. The pressure drop across a straight pipe/hose can be modeled by the equation:

$$\begin{aligned} p_\lambda = & \frac{0.3164 l_{hose}\rho}{2Re^{0.25} d_{hose}} \frac{Q_{out} \mid Q_{out} \mid}{(0.25 d_{hose}^2 \pi)^2} (0.5 + 0.5 \tanh(\frac{2300 - Re}{100})) \\ & + \frac{128 \nu \rho l_{hose} Q_{out}}{\pi d_{hose}^4} (0.5 + 0.5 \tanh(\frac{-2300 + Re}{100})) \end{aligned} \tag{6.13}$$

where ν is the kinematic viscosity of the fluid. Re represents the Reynold number which can be computed by Equation (6.14):

$$Re = \frac{v_{out} d_{hose}}{\nu} \tag{6.14}$$

Equation (6.13) combines the pressure loss of the laminar flow and the turbulent flow by the hyperbolic-tangent expression. Consequently, a continuous transition of the pressure loss between the laminar and turbulent flow can be created. When the Reynold number is less than 2200, $(0.5 + \ 0.5\tanh(\frac{2300-Re}{100}))$ is close to zero, which means the pressure drop is contributed by the laminar flow. On the other hand, when the Reynold number is greater than 2400, $(0.5 + 0.5\tanh(\frac{-2300+Re}{100}))$ is close to zero, which means the pressure drop is contributed by the turbulent flow. Another source of pressure drop is the fitting loss, which can be computed by Equation (6.15):

$$p_\zeta = \zeta \frac{\rho}{2} Q_{out} \mid Q_{out} \mid \frac{1}{(0.25 d_{hose}^2 \pi)^2} \tag{6.15}$$

where ζ is the friction coefficient for a given fitting type. Finally, the total resistance in the hose with n line pieces and m fittings can be computed by Equation (6.16):

$$p_f(Q_{out}) = p_{\lambda,1}(Q_{out}) + ... + p_{\lambda,n}(Q_{out}) + p_{\zeta,1}(Q_{out}) + ... + p_{\zeta,m}(Q_{out}) \tag{6.16}$$

In this dissertation, the pressure loss of the hoses is modeled by the Equation (6.17):

$$p_f(Q_{out}) = p_\lambda(Q_{out}) + p_{\zeta,M}(Q_{out}) + p_{\zeta,C}(Q_{out}) \tag{6.17}$$

where $p_{\zeta,M}$ represents the fitting resistance which considers the internal pressure drops in the manifold and $p_{\zeta,C}$ represents the cylinder inlet loss.

6.1.3 The Directional Valves

The two-way two-position directional valves are used in this model. The flow across the valve can be described by the following orifice Equation (6.18):

$$Q_v = sign(\Delta p) C_d A_v(\alpha) \sqrt{\frac{2}{\rho} \mid \Delta p \mid} \tag{6.18}$$

where Δp is the pressure difference cross the valve, C_d is the discharge coefficient, and $A_v(\alpha)$ is the opening area which can be computed by Equations (6.19)–(6.21):

$$A_v(\alpha) = \alpha A_0 \tag{6.19}$$

$$\dot{\alpha} = \begin{cases} \frac{1}{t_v}, & \text{if } u_v = 1 \\ -\frac{1}{t_v}, & \text{if } u_v = 0 \end{cases} \tag{6.20}$$

$$0 \leqslant \alpha \leqslant 1 \tag{6.21}$$

where A_0 is the maximum opening area of the valve. In this paper, a total of eight valves are used to control the actuator force. The t_v represents the opening and closing time of the valve. The shifting algorithm of the valve applied in this paper can be further improved [162] to reduce the pressure oscillations and improve the energy efficiency. Moreover, the different opening time has a significant impact on the cylinder pressure [163]. The opening time t_v is selected to be 30 ms in this paper

to avoid the cavitation or pressure spikes and to have a relatively fast response to the reference control command. Since the focus of this paper is to examine the controllers' performance practically, the influence of different opening times is not investigated in this paper.

6.1.4 The Pressure Accumulators

The accumulators in the DDC system are used as pressure sources and also for energy storage. The dynamics of the pressure accumulator can be modeled with the Equations (6.22)–(6.24) [15]:

$$\dot{p}_{acc} = \frac{Q_{acc} + \frac{1}{1+\frac{R_{gas}}{C_v}} \frac{V_g}{T_{gas}} \frac{1}{\tau_a}(T_w - T_{gas})}{\frac{V_{a0}-V_g+V_{ext}}{\beta} + \frac{1}{1+\frac{R_{gas}}{C_v}} \frac{V_g}{p_{acc}}} \tag{6.22}$$

$$\dot{V}_g = -Q_{acc} + \dot{p}_{acc} \frac{V_{a0} - V_g + V_{ext}}{\beta} \tag{6.23}$$

$$\dot{T}_{gas} = \frac{1}{\tau_a}(T_w - T_{gas}) - \frac{R_{gas} T_{gas}}{C_v V_g} \dot{V}_g \tag{6.24}$$

where p_{acc} is the pressure of the accumulator, Q_{acc} is the inlet flow to the accumulator, R_{gas} is the ideal gas constant, C_v is the gas specific heat at constant volume, T_w is the wall temperature, τ_a is the thermal time constant, β is the bulk modulus of the fluid in the pipeline volume V_{ext}, V_{a0} is the size of the accumulator, V_g is the gas volume, and T_{gas} is the gas temperature. Hence the state of the accumulator contains

the pressure, the gas volume and the gas temperature. Initially, the state can be specified based on the standard gas law by Equation (6.25):

$$V_g = \frac{T_{gas}}{T_0}\frac{p_{a0}}{p_a}V_{a0} \tag{6.25}$$

where p_{a0} is the pre-charged pressure of the gas at the temperature T_0.

6.1.5 The Hydraulic Motor

For the system presented in this dissertation, there are 4 chambers and 2 different pressures: the high pressure and the low pressure. The hydraulic motor is connected between the high pressure accumulator and the low pressure accumulator. The flow of the hydraulic motor can be modeled by Equation (6.26):

$$Q_M = D_w\omega_M - \Delta p C_{Q1} \tag{6.26}$$

where D_w is the displacement of the hydraulic motor, which is constant for a fixed displacement motor, Δp is the pressure across the motor, C_{Q1} is the coefficient of the flow loss of the motor, and ω_M is the rotational speed of the motor which is defined by Equation (6.27):

$$\omega_M = \frac{p_{avg,exp}\psi}{p_H k_{gen} D_M} \tag{6.27}$$

where $p_{avg,exp}$ is the expected average power output, p_H is the pressure of the high pressure accumulator, k_{gen} is the number of generators, D_M is the total motor displacement, and ψ is a coefficient for the motor speed control to prevent the high pressure from depletion or saturation which is formulated by Equations (6.28) and (6.29):

$$k = \frac{4}{(p_{H,max} - p_{H,min})} \tag{6.28}$$

$$\psi = \begin{cases} k(p_H - p_{H,min}), & \text{if } p_H > p_{H,min} \\ 0, & \text{otherwise} \end{cases} \tag{6.29}$$

To achieve the desired motor speed introduced in Equation (6.27), the generator torque control needs to be included. In this paper, the generator and inverter are not modeled and the desired motor speed is assumed achievable. The power in the hydraulic motor can be computed by Equation (6.30):

$$P_M = \Delta p Q_M \tag{6.30}$$

This completes the modeling of DDC hydraulic system; the control algorithm is introduced in the next section.

6.2 Numerical Validation

6.2.1 The Control Algorithm

Two parts will be presented in this section: the control method for the buoy and the force-shifting algorithm for controlling the valves. The control method for controlling the buoy computes a reference value for the control force at each time step. This reference control force is then used as an input to the PTO, and the actual control force that results from the PTO is computed using the force-shifting algorithm. Each of the two parts is detailed below.

6.2.1.1 The Buoy Control Method

Several control methods will be tested in this paper using a simulator that simulates the PTO unit. Some of these controller were originally developed for heave control. It is relatively straightforward, however, to extend a control method from the heave motion to the pitch motion. For example, the singular arc (SA) control method [2] can be used to compute the control torque by the following Equation (6.31):

$$\tau_{PTO}(s) = \frac{N(s)}{D(s)} \tag{6.31}$$

where:

$$N(s) = (Js^2 + (C_r(sI + A_r)^{-1}B_r - D_r)s + K)\tau_e(s)$$

$$D(s) = s(C_r(sI + A_r)^{-1}B_r - C_r(sI - A_r)^{-1}B_r - 2D_r) \tag{6.32}$$

where the excitation torque can be expressed as Fourier series expansion by Equation (6.33):

$$\tau_e = \sum_{i=1}^{n} \Re(\tau_{ew}(\omega_i)\eta(\omega_i)e^{i(-\omega_i t + \phi_i)}) \tag{6.33}$$

An inverse Laplace transformation is then applied to the SA control to obtain the control in the time domain. The required information to compute the control is the time t, the excitation torque coefficient τ_{ew}, the wave frequency vector $\vec{\omega}$ and the time domain phase shift vector $\vec{\phi}$. A reference control method is the feedback proportional-derivative (PD) control. The PD control takes the form of Equation (6.34):

$$\tau_{PTO} = K_p\theta + K_d\dot{\theta} \tag{6.34}$$

where K_p is the proportional gain and K_d is the derivative gain. In addition to the above two control methods, simulated with the hydraulic system are model predictive control (MPC) [164], shape-based (SB) control [5], proportional-derivative complex conjugate control (PDC3) [24], and pseudo-spectral (PS) control [165]. Each one of these methods is well documented in the literature, so the details of each control methods are avoided in this section.

In the original developments, the SA control and the PDC3 control compute a control force that is equivalent to the complex conjugate control (C3), and hence the maximum possible harvested energy in the linear domain. However, the C3 does not account for constraints on the buoy displacement. In fact, since the C3 criterion is to resonate the buoy with the excitation force, the motion of the buoy always violates displacement constraints when controlled using the SA and PDC3 controls. On the other hand, the MPC, SB, and PS control methods compute a control force in an optimal sense, taking displacement constraints into account. Figure 6.2 shows a simulation for 5 min for the above six control methods when a constraint on the buoy displacement is assumed. The simulation parameters are detailed in Section 6.2.3. This simulation does not account for the PTO dynamics and is here presented to highlight the impact of including the PTO into the simulations in Section 6.2.3. As can be seen from Figure 6.2, among the six control methods, the MPC and PD controls performed best, then the SB method, then the PS, and then the PDC3 and SA methods. The two methods (SA and PDC3) that perform best without displacement constraints actually have the poorest performance when accounting for the constraints.

6.2.2 The Force-Shifting Algorithm

The force-shifting algorithm (FSA) is introduced in this section. The FSA used in this paper is described by Equation (6.35):

$$\{F_c(t) = \vec{F}[k] \mid k = arg \;\; min \mid F_{ref}(t) - \vec{F}[k] \mid\} \tag{6.35}$$

where F_{ref} is the reference control force (computed for instance using one of the six control methods described above), and $\vec{F}$ is the vector of the possible discrete values for the force. With different permutations of valve openings, it is possible to produce different levels of constant forces, as shown in Figure 6.3, where it is assumed that $p_H = 200$ bar and $p_L = 20$ bar. The FSA selects the discrete force level that is closest to the reference control force. It is noted here that the discrete force changes over time due to the fluctuation of the pressures in the accumulators.

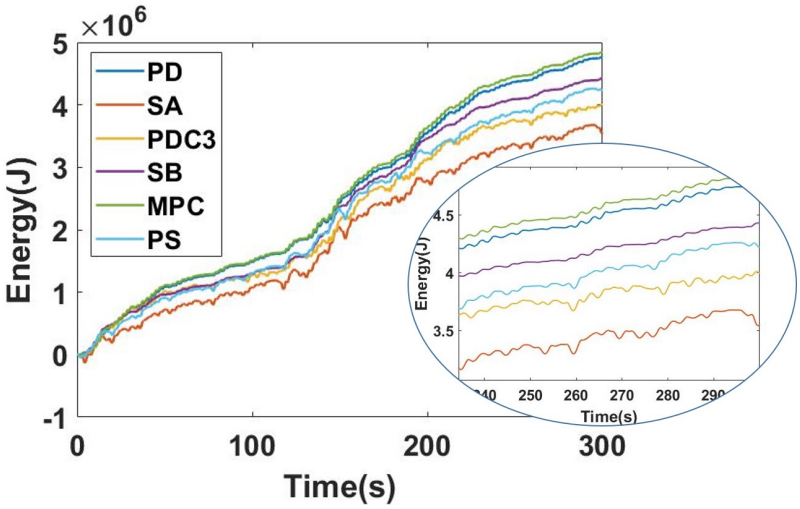

Figure 6.2: When accounting for displacement constraints, some unconstrained methods harvest less energy. PD: proportional-derivative; SA: singular arc; PDC3: proportional-derivative complex conjugate control; SB: shape-based; MPC: model predictive control; PS: pseudo-spectral.

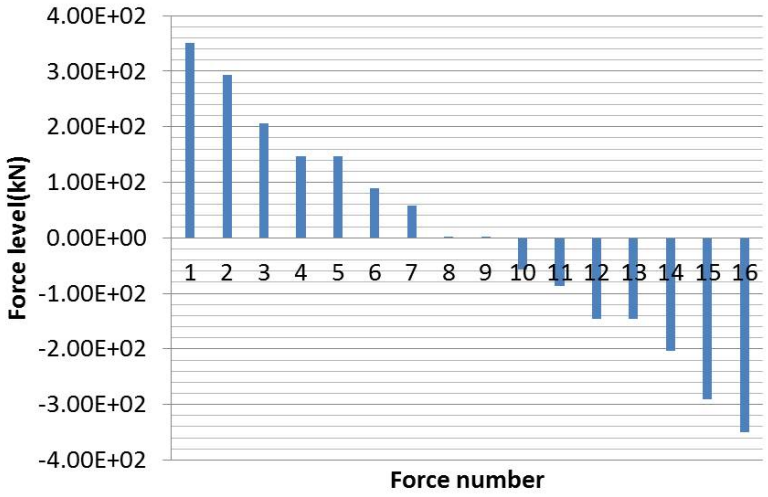

Figure 6.3: An example for all discrete possible values for a PTO force.

6.2.3 Simulation Tool

A tool for simulating the dynamics of the WEC including the motion dynamics, the hydrodynamic/hydrostatic force calculations, and the PTO hardware model was developed in MathWorks Simulink®. The detailed Simulink model of the wave energy conversion system is shown in Figure 6.4. The Plant block simulates the dynamics of the buoy. The PTO block simulates all the equations of the valves, hoses, and accumulators. As can be seen in Figure 6.4, the excitation force is an input that is computed outside the Plant block. The control force command is computed in the block 'Control Command'. Despite the name, six different controllers were tested in the 'Control Command' block. A detailed Simulink model of the hydraulic system is shown in Figure 6.5, this model is inside the PTO block in Figure 6.4. The parameters of the dynamic model of the WaveStar used in the simulations in this dissertation are listed in Table 2.1.

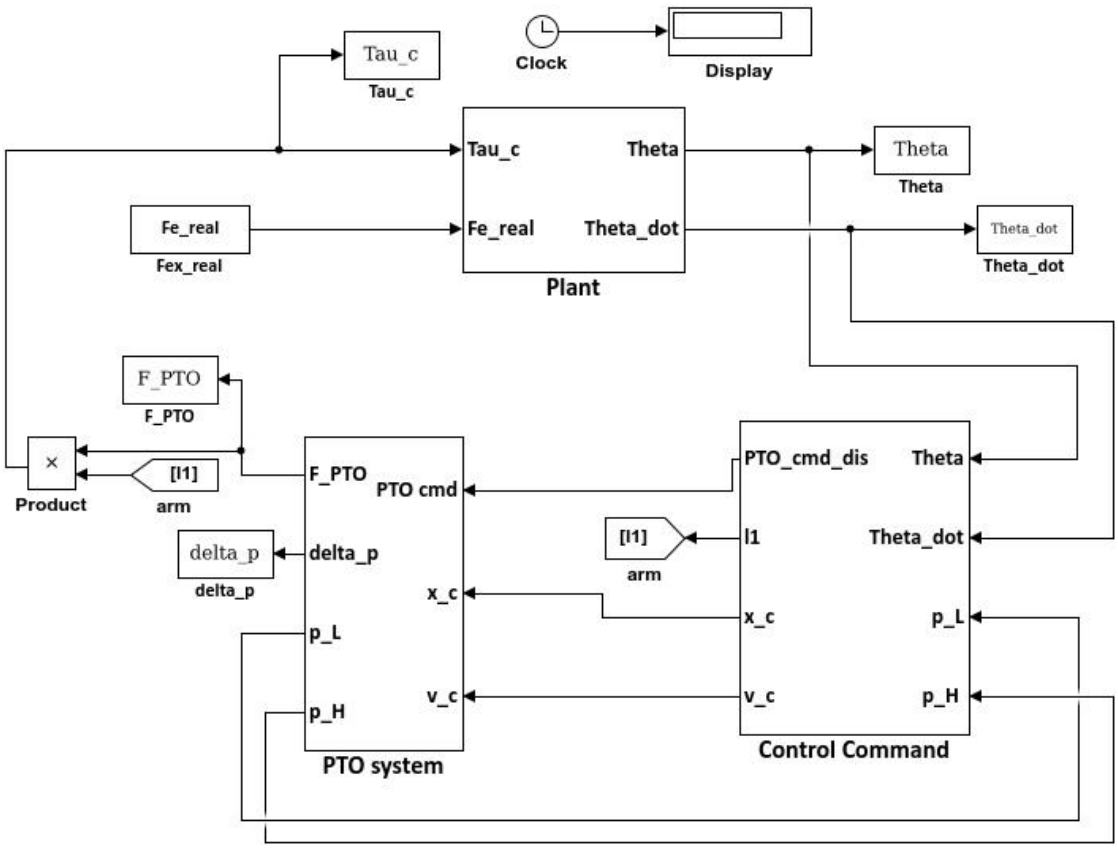

Figure 6.4: The Simulink model of the wave energy conversion system.

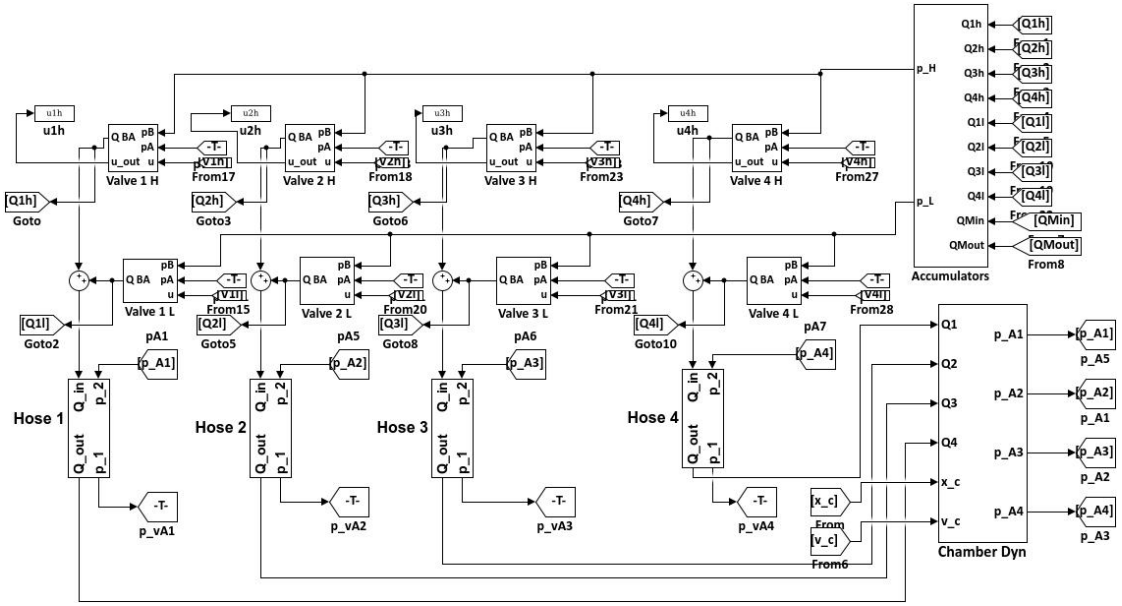

Figure 6.5: The Simulink model of the hydraulic PTO system.

The irregular waves are simulated in this study using the stochastic Pierson–Moskowitz (PM) spectrum. The wave used in the simulation has a significant height of 1.75 m and a peak period 5.57 s. With regard to the significant height and peak period applied in the simulation, they are selected from the validated wave climate in [112, 166] for the Wavestar C5. The proper range so that the wave for C5 can have major energy absorption is with a significant height from 0.5 m to 3 m and peak period from 2 s to 7 s. The wave climate applied in this study is in the middle of the range to avoid losing generality.

6.2.3.1 The System Losses

The system losses are computed in this study. The system losses include the pressure loss of the hoses, the flow loss of the generator, and the friction of the cylinder. The pressure loss is shown in Figure 6.6, in which the vertical line represents the transition between the laminar flow and the turbulent flow when the Reynold number is $Re = 2300$, for each of the two possible directions of the fluid flow. The amount of the flow loss and the friction force of the cylinder are shown in Figures 6.7 and 6.8. All the system parameters used in the simulations are listed in Table 6.1.

6.2.4 Simulation Results

The above Simulink tool is used to simulate the performance of the above six control methods. The energy extracted by those methods is shown in Figure 6.9. In this simulation, there are limitations on the maximum stroke and the maximum control force. In addition, the PTO dynamics are simulated. The maximum control force in the cylinder in the simulations presented in this paper is assumed to be 215 kN. The maximum allowable displacement in the simulations presented in this paper is assumed to be 1.2 m. As can be seen in Figure 6.9, the MPC and PD control methods harvest the highest energy level compared to the other methods. The SB

method comes next. The SA, PDC3, and PS control methods come next, and the three of them perform about the same. For further analysis of the performance of the controllers, the capture width ratio (CWR) is evaluated:

$$CWR = \frac{P_{ave}}{DP_w} \tag{6.36}$$

where P_{ave} is the average power extraction of the buoy, P_w is the wave energy transport, and D is the characteristic dimension of the buoy. The CWRs of the MPC, PD, SB, SA, PDC3, and PS controllers are 51.21%, 50.92%, 44.68%, 37.60%, 37.14%, and 36.86% respectively. According to the [166], the CWR of the performance of the floater with the applied wave ranges from 40% to 50%. Hence, the performance of the proposed controllers is in the reasonable range in terms of energy extraction. Comparing Figure 6.9 to Figure 6.2 we can see that by including the PTO model, the performance of the SA method improves slightly, while the performance of the PS degrades slightly, and as a result, the three methods PS, SA, and PDC3 perform about the same. The performance of the MPC, PD, and SB control methods actually slightly improve when the PTO model is included.

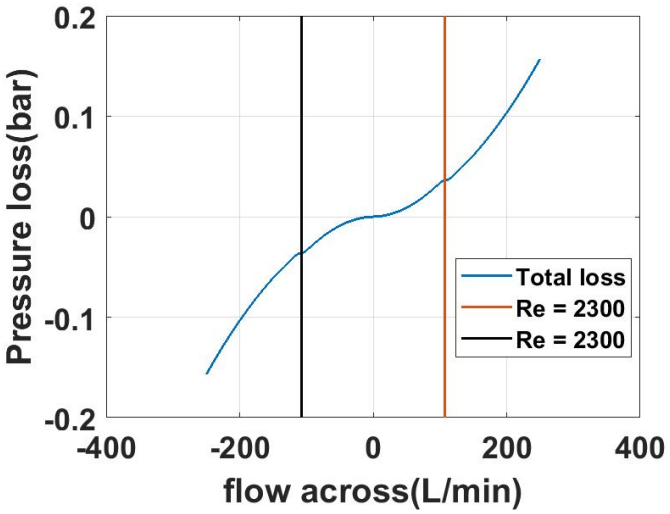

Figure 6.6: The pressure loss of the hose which has a 1-m length and 3.81×10^{-2} m diameter with different flow rates across the hose.

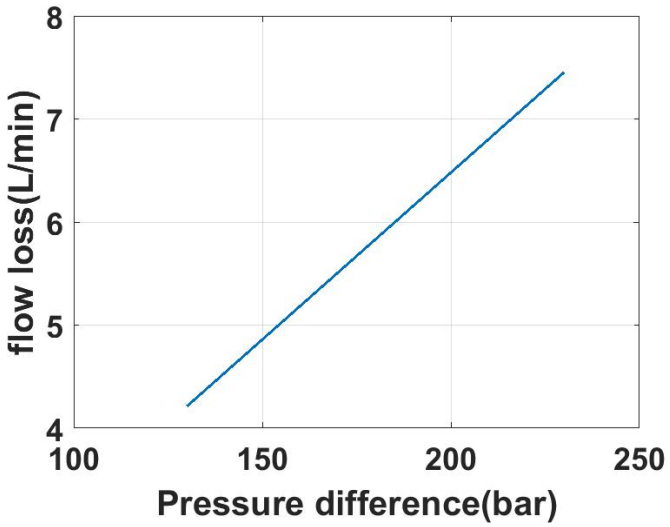

Figure 6.7: The flow loss of the generator.

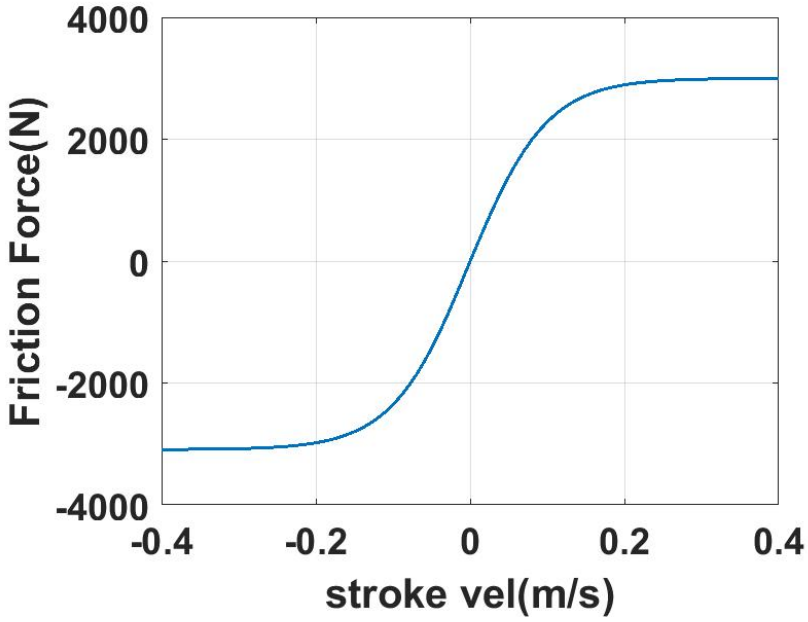

Figure 6.8: The friction force of the cylinder with different velocities when the cylinder force is 100 kN.

Another important result to examine is the output mechanical power at the actuator and the output power from the generator. These two quantities are compared in the first part of Figure 6.10. From the figure, we can tell that the power absorbed in the generator side is much smoother than the power extracted by the actuator. The hydraulic accumulators act as a power capacitor for energy storage, resulting in this relatively smooth power profile at the generator output. As can be seen in the figure also, the actuator power includes reactive power; these are the times at which the actuator power is negative. At these times, the PTO actually pumps power into the ocean through the actuator. The generator output power does not have any reactive power, confirming that all the reactive power come from the accumulators.

The efficiency of the system is defined by Equation (6.37):

$$\eta_{out} = \frac{P_{gen}}{P_{actuator}} \tag{6.37}$$

The efficiency depends on the control method. For example, in this test case, the efficiency of the SB controller is 80.15%, for the MPC it is 72.58%, for the PS it is 67.34%, for the SA it is 64.36%, and for the PD controller it is 71.76%, over 300 s.

In the context of comparing the performance of different control methods, it is important to highlight one significant difference between them that emanates from the theory behind each control method. Each of the MPC, SB, and PS control methods requires wave prediction. That is, wave information (or excitation force) is needed over a future horizon at each time step in the simulation. In the simulations in this paper, this future horizon is assumed to be 0.6 s for the SB and MPC control methods and is assumed to be 60 s for the PS control. Wave prediction is assumed perfect in these simulations. Non-perfect wave prediction would affect the results obtained using these methods. The PD, SA, and PDC3 control methods do not need future wave prediction.

This simulation tool also provides detailed operation information that is useful for characterizing different components in the system. For example, the generator speed is computed in the simulation and is shown in the second part of Figure 6.10. As

shown in the figure, the speed is oscillating around 1200 RPM.

Table 6.1
The data used in the simulation of the overall WEC system.

Symbol	**Value**	**Unit**
Length of the arms		
l_2	3	m
l_3	2.6	m
l_4	1.6	m
Length of the hoses C2M		
l_{A1}	1	m
l_{A2}	1	m
l_{A3}	1	m
l_{A4}	1	m
Diameter of the hoses C2M		
d_{A1}	1.5	in
d_{A2}	1.5	in
d_{A3}	1.5	in
d_{A4}	1.5	in
Maximum stroke		
$x_{c,max}$	3	m
Area of the chambers		

A_1	113.4×10^{-4}	m^2
A_2	32.55×10^{-4}	m^2
A_3	80.85×10^{-4}	m^2
A_4	162.75×10^{-4}	m^2
Max Area of the valves		
A_{01}	1.6×10^{-4}	m^2
A_{02}	1.6×10^{-4}	m^2
A_{03}	1.6×10^{-4}	m^2
A_{04}	1.6×10^{-4}	m^2
Accumulator size		
V_{a0}	100×10^{-3}	m^3
Pressure drop coef		
ζ_M	1.3	
ζ_C	1	
Specific time constant S		
τ_l	23	s
τ_h	34	s
Initial pressure of the accumulators		
$p_{a,l}$	20	bar
$p_{a,h}$	130	bar

Initial angle		
α_0	1.0821	rad
Control parameters		
K	-9.16×10^6	Nm/rad
B	4.4×10^6	Nms/rad
Valve opening time		
t_v	30×10^{-3}	s
Wall temperature		
T_w	50	^{o}C
Ideal gas constant		
R	276	J/kg/K
Gas specific heat at constant volume		
C_v	760	J/kg/K
Motor displacement		
D_w	100	cc/rev
Flow loss coefficient		
C_{Q1}	5.4×10^{-12}	m^3/s/Pa
Fluid bulk modulus		
β	1.5×10^9	Pa

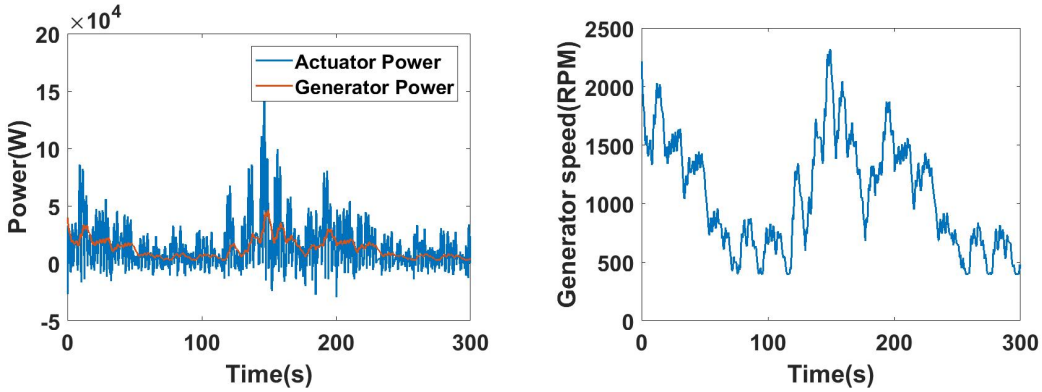

Figure 6.10: The power extracted by the actuator and the generator and the generator speed

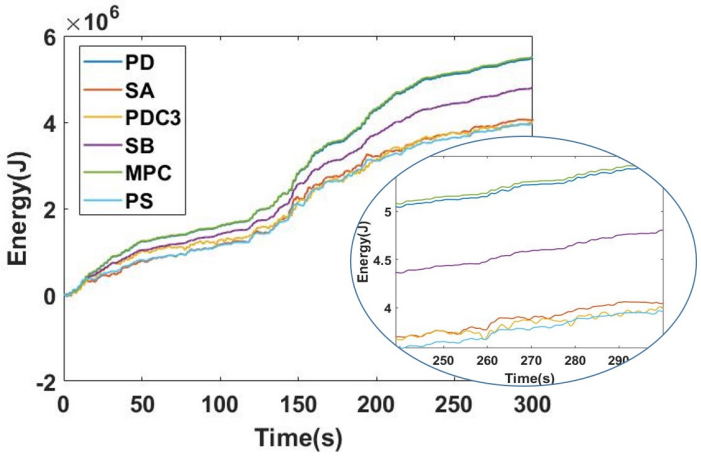

Figure 6.9: The energy extracted accounting for displacement and force constraints, including the hydraulic system dynamics model.

To present detailed plots for the response of the buoy, only one control method is selected as a sample to avoid excessive figures in the paper. The SB method is selected here to present the detailed WEC response in this section. The angular displacement of the buoy is shown in the first part in Figure 6.11; the maximum angular displacement is about 10 degrees and it is below 5 degrees most of the time. The angular

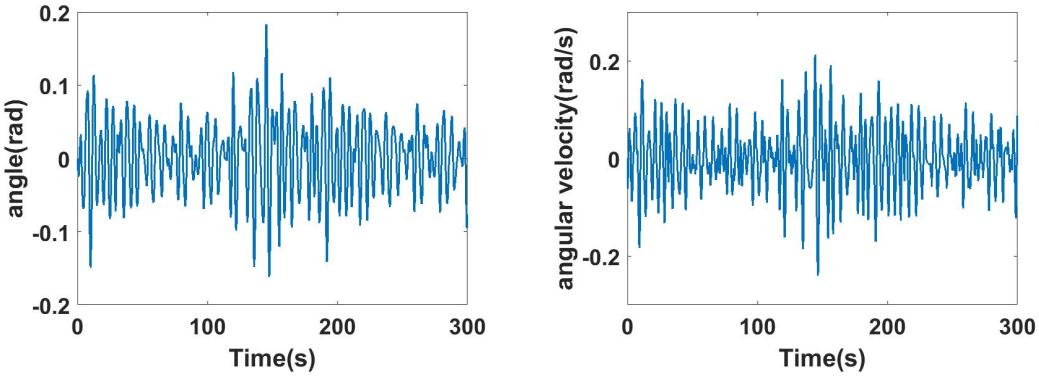

Figure 6.11: The rotational angle and the angular velocity

velocity of the buoy is shown in the second part in Figure 6.11. The cylinder force and the PTO torque are shown in Figures 6.12, respectively. Both the reference and actual values are plotted in each of the two figures. As can be seen in Figure 6.12, the control force is below the force limit of 215 kN. The accumulator pressure is shown in Figure 6.13. The high pressure is oscillating around 100 bar, while the low pressure is stable around 20 bar. The chamber pressure is also shown in Figure 6.13. Significant fluctuations can be observed when the hydraulic system is extracting energy. This is necessary to be able to track the reference control command effectively. However, those fluctuations may be reduced by increasing the valve opening area or including relief valves.

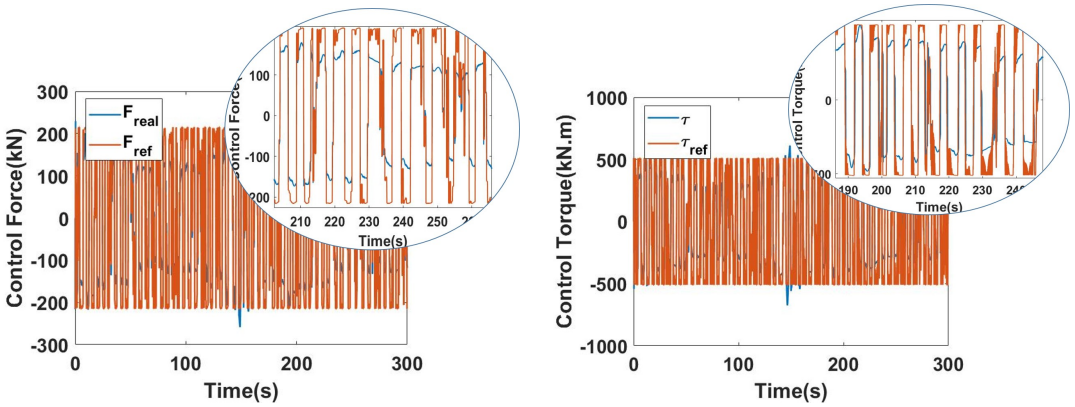

Figure 6.12: The cylinder force and the PTO torque

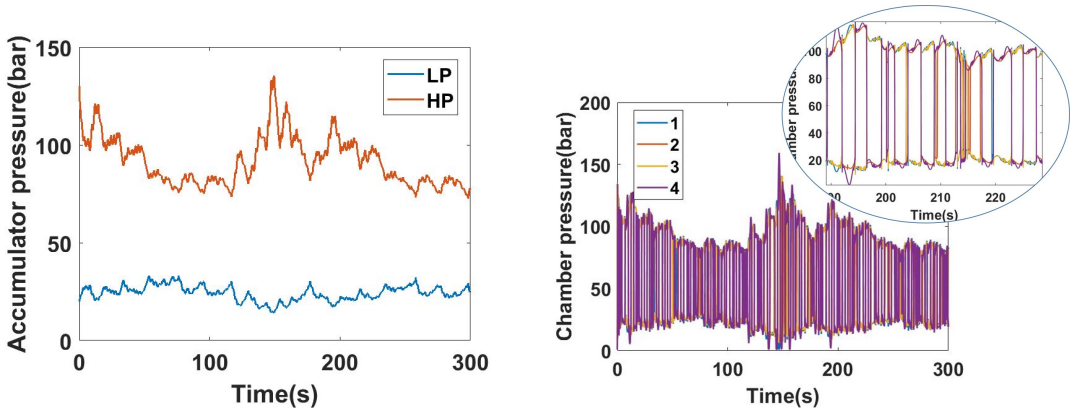

Figure 6.13: The pressure of the accumulator and the chamber

6.2.5 Discussion

In this study, different recent control methods are tested using a simulation tool that simulates a hydraulic PTO system. In a theoretical test (where PTO is assumed to track the reference control command ideally and in the absence of all constraints,) the SA controller has the best performance in terms of energy extraction. However, the performance of the SA controller with the hydraulic system model included is

the poorest among the tested six control methods. To get more insight into this phenomenon, consider Table 6.2 that presents data for three controllers (SA, PD, and PDC3) in the theoretical test case. As can be seen in Table 6.2, the energy extracted by the PD controller in this theoretical test is about 60% of that of the SA controller. However, the buoy maximum displacement associated with the SA control is significantly greater than that of the PD control (almost three times higher) which makes it more difficult to achieve. Similarly, the maximum control force required by the SA control is significantly greater than that of the PD control, which means a PTO might not be able to track the command force at all times when using a SA control, while it is more likely to track a command force generated using a PD control. The data of the PDC3 control in Table 6.2 also highlights that the PDC3 control in this test case generates about the same level of average power, but in a higher displacement range and with higher force capability. This indicates that including a model for the PTO would result in favorable performance for the PD control compared to the PDC3. To highlight the impact of the PTO model on the performance of the different control strategies, consider Table 6.3. The data are presented for all the six control methods. As can be seen from Table 6.3, all the control methods reached the maximum possible control capacity allowable by the PTO. Since this maximum control force is well below that needed by the SA in Table 6.2, the amount of harvested energy in this practical case is significantly less than that computed in the theoretical case (13.49 kW compared to 35.11 kW in average power). The drop

in energy harvested using the PD control, however, is less since the maximum force needed theoretically was as high as that of the SA. The displacement of the PDC3 reached the maximum displacement allowable by the WEC (1.2 m.) This is expected since the PDC3 tends to increase the displacement and hence it would reach a limit imposed by the WEC system.

Table 6.2
Capacity requirement of the controllers without hydraulic system.

Symbol	**Value**	**Unit**
The SA controller		
$F_{PTO,max}$	3705	kN
$x_{c,max} - x_{c,min}$	3.2	m
P_{ave}	35.11	kW
The PD controller		
$F_{PTO,max}$	1119	kN
$x_{c,max} - x_{c,min}$	1.1	m
P_{ave}	21.00	kW
The PDC3 controller		
$F_{PTO,max}$	1404	kN
$x_{c,max} - x_{c,min}$	1.6	m
P_{ave}	21.08	kW

Table 6.3
Capacity requirement of the controllers with hydraulic system.

Symbol	Value	Unit
The SA controller		
$F_{PTO,max}$	215	kN
$x_{c,max} - x_{c,min}$	0.96	m
P_{ave}	13.49	kW
The PD controller		
$F_{PTO,max}$	215	kN
$x_{c,max} - x_{c,min}$	1.1	m
P_{ave}	18.26	kW
The PDC3 controller		
$F_{PTO,max}$	215	kN
$x_{c,max} - x_{c,min}$	1.2	m
P_{ave}	13.32	kW
The SB controller		
$F_{PTO,max}$	215	kN
$x_{c,max} - x_{c,min}$	0.8	m
P_{ave}	16.02	kW
The MPC controller		
$F_{PTO,max}$	215	kN

$x_{c,max} - x_{c,min}$	1.1	m
P_{ave}	18.37	kW
The PS controller		
$F_{PTO,max}$	215	kN
$x_{c,max} - x_{c,min}$	0.90	m
P_{ave}	13.22	kW

Chapter 7

Conclusion

The optimal control of the Wave Energy Converters is presented in this dissertation. The proposed controllers aim at absorbing the maximum wave energy. Several controllers are derived without considering the constraints on the displacement, velocity and the control force. However, most of the controllers consider the constraints without losing the optimality in terms of the energy extraction. The wave estimation is required for the controller, several wave estimation techniques are introduced. Further, the novel consensus estimator is developed for the estimation of the wave field in the WEC array by applying the timely communication technology. To further validate the performance of the controller, the hydraulic Power Take off unit is implemented to examine the controllers. The focus of this dissertation is on developing and validating optimal controllers.

The first part of this dissertation is regarding the development and validation of the optimal controllers for the single body WEC. The single body WEC, in this study, can be categorized as the single body heaving WEC and the single body pitching WEC. The controllers developed for these two systems have similar derivation and format since they are all single-degree-of-freedom. The single body WEC has relatively simple dynamics, hence it is convenient for the control design. The Singular Arc control (Section 3.1), the Simple Model Control (Section 3.2) and the Shape-based control (Section 4.1) are proposed for the single body WEC. The SA control and SMC control are derived based on the optimal control theory without considering the motion and control constraints. Both controllers require the wave estimation, specifically, the performance of the SA controller relies on the goodness of the estimation of the excitation force. On the other hand, the performance of the SMC control relies on the estimation of the total wave force acting on the floater. The simulation results of the SA controller is presented in Section 5.1. The results show that when the SA controller has perfect knowledge of the wave, the energy extracted by the SA controller is the same as the Complex Conjugate Controller. That confirms the SA controller is a time domain implementation of the Complex Conjugate Control. Further, the energy extracted by the SA controller with wave estimation is still close to the Complex Conjugate Controller. Section 5.2.1 shows the simulation results of the SMC. When there is an accurate estimation of the total wave force, the energy extracted by the SMC controller can be very close to the Ideal SA controller which is simulated based

on perfect knowledge of the wave.

Considering the constrained optimal control developed for the single body WEC. The SB controller is derived by assuming the trajectory of the velocity of the buoy and solve the coefficients of the velocity profile by optimization. It can be considered as a numerical optimal control. The SB controller is further validated with the hydraulic system which is shown in Section 6.2.4. The performance of the SB controller is worse than the PD and MPC controller, however, it is better than the PDC3, PS and SA controller. Hence it has a good robustness with the complex dynamics.

The second part of this dissertation presents the control design for the single body three-degree-of-freedom WEC. The three-degree-of-freedom WEC moves in the surge, heave and pitch mode. The heave motion is proven to be independent of the other two modes when the motion is small. Hence, the control design can be separated as the control design for the heave motion (1-DoF) and for the surge-pitch coupled motion (2-DoF). The Pseudospectral optimal control and the Linear Quadratic Gaussian optimal control are implemented for the 3-DoF system. Although those two controllers both require the wave estimation, only the performance with wave estimation of the LQG controller is discussed in this dissertation. The simulation results of the LQG controller is shown in Section 5.2.2. The results show that with a good accuracy of the estimation, the LQG controller can extract the major amount of energy of the LQ controller which assumes the perfect knowledge of the wave. Additionally, the

energy extracted from the three modes is significantly higher than 3 times the heave-only mode due to the parametric excitation. That also indicates with the proper controller, the nonlinearity of the wave energy conversion problem can be utilized to generate more energy. The PS control is validated with the hydraulic system presented in Section 6.2.4. The performance of the PS controller is worse than the other optimal controllers which indicate the PS controller is hard to be adaptive to complex dynamics.

Based on the simulation results shown in Section 6.2.4. We can also point out the PD control and the MPC control has the best performance. However, to implement the MPC control, the wave prediction is required and it is relatively computational expensive than the PD control. Although the optimal controls are derived based on maximizing the energy capture, the PD control is very simple to be implemented and is very robust. Additionally, most of the optimal controllers, although shows a good performance theoretically (without real PTO implementation), they are not robust when they are implemented with the PTO unit. That does not mean the optimal control are always worse than the PD control. That indicates the optimal control needs to be solved by considering the dynamics not only of the wave-buoy interaction but also of the wave estimation unit and PTO unit.

In the last, we discuss the Collective Control and the consensus estimation of the WEC array. The Collective Controller applies the PD feedback control law, where the PD

feedback control gains are optimized in terms of energy extraction and constraints. The Consensus estimation of the WEC array applies the communication technology to improve the estimation. The simulation results show a significant improvement of the accuracy of the estimation and the disagreement among all the agents in the WEC array.

7.1 Future work

Regarding the research of the WEC array, the Collective Control is only preliminarily constructed for the WEC array. Additionally, the Consensus estimation of the wave field is only validated for an uncoupled, unforced WEC array. Hence, the future work will focus on the development of the controllers, estimators and PTO units of the WEC array.

First, the Collective control needs to be further optimized to have a robust performance. Second, the consensus estimation needs to be extended to a coupled, forced WEC array. Finally, the PTO units need to be considered in the control design. So that we can validate our controllers through a realistic wave to wire model.

References

[1] O. Abdelkhalik, S. Zou, R. Robinett, G. Bacelli, D. Wilson, and R. Coe, "Control of three degrees-of-freedom wave energy converters using pseudo-spectral methods." *Journal of Dynamic Systems, Measurement, and Control*, vol. 140(7), no. 9, pp. 074 501–074 501–9, 2018.

[2] S. Zou, O. Abdelkhalik, R. Robinett, G. Bacelli, and D. Wilson, "Optimal control of wave energy converters," *Renewable energy*, vol. 103, pp. 217–225, 2017.

[3] O. Abdelkhalik and S. Zou, "Control of wave energy converters using a simple dynamic model," *IEEE Transactions on Sustainable Energy*, 2018.

[4] O. Abdelkhalik, S. Zou, R. Robinett, G. Bacelli, and D. Wilson, "Estimation of excitation forces for wave energy converters control using pressure measurements," *International Journal of Control*, vol. 90, no. 8, pp. 1793–1805, 2017.

[5] O. Abdelkhalik, R. Robinett, S. Zou, G. Bacelli, R. Coe, D. Bull, D. Wilson,

and U. Korde, "On the control design of wave energy converters with wave prediction," *Journal of Ocean Engineering and Marine Energy*, vol. 2, no. 4, pp. 473–483, 2016.

[6] S. Zou and O. Abdelkhalik, "Control of wave energy converters with discrete displacement hydraulic power take-off units," *Journal of Marine Science and Engineering*, vol. 6, no. 2, p. 31, 2018.

[7] ——, "Time-varying linear quadratic gaussian optimal control for three-degree-of-freedom wave energy converters." *Renewable Energy*, under review.

[8] ——, "Consensus estimation in arrays of wave energy converters," *IEEE Transactions on Sustainable Energy*, 2018.

[9] O. Abdelkhalik and S. Zou, "The collective control of the wec array surrogate model," draft.

[10] F. d. O. Antonio, "Wave energy utilization: A review of the technologies," *Renewable and sustainable energy reviews*, vol. 14, no. 3, pp. 899–918, 2010.

[11] M.-F. Hsieh, I.-H. Lin, D. G. Dorrell, M.-J. Hsieh, and C.-C. Lin, "Development of a wave energy converter using a two chamber oscillating water column," *IEEE Transactions on Sustainable Energy*, vol. 3, no. 3, pp. 482–497, 2012.

[12] A. Sproul and N. Weise, "Analysis of a wave front parallel wec prototype," *IEEE Transactions on Sustainable Energy*, vol. 4, no. 6, pp. 1183–1189, 2015.

[13] J. Falnes, "A review of wave-energy extraction," *Marine structures*, vol. 20, no. 4, pp. 185–201, 2007.

[14] E. Renzi and F. Dias, "Hydrodynamics of the oscillating wave surge converter in the open ocean," *European Journal of Mechanics-B/Fluids*, vol. 41, pp. 1–10, 2013.

[15] R. H. Hansen, M. M. Kramer, and E. Vidal, "Discrete displacement hydraulic power take-off system for the wavestar wave energy converter," *Energies*, vol. 6, no. 8, pp. 4001–4044, 2013.

[16] K. Budal and J. Falnes, "Optimum operation of improved wave-power converter," *Mar. Sci. Commun.;(United States)*, vol. 3, no. 2, 1977.

[17] S. H. Salter, "Power conversion systems for ducks." IEE'Future Energy Concepts' Conference, 1979.

[18] U. A. Korde, "On control approaches for efficient primary energy conversion in irregular waves," in *OCEANS'98 Conference Proceedings*, vol. 3. IEEE, 1998, pp. 1427–1431.

[19] F. Fusco and J. V. Ringwood, "Hierarchical robust control of oscillating wave energy converters with uncertain dynamics," *IEEE Trans. Sustain. Energy*, vol. 5, no. 3, pp. 958–966, 2014.

[20] J. V. Ringwood, G. Bacelli, and F. Fusco, "Energy-maximizing control of wave-energy converters: The development of control system technology to optimize their operation," *IEEE Control Systems*, vol. 34, no. 5, pp. 30–55, 2014.

[21] J. Scruggs, S. Lattanzio, A. Taflanidis, and I. Cassidy, "Optimal causal control of a wave energy converter in a random sea," *Applied Ocean Research*, vol. 42, pp. 1–15, 2013.

[22] G. Li and M. R. Belmont, "Model predictive control of a sea wave energy converter: a convex approach," *IFAC Proceedings Volumes*, vol. 47, no. 3, pp. 11 987–11 992, 2014.

[23] G. Bacelli and J. V. Ringwood, "Numerical optimal control of wave energy converters," *IEEE Trans. Sustain. Energy*, vol. 6, no. 2, pp. 294–302, 2015.

[24] J. Song, O. Abdelkhalik, R. Robinett, G. Bacelli, D. Wilson, and U. Korde, "Multi-resonant feedback control of heave wave energy converters," *Ocean Engineering*, vol. 127, pp. 269–278, 2016.

[25] J. Falnes, *Ocean waves and oscillating systems: linear interactions including wave-energy extraction*. Cambridge university press, 2002.

[26] G. Li, G. Weiss, M. Mueller, S. Townley, and M. R. Belmont, "Wave energy converter control by wave prediction and dynamic programming," *Renewable Energy*, vol. 48, pp. 392–403, 2012.

[27] A. E. Bryson, *Applied optimal control: optimization, estimation and control*. Routledge, 2018.

[28] J. Cortes, "Discontinuous dynamical systems," *IEEE Control Systems*, vol. 28, no. 3, 2008.

[29] A. A. Agrachev and Y. Sachkov, *Control theory from the geometric viewpoint*. Springer Science & Business Media, 2013, vol. 87.

[30] S. Bennett, *A history of control engineering, 1930-1955*. IET, 1993, no. 47.

[31] B. Brogliato, "Nonsmooth impact mechanicsmodels, dynamics and control, ser," *Lecture Notes in Control and Information Sciences. London: Springer*, vol. 220, 1996.

[32] V. I. Utkin, *Sliding modes in control and optimization*. Springer Science & Business Media, 2013.

[33] D. Evans, "Some theoretical aspects of three-dimensional wave-energy absorbers," in *Proceedings of the first symposium on wave energy utilization, Chalmers University of Technology, Gothenburg, Sweden*, 1979, pp. 77–106.

[34] M. French and R. Bracewell, "Ps frog a point-absorber wave energy converter working in a pitch/surge mode," in *Fifth International Conference on Energy Options: The Role of Alternatives in the World Energy Scene, University of*

Reading, Reading, UK. http://citeseerx. ist. psu. edu/viewdoc/download. Citeseer, 1987.

[35] H. Yavuz, "On control of a pitching and surging wave energy converter," *International journal of green energy*, vol. 8, no. 5, pp. 555–584, 2011.

[36] C. Villegas and H. van der Schaaf, "Implementation of a pitch stability control for a wave energy converter," in *Proc. 10th Euro. Wave and Tidal Energy Conf. Southampton, UK*, 2011.

[37] H. E. Young and J. Pollock, "Variable coefficient control of a wave-energy device," The University of Edinburgh, Tech. Rep., 1985.

[38] K. Budal, "Theory for absorption of wave power by a system of interacting bodies," *Journal of Ship Research*, vol. 21, no. 4, 1977.

[39] J. Falnes and K. Budal, "Wave-power absorption by parallel rows of interacting oscillating bodies," *Applied Ocean Research*, vol. 4, no. 4, pp. 194–207, 1982.

[40] G. Thomas and D. Evans, "Arrays of three-dimensional wave-energy absorbers," *Journal of Fluid Mechanics*, vol. 108, pp. 67–88, 1981.

[41] P. McIver, "Some hydrodynamic aspects of arrays of wave-energy devices," *Applied Ocean Research*, vol. 16, no. 2, pp. 61–69, 1994.

[42] S. Mavrakos and P. Koumoutsakos, "Hydrodynamic interaction among vertical axisymmetric bodies restrained in waves," *Applied Ocean Research*, vol. 9, no. 3, pp. 128–140, 1987.

[43] H. Kagemoto and D. K. Yue, "Interactions among multiple three-dimensional bodies in water waves: an exact algebraic method," *Journal of Fluid mechanics*, vol. 166, pp. 189–209, 1986.

[44] T. Kinoshita, W. Bao, and S. Sunahara, "The hydrodynamic forces acting on a cylinder array oscillating in waves and current," *Journal of Marine Science and Technology*, vol. 2, no. 3, pp. 135–147, 1997.

[45] D. Evans, "Some analytic results for two and three dimensional wave-energy absorbers," *Power from sea waves*, pp. 213–249, 1980.

[46] M. Simon, "Multiple scattering in arrays of axisymmetric wave-energy devices. part 1. a matrix method using a plane-wave approximation," *Journal of Fluid Mechanics*, vol. 120, pp. 1–25, 1982.

[47] B. F. M. Child, "On the configuration of arrays of floating wave energy converters," 2011.

[48] S. Mavrakos, "Hydrodynamic coefficients for groups of interacting vertical axisymmetric bodies," *Ocean Engineering*, vol. 18, no. 5, pp. 485–515, 1991.

[49] B. Child and V. Venugopal, "Interaction of waves with an array of floating wave energy devices," in *Proceedings of the 7th European Wave and Tidal Energy Conference, Porto, Portugal*, 2007.

[50] ——, "Modification of power characteristics in an array of floating wave energy devices," in *Proceedings of the 8th European Wave and Tidal Energy Conference, Uppsala, Sweden*, 2009, pp. 309–318.

[51] ——, "Optimal configurations of wave energy device arrays," *Ocean Engineering*, vol. 37, no. 16, pp. 1402–1417, 2010.

[52] ——, "Non-optimal tuning of wave energy device arrays," in *2nd International conference on Ocean Energy (ICOE)*, 2008, pp. 15–17.

[53] H. Wolgamot, P. Taylor, and R. E. Taylor, "The interaction factor and directionality in wave energy arrays," *Ocean Engineering*, vol. 47, pp. 65–73, 2012.

[54] P. C. Vicente, F. d. O. António, L. M. Gato, and P. A. Justino, "Dynamics of arrays of floating point-absorber wave energy converters with inter-body and bottom slack-mooring connections," *Applied Ocean Research*, vol. 31, no. 4, pp. 267–281, 2009.

[55] M. Folley and T. Whittaker, "The effect of sub-optimal control and the spectral wave climate on the performance of wave energy converter arrays," *Applied Ocean Research*, vol. 31, no. 4, pp. 260–266, 2009.

[56] B. Borgarino, A. Babarit, and P. Ferrant, "Impact of wave interactions effects on energy absorption in large arrays of wave energy converters," *Ocean Engineering*, vol. 41, pp. 79–88, 2012.

[57] C. Fitzgerald and G. Thomas, "A preliminary study on the optimal formation of an array of wave power devices," in *Proceedings of the 7th European Wave and Tidal Energy Conference, Porto, Portugal*, 2007, pp. 11–14.

[58] D. Sarkar, E. Contal, N. Vayatis, and F. Dias, "Prediction and optimization of wave energy converter arrays using a machine learning approach," *Renewable Energy*, vol. 97, pp. 504–517, 2016.

[59] E. Jansson, "Multi-buoy wave energy converter: Electrical power smoothening from array configuration," 2016.

[60] P. Justino and A. Clément, "Hydrodynamic performance for small arrays of submerged spheres," in *5th European Wave Energy Conference*, 2003.

[61] P. Ricci, J.-B. Saulnier, and A. Falcão, "Point-absorber arrays: a configuration study off the portuguese west-coast," in *Proceedings of 7th European Wave and Tidal Energy Conference, Porto, Portugal, September*, 2007, pp. 11–13.

[62] B. Borgarino, A. Babarit, and P. Ferrant, "Impact of long separating distance between interacting wave energy converters on the overall energy extraction of a dense array." in *9th European Wave and Tidal Energy Conference*, 2011.

[63] J. Cruz, R. Sykes, P. Siddorn, and R. E. Taylor, "Estimating the loads and energy yield of arrays of wave energy converters under realistic seas," *IET Renewable Power Generation*, vol. 4, no. 6, pp. 488–497, 2010.

[64] G. Bacelli, P. Balitsky, and J. V. Ringwood, "Coordinated control of arrays of wave energy devicesbenefits over independent control," *IEEE Transactions on Sustainable Energy*, vol. 4, no. 4, pp. 1091–1099, 2013.

[65] P. Balitsky, "Modelling controlled arrays of wave energy converters," Ph.D. dissertation, National University, 2013.

[66] D. Oetinger, M. E. Magaña, and O. Sawodny, "Decentralized model predictive control for wave energy converter arrays," *IEEE Transactions on Sustainable Energy*, vol. 5, no. 4, pp. 1099–1107, 2014.

[67] M. Starrett, R. So, T. K. Brekken, and A. McCall, "Increasing power capture from multibody wave energy conversion systems using model predictive control," in *Technologies for Sustainability (SusTech), 2015 IEEE Conference on*. IEEE, 2015, pp. 20–26.

[68] P. B. Garcia-Rosa, G. Bacelli, and J. V. Ringwood, "Control-informed optimal array layout for wave farms," *IEEE Transactions on Sustainable Energy*, vol. 6, no. 2, pp. 575–582, 2015.

[69] K. Budal, "Model experiment with a phase-controlled point absorber," in *2nd*

International Symposium on Wave and Tidal Energy, Cambridge, UK, 23-25 September 1981, 1981, pp. 191–206.

[70] H. Eidsmoen, "Simulation of a slack-moored heaving-buoy wave-energy converter with phase control," 1996.

[71] B. Drew, A. R. Plummer, and M. N. Sahinkaya, "A review of wave energy converter technology," 2009.

[72] P. Ricci, J. Lopez, M. Santos, J. Villate, P. Ruiz-Minguela, F. Salcedo, and A. d. O. Falcao, "Control strategies for a simple point-absorber connected to a hydraulic power take-off," in *Proceedings of 8th European Wave and Tidal Energy Conference, Uppsala, Sweden*, 2009, pp. 7–10.

[73] A. Têtu, "Power take-off systems for wecs," in *Handbook of Ocean Wave Energy*. Springer, 2017, pp. 203–220.

[74] S. H. Salter, J. Taylor, and N. Caldwell, "Power conversion mechanisms for wave energy," *Proceedings of the Institution of Mechanical Engineers, Part M: Journal of Engineering for the Maritime Environment*, vol. 216, no. 1, pp. 1–27, 2002.

[75] U. A. Korde, "A power take-off mechanism for maximizing the performance of an oscillating water column wave energy device," *Applied ocean research*, vol. 13, no. 2, pp. 75–81, 1991.

[76] L. Gato and A. d. O. Falcão, "Aerodynamics of the wells turbine," *International Journal of Mechanical Sciences*, vol. 30, no. 6, pp. 383–395, 1988.

[77] L. Gato *et al.*, "Performance of the wells turbine with a double row of guide vanes," *JSME international journal. Ser. 2, Fluids engineering, heat transfer, power, combustion, thermophysical properties*, vol. 33, no. 2, pp. 265–271, 1990.

[78] M. Inoue, K. Kaneko, and T. Setoguchi, "Studies on wells turbine for wave power generator: Part 3; effect of guide vanes," *Bulletin of JSME*, vol. 28, no. 243, pp. 1986–1991, 1985.

[79] M. Inoue, K. Kaneko, T. Setoguchi, and S. Raghunathan, "Simulation of starting characteristics of the wells turbine," in *4th Joint Fluid Mechanics, Plasma Dynamics and Lasers Conference*, 1986, p. 1122.

[80] K. Kaneko, T. Setoguchi, and M. Inoue, "Performance of wells turbine in oscillating flow," *Proc Current Practices and New Tech in Ocean Eng*, pp. 447–452, 1986.

[81] S. Raghunathan, "The wells air turbine for wave energy conversion," *Progress in Aerospace Sciences*, vol. 31, no. 4, pp. 335–386, 1995.

[82] S. Raghunathan and C. Tan, "Performance of the wells turbine at starting," *Journal of Energy*, vol. 6, no. 6, pp. 430–431, 1982.

[83] M. Inoue, K. Kaneko, and T. Setoguchi, "Determination of optimum geometry of wells turbine rotor for wave power generator–part ii: considerations for practical use," *Proc curr pract new tech Ocean Engg*, vol. 2, pp. 441–446, 1986.

[84] T. Setoguchi, M. Takao, K. Kaneko, M. Inoue *et al.*, "Effect of guide vanes on the performance of a wells turbine for wave energy conversion," *International Journal of Offshore and Polar Engineering*, vol. 8, no. 02, 1998.

[85] M. Inoue, K. Kaneko, T. Setoguchi, and H. Hamakawa, "Air turbine with self-pitch-controlled blades for wave power generator (estimation of performance by model testing)," *JSME international journal. Ser. 2, Fluids engineering, heat transfer, power, combustion, thermophysical properties*, vol. 32, no. 1, pp. 19–24, 1989.

[86] M. Katsuhara, F. Kitamura, K. Kajiwara, and Y. Ohta, "Characteristics of air turbines for wave activated generator used as light beacon," in *Proceedings of 2nd symposium on wave energy utilization in Japan, JAMSTEC*, 1987, pp. 83–91.

[87] T. Kim, T. Setoguchi, K. Kaneko, and M. Takao, "The optimization of blade pitch settings of an air turbine using self-pitch-controlled blades for wave power conversion," *Journal of solar energy engineering*, vol. 123, no. 4, pp. 382–386, 2001.

[88] D. Richards and F. B. Weiskopf, "Studies with, and testing of the mccormick pneumatic wave energy turbine with some comments on pwecs systems," in *Utilization of Ocean WavesWave to Energy Conversion*. ASCE, 1986, pp. 80–102.

[89] M. McCormick, J. Rehak, and B. Williams, "An experimental study of a bidirectional radial turbine for pneumatic wave energy conversion," in *OCEANS'92. Mastering the Oceans Through Technology. Proceedings.*, vol. 2. IEEE, 1992, pp. 866–870.

[90] T. Setoguchi, K. Kaneko, H. Maeda, T. Kim, M. Inoue *et al.*, "Impulse turbine with self-pitch-controlled guide vanes for wave power conversion: performance of mono-vane type," *International Journal of Offshore and Polar Engineering*, vol. 3, no. 01, 1993.

[91] T. Setoguchi, M. Takao, Y. Kinoue, K. Kaneko, S. Santhakumar, M. Inoue *et al.*, "Study on an impulse turbine for wave energy conversion," in *The Ninth International Offshore and Polar Engineering Conference*. International Society of Offshore and Polar Engineers, 1999.

[92] M. Takao and T. Setoguchi, "Air turbines for wave energy conversion," *International Journal of Rotating Machinery*, vol. 2012, 2012.

[93] S. Santhakumar, "Report of workshop on turbine for ocean energy application," *Indian Institute of Technology, Madras, India*, 1996.

[94] S. Santhakumar, V. Jayashankar, M. Atmanand, A. Pathak, M. Ravindran, T. Setoguchi, M. Takao, K. Kaneko *et al.*, "Performance of an impulse turbine based wave energy plant," in *The Eighth International Offshore and Polar Engineering Conference*. International Society of Offshore and Polar Engineers, 1998.

[95] T. Setoguchi, S. Santhakumar, M. Takao, T. Kim, and K. Kaneko, "A performance study of a radial turbine for wave energy conversion," *Proceedings of the Institution of Mechanical Engineers, Part A: Journal of Power and Energy*, vol. 216, no. 1, pp. 15–22, 2002.

[96] M. Takao, Y. Fujioka, and T. Setoguchi, "Effect of pitch-controlled guide vanes on the performance of a radial turbine for wave energy conversion," *Ocean engineering*, vol. 32, no. 17, pp. 2079–2087, 2005.

[97] K. Rhinefrank, J. Prudell, and A. Schacher, "Development and characterization of a novel direct drive rotary wave energy point absorber mts-ieee oceans conference proceedings," in *OCEANS 2009, MTS/IEEE Biloxi-Marine Technology for Our Future: Global and Local Challenges*. IEEE, 2009, pp. 1–5.

[98] K. Rhinefrank, A. Schacher, J. Prudell, T. K. Brekken, C. Stillinger, J. Z. Yen, S. G. Ernst, A. von Jouanne, E. Amon, R. Paasch *et al.*, "Comparison of direct-drive power takeoff systems for ocean wave energy applications," *IEEE Journal of Oceanic Engineering*, vol. 37, no. 1, pp. 35–44, 2012.

[99] Y. Sang, *A suboptimal control strategy for a slider crank wave energy converter power take-off system.* Western Carolina University, 2015.

[100] N. Baker and M. A. Mueller, "Direct drive wave energy converters," *Rev. Energ. Ren.: Power Engineering*, vol. 1, pp. 1–7, 2001.

[101] M. Mueller, "Electrical generators for direct drive wave energy converters," *IEE Proceedings-generation, transmission and distribution*, vol. 149, no. 4, pp. 446–456, 2002.

[102] N. Baker, M. Mueller, and P. Brooking, "Electrical power conversion in direct drive wave energy converters," in *Proceedings of the European Wave Energy Conference, Cork, Ireland*, 2003, pp. 197–204.

[103] E. Enferad, D. Nazarpour, S. Golshannavaz, and F. Aminifar, "Direct drive surge wave energy converter with grid integration functionality," *International Transactions on Electrical Energy Systems*, vol. 26, no. 5, pp. 1066–1084, 2016.

[104] T. Kovaltchouk, B. Multon, H. B. Ahmed, J. Aubry, F. Rongere, and A. Glumineau, "Influence of control strategy on the global efficiency of a direct wave energy converter with electric power take-off," in *Ecological Vehicles and Renewable Energies (EVER), 2013 8th International Conference and Exhibition on.* IEEE, 2013, pp. 1–10.

[105] H. Mendonca and S. Martinez, "A resistance emulation approach to optimize

the wave energy harvesting for a direct drive point absorber," *IEEE Transactions on Sustainable Energy*, vol. 7, no. 1, pp. 3–11, 2016.

[106] J. K.-H. Shek, D. E. Macpherson, M. A. Mueller, and J. Xiang, "Reaction force control of a linear electrical generator for direct drive wave energy conversion," *IET renewable power generation*, vol. 1, no. 1, pp. 17–24, 2007.

[107] F. Ferri and P. Kracht, "Implementation of a hydraulic power take-off for wave energy applications," *Recuperado de http://www. sdwed. civil. aau. dk/digitalAssets/97/97533_d4*, vol. 7, 2013.

[108] A. Plummer and C. Cargo, "Power transmissions for wave energy converters: a review," in *8th International Fluid Power Conference (IFK)*. University of Bath, 2012.

[109] F. d. O. Antonio, "Modelling and control of oscillating-body wave energy converters with hydraulic power take-off and gas accumulator," *Ocean engineering*, vol. 34, no. 14, pp. 2021–2032, 2007.

[110] F. d. O. António, "Phase control through load control of oscillating-body wave energy converters with hydraulic pto system," *Ocean Engineering*, vol. 35, no. 3, pp. 358–366, 2008.

[111] P. Ricci, J. Lopez, M. Santos, P. Ruiz-Minguela, J. Villate, F. Salcedo *et al.*, "Control strategies for a wave energy converter connected to a hydraulic power take-off," *IET renewable power generation*, vol. 5, no. 3, pp. 234–244, 2011.

[112] R. H. Hansen, *Design and control of the powertake-off system for a wave energy converter with multiple absorbers.* Videnbasen for Aalborg UniversitetVBN, Aalborg UniversitetAalborg University, Det Teknisk-Naturvidenskabelige FakultetThe Faculty of Engineering and Science.

[113] A. Babarit, M. Guglielmi, and A. H. Clément, "Declutching control of a wave energy converter," *Ocean Engineering*, vol. 36, no. 12, pp. 1015–1024, 2009.

[114] H. Eidsmoen, "Tight-moored amplitude-limited heaving-buoy wave-energy converter with phase control," *Applied Ocean Research*, vol. 20, no. 3, pp. 157–161, 1998.

[115] C. Josset, A. Babarit, and A. Clément, "A wave-to-wire model of the searev wave energy converter," *Proceedings of the institution of mechanical engineers, Part M: Journal of Engineering for the Maritime Environment*, vol. 221, no. 2, pp. 81–93, 2007.

[116] R. Henderson, "Design, simulation, and testing of a novel hydraulic power take-off system for the pelamis wave energy converter," *Renewable energy*, vol. 31, no. 2, pp. 271–283, 2006.

[117] D. Zhang, W. Li, Y. Ying, H. Zhao, Y. Lin, and J. Bao, "Wave energy converter of inverse pendulum with double action power take off," *Proceedings of the Institution of Mechanical Engineers, Part C: Journal of Mechanical Engineering Science*, vol. 227, no. 11, pp. 2416–2427, 2013.

[118] J. C. Antolín-Urbaneja, A. Cortés, I. Cabanes, P. Estensoro, J. Lasa, and M. Marcos, "Modeling innovative power take-off based on double-acting hydraulic cylinders array for wave energy conversion," *Energies*, vol. 8, no. 3, pp. 2230–2267, 2015.

[119] C. Cargo, A. Hillis, and A. Plummer, "Optimisation and control of a hydraulic power take-off unit for a wave energy converter in irregular waves," *Proceedings of the Institution of Mechanical Engineers, Part A: Journal of Power and Energy*, vol. 228, no. 4, pp. 462–479, 2014.

[120] K. Sun, W. Ge, L. Luo, H. Liang, C. Xu, J. Leng, Z. Yuan, and H. Huang, "Research on the hydraulic power take-off unit of a hybrid wave energy converter," in *OCEANS 2016-Shanghai*. IEEE, 2016, pp. 1–4.

[121] R. H. Hansen, T. O. Andersen, and H. C. Pedersen, "Model based design of efficient power take-off systems for wave energy converters," in *12th Scandinavian International Conference on Fluid Power, SICFP 2011*. Tampere University Press, 2011, pp. 35–49.

[122] Y. Kamizuru, *Development of hydrostatic drive trains for wave energy converters*. Shaker, 2014.

[123] J. Hals, R. Taghipour, and T. Moan, "Dynamics of a force-compensated two-body wave energy converter in heave with hydraulic power take-off subject to

phase control," in *Proceedings of the 7th European Wave and Tidal Energy Conference, Porto, Portugal*, 2007, pp. 11–14.

[124] R. Costello, J. Ringwood, and J. Weber, "Comparison of two alternative hydraulic pto concepts for wave energy conversion," in *Proceedings of the 9th European wave and tidal energy conference (EWTEC)*. School of Civil Engineering and the Environment, University of Southampton, 2011.

[125] Y. Kamizuru, M. Liermann, and H. Murrenhoff, "Simulation of an ocean wave energy converter using hydraulic transmission."

[126] M. Penalba, N. P. Sell, A. J. Hillis, and J. V. Ringwood, "Validating a wave-to-wire model for a wave energy converterpart i: The hydraulic transmission system," *Energies*, vol. 10, no. 7, p. 977, 2017.

[127] K. Schlemmer, F. Fuchshumer, N. Böhmer, R. Costello, and C. Villegas, "Design and control of a hydraulic power take-off for an axi-symmetric heaving point absorber," in *Proceedings of the Nineth European Wave and Tidal Energy Conference, Southampton*, 2011.

[128] J. F. Gaspar, M. Calvário, M. Kamarlouei, and C. G. Soares, "Power take-off concept for wave energy converters based on oil-hydraulic transformer units," *Renewable Energy*, vol. 86, pp. 1232–1246, 2016.

[129] E. V. Sánchez, R. H. Hansen, and M. M. Kramer, "Control performance assessment and design of optimal control to harvest ocean energy," *IEEE Journal of Oceanic Engineering*, vol. 40, no. 1, pp. 15–26, 2015.

[130] W. Cummins, "The impulse response function and ship motions," David Taylor Model Basin Washington DC, Tech. Rep., 1962.

[131] C. Lee, *WAMIT Theory Manual*, ser. Report (Massachusetts Institute of Technology. Department of Ocean Engineering). Massachusetts Institute of Technology, Department of Ocean Engineering, 1995. [Online]. Available: http://books.google.com/books?id=fWKGHAAACAAJ

[132] A. Babarit and G. Delhommeau, "Theoretical and numerical aspects of the open source BEM solver NEMOH," in *11th European Wave and Tidal Energy Conference (EWTEC2015)*, ser. Proceedings of the 11th European Wave and Tidal Energy Conference, Nantes, France, Sep. 2015. [Online]. Available: https://hal.archives-ouvertes.fr/hal-01198800

[133] I. ANSYS, "Ansys aqwa v14. 0," *URL www. ansys. com*, 2014.

[134] H. Krogstad and Ø. Arntsen, "Linear wave theory," *Norwegian University of Science and Technology, Trondheim*, 2000.

[135] Z. Yu and J. Falnes, "State-space modelling of a vertical cylinder in heave," *Applied Ocean Research*, vol. 17, no. 5, pp. 265–275, 1995.

[136] T. Perez and T. I. Fossen, "A matlab toolbox for parametric identification of radiation-force models of ships and offshore structures," 2009.

[137] K. Szabelski, "The vibrations of self-excited system with parametric excitation and non-symmetric elasticity characteristic," *Journal of Theoretical and Applied Mechanics*, vol. 29, no. 1, pp. 57–81, 1991.

[138] M. Clifford and S. Bishop, "Locating oscillatory orbits of the parametrically-excited pendulum," *The ANZIAM Journal*, vol. 37, no. 3, pp. 309–319, 1996.

[139] F. Dohnal and B. Mace, "Amplification of damping of a cantilever beam by parametric excitation," *Proc 9th MOVIC*, 2008.

[140] P. H. Nguyen and J. H. Ginsberg, "Vibration control using parametric excitation," *Journal of Vibration and Acoustics*, vol. 123, no. 3, pp. 359–364, 2001.

[141] E. I. Butikov, "Parametric excitation of a linear oscillator," *European Journal of Physics*, vol. 25, no. 4, p. 535, 2004.

[142] B. Zaghari, M. Ghandchi Tehrani, and E. Rustighi, "Mechanical modelling of a vibration energy harvester with time-varying stiffness," 2014.

[143] B. Zaghari, G. Tehrani, and E. Rustighi, "Energy harvesting using parametric excitation," 2014.

[144] B. Sahoo, L. Panda, and G. Pohit, "Two-frequency parametric excitation and internal resonance of a moving viscoelastic beam," *Nonlinear Dynamics*, vol. 82, no. 4, pp. 1721–1742, 2015.

[145] A. Sofroniou and S. Bishop, "Dynamics of a parametrically excited system with two forcing terms," *Mathematics*, vol. 2, no. 3, pp. 172–195, 2014.

[146] A. El-Bassiouny and M. Eissa, "Resonance of non-linear systems subjected to multi-parametrically excited structures:(comparison between two methods, response and stability)," *Physica Scripta*, vol. 70, no. 2-3, p. 101, 2004.

[147] R. G. Coe and D. L. Bull, "Nonlinear time-domain performance model for a wave energy converter in three dimensions," in *Oceans-St. John's, 2014*. IEEE, 2014, pp. 1–10.

[148] S. Darwish and O. Abdelkhalik, "Approximate surrogate models of wave energy conversion arrays using mechanical elements," *Applied Ocean Research*, under review.

[149] A. Chipperfield and P. Fleming, "The matlab genetic algorithm toolbox," 1995.

[150] P. Kasturi and P. Dupont, "Constrained optimal control of vibration dampers," *Journal of Sound and vibration*, vol. 215, no. 3, pp. 499–509, 1998.

[151] A. Forsgren, P. E. Gill, and M. H. Wright, "Interior methods for nonlinear optimization," *SIAM review*, vol. 44, no. 4, pp. 525–597, 2002.

[152] G. Bacelli, "Optimal control of wave energy converters," Ph.D. dissertation, National University of Ireland Maynooth, 2014.

[153] V. Garber, "Optimum intercept laws for accelerating targets." *AIAA Journal*, vol. 6, no. 11, pp. 2196–2198, 1968.

[154] P. Venkataraman, *Applied optimization with MATLAB programming*. John Wiley & Sons, 2009.

[155] J. L. Crassidis and J. L. Junkins, *Optimal Estimation of Dynamic Systems*. CHAPMAN&HALL/CRC, 2004.

[156] R. Olfati-Saber, "Kalman-consensus filter: Optimality, stability, and performance," in *Decision and Control, 2009 held jointly with the 2009 28th Chinese Control Conference. CDC/CCC 2009. Proceedings of the 48th IEEE Conference on*. IEEE, 2009, pp. 7036–7042.

[157] M. Folley, *Numerical Modelling of Wave Energy Converters: State-of-the-Art Techniques for Single Devices and Arrays*. Academic Press, 2016.

[158] R. Salmon, "Introduction to ocean waves," *Scripps Inst. of Oceanogr., Univ. of Calif., San Diego.[Available at http://www-pord. ucsd. edu/rsalmon/111. textbook. pdf, from SIO 111/Physics 111 Textbook, http://www-pord. ucsd. edu/rsalmon/waves. html.]*, 2014.

[159] A. Pecher and J. P. Kofoed, *Handbook of Ocean Wave Energy*. Springer, 2017.

[160] H.-N. Nguyen and P. Tona, "Wave excitation force estimation for wave energy converters of the point-absorber type," *IEEE Transactions on Control Systems Technology*, 2017.

[161] C. Cargo, A. Hillis, and A. Plummer, "Strategies for active tuning of wave energy converter hydraulic power take-off mechanisms," *Renewable Energy*, vol. 94, pp. 32–47, 2016.

[162] A. H. Hansen and H. C. Pedersen, "Reducing pressure oscillations in discrete fluid power systems," *Proceedings of the Institution of Mechanical Engineers, Part I: Journal of Systems and Control Engineering*, vol. 230, no. 10, pp. 1093–1105, 2016.

[163] R. H. Hansen, T. O. Andersen, H. C. Pedersen, and A. H. Hansen, "Control of a 420 kn discrete displacement cylinder drive for the wavestar wave energy converter," in *Proceedings of the ASME/BATH 2014 Symposium on Fluid Power and Motion Control, Bath, UK*, 2014, pp. 10–12.

[164] J. Hals, J. Falnes, and T. Moan, "Constrained optimal control of a heaving buoy wave-energy converter," *Journal of Offshore Mechanics and Arctic Engineering*, vol. 133, no. 1, pp. 1–15, 2011.

[165] D. R. Herber and J. T. Allison, "Wave energy extraction maximization in irregular ocean waves using pseudospectral methods," in *ASME 2013 International Design Engineering Technical Conferences and Computers and Information in*

Engineering Conference. American Society of Mechanical Engineers, 2013, pp. V03AT03A018–V03AT03A018.

[166] M. Kramer, L. Marquis, and P. Frigaard, "Performance evaluation of the wavestar prototype," in *EWTEC Conference-Proceedings*. Citeseer, 2011.

[167] G. Takács *et al.*, "Basics of vibration dynamics," in *Model Predictive Vibration Control*. Springer, 2012, pp. 25–64.

[168] W. J. Palm, *Mechanical vibration*. John Wiley Hoboken, NJ, 2007.

[169] J. Falnes, "Wave-energy conversion through relative motion between two single-mode oscillating bodies," *Journal of Offshore Mechanics and Arctic Engineering*, vol. 121, no. 1, pp. 32–38, 1999.

[170] S. Olaya, J.-M. Bourgeot, and M. Benbouzid, "Optimal control for a self-reacting point absorber: A one-body equivalent model approach," in *IEEE PEAC 2014*. IEEE, 2014, pp. 332–337.

[171] O. Abdelkhalik, S. Zou, R. Robinett, and U. Korde, "Time-varying linear quadratic gaussian optimal control for three-degree-of-freedom wave energy converters," in *12th European Wave and Tidal Energy Conference (EWTEC 2017)*, 2018.

[172] J. Falnes and P. M. Lillebekken, "Budal's latching-controlled-buoy type wave-power plant," 2003.

[173] G. Nolan, M. Ó Catháin, J. Murtagh, and J. Ringwood, "Modelling and simulation of the power take-off system for a hinge-barge wave-energy converter," 2003.

[174] I. Istif, A. Sagirli, and K. Kutlu, "Bond graph modeling and position control of an electrohydraulic elevator," in *Proceedings of ESDA: 6th Biennial Conference on Engineering Systems Design and Analysis, Istanbul, Turkey*, 2002.

[175] J. P. Kofoed, P. Frigaard, E. Friis-Madsen, and H. C. Sørensen, "Prototype testing of the wave energy converter wave dragon," *Renewable energy*, vol. 31, no. 2, pp. 181–189, 2006.

[176] T. Yoshida, M. Sanada, S. Morimoto, and Y. Inoue, "Study of flywheel energy storage system for power leveling of wave power generation system," in *Electrical Machines and Systems (ICEMS), 2012 15th International Conference on*. IEEE, 2012, pp. 1–5.

[177] W. Sheng, R. Alcorn, and A. Lewis, "Assessment of primary energy conversions of oscillating water columns. ii. power take-off and validations," *Journal of Renewable and Sustainable Energy*, vol. 6, no. 5, p. 053114, 2014.

[178] V. Jayashankar, S. Anand, T. Geetha, S. Santhakumar, V. J. Kumar, M. Ravindran, T. Setoguchi, M. Takao, K. Toyota, and S. Nagata, "A twin unidirectional impulse turbine topology for owc based wave energy plants," *Renewable Energy*, vol. 34, no. 3, pp. 692–698, 2009.

[179] K. Mala, J. Jayaraj, V. Jayashankar, T. Muruganandam, S. Santhakumar, M. Ravindran, M. Takao, T. Setoguchi, K. Toyota, and S. Nagata, "A twin unidirectional impulse turbine topology for owc based wave energy plants–experimental validation and scaling," *Renewable energy*, vol. 36, no. 1, pp. 307–314, 2011.

[180] A. Serena, M. Molinas, and I. Cobo, "Design of a direct drive wave energy conversion system for the seaquest concept," *Energy Procedia*, vol. 20, pp. 271–280, 2012.

[181] S. Salter and C. Lin, "The sloped ips wave energy converter," in *2nd European Wave Energy Conference, Lisbon, Portugal, November*, 1995, pp. 337–344.

[182] S. Salter and C.-P. Lin, "Wide tank efficiency measurements on a model of the sloped ips buoy," in *Proceedings of 3rd European Wave Energy Conference*, 1998, pp. 200–6.

[183] P. Brooking and M. Mueller, "Power conditioning of the output from a linear vernier hybrid permanent magnet generator for use in direct drive wave energy converters," *IEE Proceedings-Generation, Transmission and Distribution*, vol. 152, no. 5, pp. 673–681, 2005.

[184] Y. Sang, H. B. Karayaka, Y. Yan, and J. Z. Zhang, "Resonance control strategy for a slider crank wec power take-off system," in *Oceans-St. John's, 2014*. IEEE, 2014, pp. 1–8.

[185] Y. Sang, H. B. Karayaka, Y. Yan, J. Z. Zhang, E. Muljadi, and Y.-H. Yu, "Energy extraction from a slider-crank wave energy converter under irregular wave conditions," in *OCEANS'15 MTS/IEEE Washington*. IEEE, 2015, pp. 1–7.

[186] O. Keysan, A. McDonald, M. Mueller, R. Doherty, and M. Hamilton, "C-gen, a lightweight direct drive generator for marine energy converters," 2010.

[187] N. Hodgins, A. McDonald, J. Shek, O. Keysan, and M. Mueller, "Current and future developments of the c-gen lightweight direct drive generator for wave & tidal energy."

[188] E. Tedeschi, M. Molinas, M. Carraro, and P. Mattavelli, "Analysis of power extraction from irregular waves by all-electric power take off," in *Energy Conversion Congress and Exposition (ECCE), 2010 IEEE*. IEEE, 2010, pp. 2370–2377.

[189] F. d. O. António, P. A. Justino, J. C. Henriques, and J. M. André, "Reactive versus latching phase control of a two-body heaving wave energy converter," in *Control Conference (ECC), 2009 European*. IEEE, 2009, pp. 3731–3736.

[190] G. Bacelli, J. V. Ringwood, and J.-C. Gilloteaux, "A control system for a self-reacting point absorber wave energy converter subject to constraints," *Proceedings of 18th IFAC World Congress*, vol. 44, no. 1, pp. 11 387–11 392, 2011.

[191] Y. Kamizuru, L. Verdegem, P. Erhart, C. Langenstein, L. Andren, M. Lenßen, and H. Murrenhoff, "Efficient power take-offs for ocean energy conversion," in *Proceedings of the 4th International Conference on Ocean Energy, Dublin, Ireland*, vol. 1719, 2012, p. 18.

[192] J. Lasa, J. C. Antolin, C. Angulo, P. Estensoro, M. Santos, and P. Ricci, "Design, construction and testing of a hydraulic power take-off for wave energy converters," *Energies*, vol. 5, no. 6, pp. 2030–2052, 2012.

[193] G. Bacelli, J.-C. Gilloteaux, and J. Ringwood, "State space model of a hydraulic power take off unit for wave energy conversion employing bondgraphs." WREC, 2008.

[194] Y. You-Guan, G. Guo-fang, and H. Guo-Liang, "Simulation technique of amesim and its application in hydraulic system [j]," *Hydraulics Pneumatics & Seals*, vol. 3, pp. 28–31, 2005.

[195] C. J. Taylor, M. Stables, P. Cross, K. Gunn, and G. A. Aggidis, "Linear and non–linear control of a power take–off simulation for wave energy conversion," 2009.

[196] H. Engja and J. Hals, "Modelling and simulation of sea wavepower conversion systems," in *7th European Wave and Tidal Energy Conference-EWTEC*, 2007.

[197] D. C. Karnopp, D. L. Margolis, and R. C. Rosenberg, *System dynamics: modeling, simulation, and control of mechatronic systems*. John Wiley & Sons, 2012.

[198] J. F. Gaspar, M. Kamarlouei, A. Sinha, H. Xu, M. Calvário, F.-X. Faÿ, E. Robles, and C. G. Soares, "Analysis of electrical drive speed control limitations of a power take-off system for wave energy converters," *Renewable Energy*, 2017.

[199] J. Gaspar, M. Calvário, and C. G. Soares, "Pump and gas accumulator based phase control of wave energy converters," *Renewable Energies Offshore*, pp. 295–303, 2015.

[200] J. F. Gaspar, M. Kamarlouei, A. Sinha, H. Xu, M. Calvário, F.-X. Faÿ, E. Robles, and C. G. Soares, "Speed control of oil-hydraulic power take-off system for oscillating body type wave energy converters," *Renewable Energy*, vol. 97, pp. 769–783, 2016.

[201] R. H. Hansen, A. Hansen, and T. O. Andersen, "Simulation of utilisation of pressure propagation for increased efficiency of secondary controlled discrete displacement cylinders," in *Applied Mechanics and Materials*, vol. 233. Trans Tech Publ, 2012, pp. 3–6.

[202] R. H. Hansen, T. O. Andersen, and H. C. Perdersen, "Analysis of discrete pressure level systems for wave energy converters," in *Fluid Power and Mechatronics (FPM), 2011 International Conference on*. IEEE, 2011, pp. 552–558.

[203] K. Rhinefrank, A. F. Yokochi, A. von Jouanne, M. Dittrich, and E. Agamloh, "Magnetic helical screw drive," Apr. 8 2009, uS Patent App. 12/420,720.

[204] J. Shek, D. Macpherson, and M. Mueller, "Phase and amplitude control of a linear generator for wave energy conversion," 2008.

[205] A. Sinha, D. Karmakar, and C. Guedes Soares, "Effect of floater shapes on the power take-off of wave energy converters," *Guedes Soares C (ed.) Renewable Energies Offshore. London: Taylor & Francis Group*, pp. 375–382, 2015.

[206] S. Pakdelian and H. A. Toliyat, "Dynamic modeling of the trans-rotary magnetic gear for the point-absorbing wave energy conversion systems," in *Energy Conversion Congress and Exposition (ECCE), 2014 IEEE*. IEEE, 2014, pp. 3163–3170.

[207] R. H. Hansen, T. O. Andersen, and H. C. Pedersen, "Determining required valve performance for discrete control of pto cylinders for wave energy," in *ASME 2012 6th International Conference on Energy Sustainability & 10th Fuel Cell Science, Engineering and Technology Conference*. American Society of Mechanical Engineers, 2012, pp. 565–578.

[208] R. N. F. P. KIN, "Wave star energy," 2004.

[209] C. Guedes Soares, J. Bhattacharjee, M. Tello, and L. Pietra, "Review and classification of wave energy converters," *Maritime engineering and technology*, pp. 585–594, 2012.

[210] M. Ohkusu, "On the heaving motion of two circular cylinders on the surface of a fluid," *Reports of Research Institute for Applied Mechanics*, vol. 17, no. 58, pp. 167–185, 1969.

[211] ——, "Wave action on groups of vertical circular cylinders," *Journal of the Society of Naval Architects of Japan*, vol. 1972, no. 131, pp. 53–64, 1972.

[212] ——, "Hydrodynamic forces on multiple cylinders in waves," in *Int. Symp. on the Dynamics of Marine Vehicles and Structures in Waves, 1974*, 1974.

[213] G. De Backer, M. Vantorre, and J. De Rouck, "Wave energy absorption by point absorber arrays," 2011.

[214] C. M. Linton and P. McIver, *Handbook of mathematical techniques for wave/structure interactions*. CRC Press, 2001.

[215] C. Linton and D. Evans, "The interaction of waves with arrays of vertical circular cylinders," *Journal of Fluid Mechanics*, vol. 215, pp. 549–569, 1990.

[216] S. Mavrakos and P. McIver, "Comparison of methods for computing hydrodynamic characteristics of arrays of wave power devices," *Applied Ocean Research*, vol. 19, no. 5-6, pp. 283–291, 1997.

[217] B. Borgarino, A. Babarit, P. Ferrant *et al.*, "Extension of free-surface green's function multipole expansion for infinite water depth case," *International Journal of Offshore and Polar Engineering*, vol. 21, no. 03, 2011.

[218] A. Babarit, "Impact of long separating distances on the energy production of two interacting wave energy converters," *Ocean Engineering*, vol. 37, no. 8, pp. 718–729, 2010.

[219] R. Taghipour, T. Moan *et al.*, "Efficient frequency-domain analysis of dynamic response for the multi-body wave energy converter in multi-directional wave," in *The Eighteenth International Offshore and Polar Engineering Conference*. International Society of Offshore and Polar Engineers, 2008.

[220] M. Folley and T. Whittaker, "The adequacy of phase-averaged models for modelling wave farms," in *ASME 2011 30th International Conference on Ocean, Offshore and Arctic Engineering*. American Society of Mechanical Engineers, 2011, pp. 663–671.

[221] A. Alexandre, T. Stallard, and P. Stansby, "Transformation of wave spectra across a line of wave devices," in *Proceedings of the 8th European Wave and Tidal Energy Conference, Uppsala, Sweden*, vol. 710, 2009.

[222] J. A. Oskamp and H. T. Özkan-Haller, "Wave predictions at the site of a wave energy conversion array," *Coastal Engineering Proceedings*, vol. 1, no. 32, p. 39, 2011.

[223] N. Booij, R. Ris, and L. H. Holthuijsen, "A third-generation wave model for coastal regions: 1. model description and validation," *Journal of geophysical research: Oceans*, vol. 104, no. C4, pp. 7649–7666, 1999.

[224] C. Wang and G. Wu, "Interactions between fully nonlinear water waves and cylinder arrays in a wave tank," *Ocean Engineering*, vol. 37, no. 4, pp. 400–417, 2010.

[225] C. Yang, R. Lohner, and S. C. Yim, "Development of a cfd simulation method for extreme wave and structure interactions," in *ASME 2005 24th International Conference on Offshore Mechanics and Arctic Engineering*. American Society of Mechanical Engineers, 2005, pp. 951–963.

[226] E. B. Agamloh, A. K. Wallace, and A. Von Jouanne, "Application of fluid–structure interaction simulation of an ocean wave energy extraction device," *Renewable Energy*, vol. 33, no. 4, pp. 748–757, 2008.

[227] M. A. Bhinder, A. Babarit, L. Gentaz, and P. Ferrant, "Assessment of viscous damping via 3d-cfd modelling of a floating wave energy device," in *Proceedings of the 9th European Wave and Tidal Energy Conference, Southampton, UK*, 2011.

[228] S. Bellew and T. Stallard, "Linear modelling of wave device arrays and comparison to experimental and second order models."

[229] S. Weller, T. Stallard, and P. Stansby, "Experimental measurements of irregular wave interaction factors in closely spaced arrays," *IET renewable power generation*, vol. 4, no. 6, pp. 628–637, 2010.

[230] E. Lejerskog, H. Gravråkmo, A. Savin, E. Strömstedt, S. Tyrberg, K. Haikonen, R. Krishna, C. Boström, M. Rahm, R. Ekström *et al.*, "Lysekil research site, sweden: A status update," in *9th European Wave and Tidal Energy Conference, Southampton, UK, 5-9 September 2011*, 2011.

[231] E. Tedeschi, M. Santos, P. Ricci, M. Molinas, and J. Villate, "Control strategies for the grid integration of wave energy converters at the biscay marine energy platform," in *Proceedings of the European Wave and Tidal Energy Conference,(EWTEC2011), Southampton, UK*, vol. 59, 2011.

[232] M. Molinas, O. Skjervheim, B. Sørby, P. Andreasen, S. Lundberg, and T. Undeland, "Power smoothing by aggregation of wave energy converters for minimizing electrical energy storage requirements," in *Proceedings of the 7th European Wave and Tidal Energy Conference*, 2007, pp. 3–8.

[233] D. OSullivan and G. Dalton, "Challenges in the grid connection of wave energy devices," in *8th European wave and tidal energy conference. Uppsala, Sweden*, 2009.

[234] F. Sharkey, E. Bannon, M. Conlon, and K. Gaughan, "Dynamic electrical ratings and the economics of capacity factor for wave energy converter arrays," 2011.

[235] P. Ricci, A. Rico, P. Ruiz-Minguela, F. Boscolo, and J. Villate, "Design, modelling and analysis of an integrated mooring system for wave energy arrays," in *Proceedings of the 4th International Conference on Ocean Energy*, vol. 17, 2012.

[236] O. Langhamer, "Wave energy conversion and the marine environment: Colonization patterns and habitat dynamics," Ph.D. dissertation, Acta Universitatis Upsaliensis, 2009.

[237] A. De Andrés, R. Guanche, L. Meneses, C. Vidal, and I. Losada, "Factors that influence array layout on wave energy farms," *Ocean Engineering*, vol. 82, pp. 32–41, 2014.

[238] W. Chen, F. Gao, X. Meng, and J. Fu, "Design of the wave energy converter array to achieve constructive effects," *Ocean Engineering*, vol. 124, pp. 13–20, 2016.

[239] A. Babarit, "On the park effect in arrays of oscillating wave energy converters," *Renewable Energy*, vol. 58, pp. 68–78, 2013.

[240] B. Robertson, C. Hiles, E. Luczko, and B. Buckham, "Quantifying wave power and wave energy converter array production potential," *International Journal of Marine Energy*, vol. 14, pp. 143–160, 2016.

[241] C. Greenwood, D. Christie, V. Venugopal, J. Morrison, and A. Vogler, "Modelling performance of a small array of wave energy converters: Comparison of spectral and boussinesq models," *Energy*, vol. 113, pp. 258–266, 2016.

[242] J. Wu, S. Shekh, N. Y. Sergiienko, B. S. Cazzolato, B. Ding, F. Neumann, and M. Wagner, "Fast and effective optimisation of arrays of submerged wave energy converters," in *Proceedings of the 2016 on Genetic and Evolutionary Computation Conference*. ACM, 2016, pp. 1045–1052.

[243] C. Jones, J. Magalen, and J. Roberts, "Wave energy converter (wec) array effects on wave, current, and sediment circulation: Monteray bay, ca."

[244] J. M. Hamrick, *A three-dimensional environmental fluid dynamics computer code: Theoretical and computational aspects*. Virginia Institute of Marine Science, College of William and Mary, 1992.

[245] M. C. Haller, A. Porter, P. Lenee-Bluhm, K. Rhinefrank, E. Hammagren, T. Ozkan-Haller, and D. Newborn, "Laboratory observation of waves in the vicinity of wec-arrays," Oregon Wave Energy Trust, Tech. Rep., 2011.

[246] J. Newman, "Wave effects on multiple bodies."

[247] C. J. Sharp, "Wave energy converter array optimization: Array economic analysis and preliminary results of a genetic algorithm approach introducing cost factors," Ph.D. dissertation, 2015.

[248] A. J. Nambiar, D. I. Forehand, M. M. Kramer, R. H. Hansen, and D. M. Ingram, "Effects of hydrodynamic interactions and control within a point absorber array on electrical output," *International Journal of Marine Energy*, vol. 9, pp. 20–40, 2015.

[249] D. I. Forehand, A. E. Kiprakis, A. J. Nambiar, and A. R. Wallace, "A fully coupled wave-to-wire model of an array of wave energy converters," *IEEE Transactions on Sustainable Energy*, vol. 7, no. 1, pp. 118–128, 2016.

[250] M. Mosher, "A new methodology for frequency domain analysis of wave energy converters with periodically varying physical parameters," Ph.D. dissertation, University of Victoria, 2012.

[251] J. Engström, M. Eriksson, M. Göteman, J. Isberg, and M. Leijon, "Performance of large arrays of point absorbing direct-driven wave energy converters," *Journal of Applied Physics*, vol. 114, no. 20, p. 204502, 2013.

[252] L. B. Hernandez and J. M. E. Alzola, "Hydrodynamic interaction of ocean wave energy point absorbers," 2016.

[253] G. S. Ásgeirsson, "Hydrodynamic investigation of wavepower buoys," 2013.

[254] M. Bånkestad, "Modeling, simulation and dynamic control of a wave energy converter," 2013.

[255] J. C. McNatt, V. Venugopal, and D. Forehand, "The cylindrical wave field of wave energy converters," *International Journal of Marine Energy*, vol. 3, pp. e26–e39, 2013.

[256] ——, "A novel method for deriving the diffraction transfer matrix and its application to multi-body interactions in water waves," *Ocean Engineering*, vol. 94, pp. 173–185, 2015.

[257] A. Babarit, B. Borgarino, P. Ferrant, and A. Clément, "Assessment of the influence of the distance between two wave energy converters on energy production," *IET renewable power generation*, vol. 4, no. 6, pp. 592–601, 2010.

[258] R. Olfati-Saber and R. M. Murray, "Consensus problems in networks of agents with switching topology and time-delays," *IEEE Transactions on automatic control*, vol. 49, no. 9, pp. 1520–1533, 2004.

Appendix A

Proof of Existence

A.1 Stability of The CD-KCF

In this section, the stability of the CD-KCF is proved based on a Lyapunov-like stability analysis. Since most of the variables in the mathematical derivations and models are in the vector or matrix format, the different denotations for the scalar, vector, and matrix are neglected except a real number is included.

Proposition 1. *Consider a Continuous-discrete Kalman-Consensus Filter with the estimation model in Eq.* (5.59)*, and let* $C_{g,i} = \gamma P_i$*. Suppose* $\gamma > 0$ *is sufficiently small*

and the covariance matrix P_i is positive definite and is bounded:

$$\beta_1 I \leqslant P_i \leqslant \beta_2 I \tag{A.1}$$

Then the collective dynamics of the estimation error $e_i = \hat{x}_i - x_i$ is globally asymptotically stable.

Proof. Assume a globally positive definite Lyapunov function $V(e) = \sum_{i=1}^{N} e_i^T P_i^{-1} e_i$. The differential between the true dynamics (without noise) and the estimator dynamics gives the dynamics of the estimation error:

$$\dot{e}_i = F e_i \tag{A.2}$$

The update of the estimation is:

$$\hat{x}_{k,i}^{+} = \hat{x}_{k,i}^{-} + K_{g,k,i}(\tilde{y}_{k,i} - H_{m,k,i}\hat{x}_{k,i}^{-}) + C_{g,k,i}\sum_{N_i}(\hat{x}_{k,j}^{-} - \hat{x}_{k,i}^{-}) \tag{A.3}$$

For the true system, we have $x_{k,i}^{+} = x_{k,i}^{-}$. Hence, the update of the error is:

$$e_{k,i}^{+} = [I - K_{g,k,i}H_{m,k,i}]e_{k,i}^{-} + C_{g,i}\sum_{j=1}^{N}(e_{k,j}^{-} - e_{k,i}^{-}) \tag{A.4}$$

The derivative of the Lyapunov function can be computed as:

$$\dot{V} = \sum_{i=1}^{N} \dot{e}_i^T P_i^{-1} e_i + e_i^T P_i^{-1} \dot{e}_i + e_i^T \dot{P}_i^{-1} e_i \tag{A.5}$$

$$= \sum_{i=1}^{N} \dot{e}_i^T P_i^{-1} e_i + e_i^T P_i^{-1} \dot{e}_i - e_i^T (P_i^{-1} \dot{P}_i P_i^{-1}) e_i \tag{A.6}$$

Using the propagation model of the covariance matrix and Eq. (A.2), we get:

$$\dot{V} = \sum_{i=1}^{N} e_i^T F^T P_i^{-1} e_i + e_i^T P_i^{-1} F e_i -$$

$$e_i^T (P_i^{-1}(F(t)P_i(t) + P_i(t)F^T(t) + G_i(t)Q_p(t)G_i^T(t))P_i^{-1}) e_i \tag{A.7}$$

$$= -e_i^T P_i^{-1} G_i(t) Q_p(t) G_i^T(t) P_i^{-1} e_i \leqslant 0 \tag{A.8}$$

At any time $t = t_k$, since $\dot{V} < 0 \quad \forall e \in R^n \setminus \{0\}$, we have:

$$V(t_{k+1})^- \leqslant V(t_k)^+ \tag{A.9}$$

where the equality only holds when the estimation error $e_i = 0$. For $t = t_{k+1}$, the Lyapunov function is:

$$V(t_{k+1})^- = \sum_{i=1}^{N} (e_{k+1,i}^-)^T (P_{k+1,i}^-)^{-1} e_{k+1,i}^- \tag{A.10}$$

$$V(t_{k+1})^+ = \sum_{i=1}^{N} (e_{k+1,i}^+)^T (P_{k+1,i}^+)^{-1} e_{k+1,i}^+ \tag{A.11}$$

To make the notation simple, the t_k and k will be dropped in the rest of the derivation.

If we substitute Eq. (A.4) into Eq. (A.11), and let $M_i = I - K_{g,i}H_{m,i}$ then:

$$
\begin{aligned}
V^+ = & \sum_i (M_i e_i^- + C_{g,i} \sum_j (e_j^- - e_i^-))^T (P_i^-)^{-1} M_i^{-1} \\
& (M_i e_i^- + C_{g,i} \sum_j (e_j^- - e_i^-)) \qquad \text{(A.12)} \\
& = \sum_i ((e_i^-)^T M_i^T (P_i^-)^{-1} e_i^- + \\
& \gamma (e_i^-)^T M_i^T (P_i^-)^{-1} M_i^{-1} P_i^- \sum_j (e_j^- - e_i^-) + \\
& \gamma \sum_j (e_j^- - e_i^-)^T e_i^- + \\
& \gamma^2 \sum_j (e_j^- - e_i^-)^T M_i^{-1} P_i^- \sum_j (e_j^- - e_i^-)) \qquad \text{(A.13)}
\end{aligned}
$$

The second term can be simplified by applying the update law of the covariance matrix:

$$
\begin{aligned}
T_{a2} &= \gamma (e_i^-)^T M_i^T (P_i^-)^{-1} M_i^{-1} P_i^- \sum_j (e_j^- - e_i^-) \\
&= \gamma (e_i^-)^T (P_i^-)^{-1} (P_i^-)^T M_i^T (P_i^-)^{-1} M_i^{-1} P_i^- \sum_j (e_j^- - e_i^-) \qquad \text{(A.14)} \\
&= \gamma (e_i^-)^T (P_i^-)^{-1} P_i^+ (P_i^-)^{-1} M_i^{-1} P_i^- \sum_j (e_j^- - e_i^-) \qquad \text{(A.15)} \\
&= \gamma (e_i^-)^T (P_i^-)^{-1} P_i^+ (P_i^+)^{-1} P_i^- \sum_j (e_j^- - e_i^-) \qquad \text{(A.16)} \\
&= \gamma (e_i^-)^T \sum_j (e_j^- - e_i^-) \qquad \text{(A.17)}
\end{aligned}
$$

Hence:

$$V^+ = \sum_i ((e_i^-)^T M_i^T (P_i^-)^{-1} e_i^- +$$

$$2\gamma (e_i^-)^T \sum_j (e_j^- - e_i^-) +$$

$$\gamma^2 \sum_j (e_j^- - e_i^-)^T M_i^{-1} P_i^- \sum_j (e_j^- - e_i^-)) \tag{A.18}$$

$$= V^- - \sum_i (e_i^-)^T (K_{g,i} H_{m,i})^T (P_i^-)^{-1} e_i^- +$$

$$\sum_i 2\gamma (e_i^-)^T \sum_j (e_j^- - e_i^-) +$$

$$\sum_i \gamma^2 \sum_j (e_j^- - e_i^-)^T P_i^- (P_i^+)^{-1} P_i^- \sum_j (e_j^- - e_i^-) \tag{A.19}$$

Since the covariance matrix is bounded, hence:

$$V^+ \leqslant V^- - \sum_i (e_i^-)^T (K_{g,i} H_{m,i})^T (P_i^-)^{-1} e_i^- +$$

$$2\gamma \sum_i (e_i^-)^T \sum_j (e_j^- - e_i^-) +$$

$$\frac{\gamma^2 \beta_2^2}{\beta_1} \sum_i \sum_j (e_j^- - e_i^-)^T \sum_j (e_j^- - e_i^-) \tag{A.20}$$

The second term can be proved to be negative definite by substituting the Kalman

Gain:

$$\forall e \in R^n \setminus \{0\}$$

$$T_{b2} = -\sum_i (e_i^-)^T (K_{g,i} H_{m,i})^T (P_i^-)^{-1} e_i^- \tag{A.21}$$

$$= -\sum_i (e_i^-)^T H_{m,i}^T K_{g,i}^T (P_i^-)^{-1} e_i^- \tag{A.22}$$

$$= -\sum_i (e_i^-)^T H_{m,i}^T (R_i + H_{m,i} P_i^- H_{m,i}^T)^{-T} H_{m,i} e_i^- < 0 \tag{A.23}$$

To solve for the last two terms in Eq. (A.20), let us define a quadratic function which is similar to the disagreement function [258] as:

$$\Phi_G = \sum_i \sum_j (e_j - e_i)^T \sum_j (e_j - e_i) \tag{A.24}$$

The Φ_G is a positive definite function. Since:

$$\sum_i \sum_j e_j^T \sum_j (e_j - e_i) \tag{A.25}$$

$$= \sum_i \sum_j e_j^T \sum_j e_j - \sum_i \sum_j e_j^T \sum_j e_i \tag{A.26}$$

$$= N \sum_j e_j^T \sum_j e_j - N \sum_j e_j^T \sum_i e_i = 0 \tag{A.27}$$

The disagreement function can be simplified as:

$$\Phi_G = N \sum_i -e_i^T \sum_j (e_j - e_i) \geqslant 0 \tag{A.28}$$

So we define:

$$L = \sum_i e_i^T \sum_j (e_j - e_i) \leqslant 0 \tag{A.29}$$

Hence, Eq. (A.20) can be further simplified as:

$$V^+ \leqslant V^- - \sum_i (e_i^-)^T (K_{g,i} H_{m,i})^T (P_i^-)^{-1} e_i^- + 2\gamma L + \frac{\gamma^2 \beta_2^2}{\beta_1} \Phi_G \tag{A.30}$$

Since $\Phi_G = -NL$, then:

$$V^+ \leqslant V^- - \sum_i (e_i^-)^T (K_{g,i} H_{m,i})^T (P_i^-)^{-1} e_i^- + 2\gamma L - \frac{\gamma^2 \beta_2^2 N}{\beta_1} L \tag{A.31}$$

Since the second term is negative definite, then to guarantee the summation of the last two terms is still negative definite the following condition should be satisfied:

$$2\gamma - \frac{\gamma^2 \beta_2^2 N}{\beta_1} \geqslant 0 \tag{A.32}$$

Hence we can solve:

$$\gamma \leqslant \frac{2\beta_1}{\beta_2^2 N} \tag{A.33}$$

We define $\tilde{\gamma} \leqslant \frac{2\beta_1}{\beta_2^2 N}$, if $0 < \gamma \leqslant \tilde{\gamma}$, then $V^+ < V^- \quad \forall e \in R^n \setminus \{0\}$ which means $\delta V = V^+ - V^- < 0 \quad \forall e \in R^n \setminus \{0\}$. Recall Eq. (A.9), we can write:

$$V(t_{k+1})^+ \leqslant V(t_{k+1})^- \leqslant V(t_k)^+ \tag{A.34}$$

where the equality only holds when the estimation error e_i converges to 0. As time goes to infinity ($t \to \infty$), the Lyapunov function will asymptotically converge to zero ($V(e) \to 0$) for $0 < \gamma \leqslant \tilde{\gamma}$ which also indicates $\hat{x}_i \to x$ (reach the consensus). Moreover, since both the update δV and the derivative $\dot{V}$ of the Lyapunov function is globally negative definite. Hence the error dynamics is globally asymptotically stable. This completes the proof. □

Appendix B

Letters of Permission

In this chapter, the permission letters from the journals for approving the reuse of the materials in the papers are listed.

1. The permission letter is shown in Figure. B.1 for using the paper from the Journal of Renewable Energy, Elsevier.

2. The permission letter is shown in Figure. B.2 for using the paper from IEEE Transactions on Sustainable Energy.

Figure B.1: The permission letter of reusing the paper [2].

3. The permission letter is shown in Figure. B.3 for using the paper from International Journal of Control, Taylor & Francis.

4. The permission letter is shown in Figure. B.4, B.5 and B.6 for using the paper from Journal of Ocean Engineering and Marine Energy, Springer Nature.

5. The permission letter is shown in Figure. B.7 for using the paper from the Journal of Marine Science and Engineering, MDPI.

6. The permission letter is shown in Figure. B.8 and B.9 for using the paper from the Journal of Dynamic Systems, Measurement, and Control, ASME.

7/16/2018 Rightslink® by Copyright Clearance Center

Copyright Clearance Center RightsLink®

Home | Account Info | Help

IEEE Requesting permission to reuse content from an IEEE publication

Title: Control of Wave Energy Converters Using A Simple Dynamic Model
Author: Ossama Abdelkhalik
Publication: Sustainable Energy, IEEE Transactions on
Publisher: IEEE
Date: Dec 31, 1969
Copyright © 1969, IEEE

Logged in as:
Shangyan Zou
MICHIGAN TECHNOLOGICAL UNIVERSITY
LOGOUT

Thesis / Dissertation Reuse

The IEEE does not require individuals working on a thesis to obtain a formal reuse license, however, you may print out this statement to be used as a permission grant:

Requirements to be followed when using any portion (e.g., figure, graph, table, or textual material) of an IEEE copyrighted paper in a thesis:

1) In the case of textual material (e.g., using short quotes or referring to the work within these papers) users must give full credit to the original source (author, paper, publication) followed by the IEEE copyright line © 2011 IEEE.
2) In the case of illustrations or tabular material, we require that the copyright line © [Year of original publication] IEEE appear prominently with each reprinted figure and/or table.
3) If a substantial portion of the original paper is to be used, and if you are not the senior author, also obtain the senior author's approval.

Requirements to be followed when using an entire IEEE copyrighted paper in a thesis:

1) The following IEEE copyright/ credit notice should be placed prominently in the references: © [year of original publication] IEEE. Reprinted, with permission, from [author names, paper title, IEEE publication title, and month/year of publication]
2) Only the accepted version of an IEEE copyrighted paper can be used when posting the paper or your thesis on-line.
3) In placing the thesis on the author's university website, please display the following message in a prominent place on the website: In reference to IEEE copyrighted material which is used with permission in this thesis, the IEEE does not endorse any of [university/educational entity's name goes here]'s products or services. Internal or personal use of this material is permitted. If interested in reprinting/republishing IEEE copyrighted material for advertising or promotional purposes or for creating new collective works for resale or redistribution, please go to http://www.ieee.org/publications_standards/publications/rights/rights_link.html to learn how to obtain a License from RightsLink.

If applicable, University Microfilms and/or ProQuest Library, or the Archives of Canada may supply single copies of the dissertation.

BACK | CLOSE WINDOW

Copyright © 2018 Copyright Clearance Center, Inc. All Rights Reserved. Privacy statement. Terms and Conditions.
Comments? We would like to hear from you. E-mail us at customercare@copyright.com

https://s100.copyright.com/AppDispatchServlet#formTop 1/1

Figure B.2: The permission letter of reusing the paper [3].

Figure B.3: The permission letter of reusing the paper [4].

7. The permission letter is shown in Figure. B.10 and B.11 for using the paper from the Journal of Renewable Energy, Elsevier.

8. The permission letter is shown in Figure. B.12 for using the paper from IEEE Transactions on Sustainable Energy.

Copyright ©2018 IEEE, Reprinted, with permission, from S. Zou, O. Abdelkhalik, "Consensus Estimation in Arrays of Wave Energy Converters," *IEEE Transactions on Sustainable Energy*, 2018.

9. Since the content of the article listed below applied in this dissertation is a draft, the authors retain the copyright of the draft [9].

SPRINGER NATURE LICENSE TERMS AND CONDITIONS

Jul 16, 2018

This Agreement between MICHIGAN TECHNOLOGICAL UNIVERSITY -- Shangyan Zou ("You") and Springer Nature ("Springer Nature") consists of your license details and the terms and conditions provided by Springer Nature and Copyright Clearance Center.

License Number	4390850370486
License date	Jul 16, 2018
Licensed Content Publisher	Springer Nature
Licensed Content Publication	Journal of Ocean Engineering and Marine Energy
Licensed Content Title	On the control design of wave energy converters with wave prediction
Licensed Content Author	Ossama Abdelkhalik, Rush Robinett, Shangyan Zou et al
Licensed Content Date	Jan 1, 2016
Licensed Content Volume	2
Licensed Content Issue	4
Type of Use	Thesis/Dissertation
Requestor type	academic/university or research institute
Format	print and electronic
Portion	full article/chapter
Will you be translating?	no
Circulation/distribution	<501
Author of this Springer Nature content	yes
Title	Optimal Control of Wave Energy Converters
Instructor name	Ossama Abdelkhalik
Institution name	MICHIGAN TECHNOLOGICAL UNIVERSITY
Expected presentation date	Jul 2018
Requestor Location	Shangyan Zou 1805 Woodmar Dr Apt C HOUGHTON, MI 49931 United States Attn: Shangyan Zou
Billing Type	Invoice
Billing Address	MICHIGAN TECHNOLOGICAL UNIVERSITY 1805 Woodmar Dr Apt C HOUGHTON, MI 49931 United States Attn: Shangyan Zou
Total	0.00 USD

Figure B.4: The permission letter of reusing the paper [5]. (1)

Terms and Conditions

Springer Nature Terms and Conditions for RightsLink Permissions

Springer Customer Service Centre GmbH (the Licensor) hereby grants you a non-exclusive, world-wide licence to reproduce the material and for the purpose and requirements specified in the attached copy of your order form, and for no other use, subject to the conditions below:

1. The Licensor warrants that it has, to the best of its knowledge, the rights to license reuse of this material. However, you should ensure that the material you are requesting is original to the Licensor and does not carry the copyright of another entity (as credited in the published version).

   If the credit line on any part of the material you have requested indicates that it was reprinted or adapted with permission from another source, then you should also seek permission from that source to reuse the material.

2. Where **print only** permission has been granted for a fee, separate permission must be obtained for any additional electronic re-use.

3. Permission granted **free of charge** for material in print is also usually granted for any electronic version of that work, provided that the material is incidental to your work as a whole and that the electronic version is essentially equivalent to, or substitutes for, the print version.

4. A licence for 'post on a website' is valid for 12 months from the licence date. This licence does not cover use of full text articles on websites.

5. Where **'reuse in a dissertation/thesis'** has been selected the following terms apply: Print rights for up to 100 copies, electronic rights for use only on a personal website or institutional repository as defined by the Sherpa guideline (www.sherpa.ac.uk/romeo/).

6. Permission granted for books and journals is granted for the lifetime of the first edition and does not apply to second and subsequent editions (except where the first edition permission was granted free of charge or for signatories to the STM Permissions Guidelines http://www.stm-assoc.org/copyright-legal-affairs/permissions/permissions-guidelines/), and does not apply for editions in other languages unless additional translation rights have been granted separately in the licence.

7. Rights for additional components such as custom editions and derivatives require additional permission and may be subject to an additional fee. Please apply to Journalpermissions@springernature.com/bookpermissions@springernature.com for these rights.

8. The Licensor's permission must be acknowledged next to the licensed material in print. In electronic form, this acknowledgement must be visible at the same time as the figures/tables/illustrations or abstract, and must be hyperlinked to the journal/book's homepage. Our required acknowledgement format is in the Appendix below.

9. Use of the material for incidental promotional use, minor editing privileges (this does not include cropping, adapting, omitting material or any other changes that affect the meaning, intention or moral rights of the author) and copies for the disabled are permitted under this licence.

10. Minor adaptations of single figures (changes of format, colour and style) do not require the Licensor's approval. However, the adaptation should be credited as shown in Appendix below.

Appendix — Acknowledgements:

For Journal Content:

Reprinted by permission from **[the Licensor]**: **[Journal Publisher** (e.g.

Figure B.5: The permission letter of reusing the paper [5]. (2)

Nature/Springer/Palgrave)] [**JOURNAL NAME**] [**REFERENCE CITATION** (Article name, Author(s) Name), [**COPYRIGHT**] (year of publication)

For **Advance Online Publication papers:**
Reprinted by permission from [**the Licensor**]: [**Journal Publisher** (e.g. Nature/Springer/Palgrave)] [**JOURNAL NAME**] [**REFERENCE CITATION** (Article name, Author(s) Name), [**COPYRIGHT**] (year of publication), advance online publication, day month year (doi: 10.1038/sj.[JOURNAL ACRONYM].)

For Adaptations/Translations:
Adapted/Translated by permission from [**the Licensor**]: [**Journal Publisher** (e.g. Nature/Springer/Palgrave)] [**JOURNAL NAME**] [**REFERENCE CITATION** (Article name, Author(s) Name), [**COPYRIGHT**] (year of publication)

Note: For any republication from the British Journal of Cancer, the following credit line style applies:

Reprinted/adapted/translated by permission from [**the Licensor**]: on behalf of Cancer Research UK: : [**Journal Publisher** (e.g. Nature/Springer/Palgrave)] [**JOURNAL NAME**] [**REFERENCE CITATION** (Article name, Author(s) Name), [**COPYRIGHT**] (year of publication)

For **Advance Online Publication** papers:
Reprinted by permission from The [**the Licensor**]: on behalf of Cancer Research UK: [**Journal Publisher** (e.g. Nature/Springer/Palgrave)] [**JOURNAL NAME**] [**REFERENCE CITATION** (Article name, Author(s) Name), [**COPYRIGHT**] (year of publication), advance online publication, day month year (doi: 10.1038/sj.[JOURNAL ACRONYM])

For Book content:
Reprinted/adapted by permission from [**the Licensor**]: [**Book Publisher** (e.g. Palgrave Macmillan, Springer etc) [**Book Title**] by [**Book author**(s)] [**COPYRIGHT**] (year of publication)

Other Conditions:

Version 1.0

Questions? customercare@copyright.com or +1-855-239-3415 (toll free in the US) or +1-978-646-2777.

Figure B.6: The permission letter of reusing the paper [5]. (3)

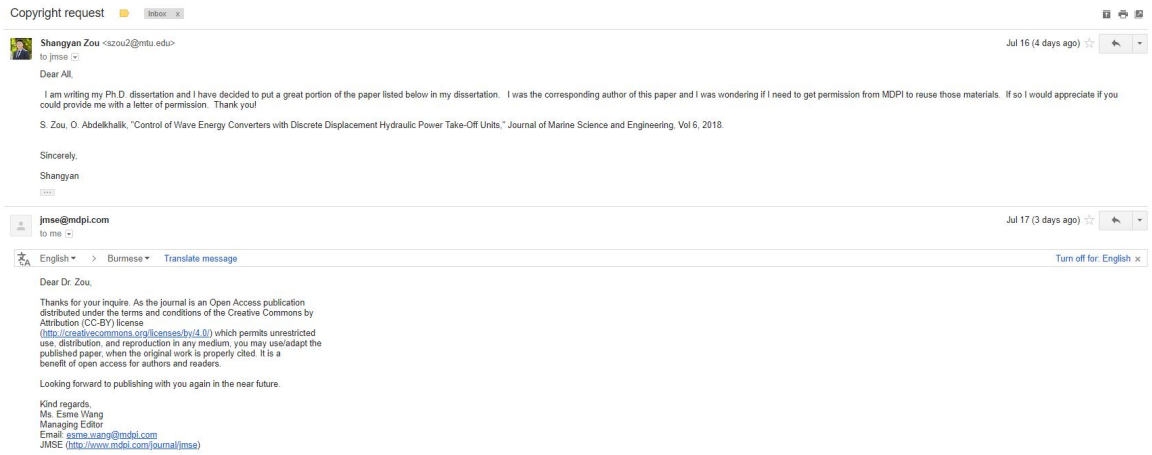
Copyright request Inbox x

Shangyan Zou <szou2@mtu.edu> Jul 16 (4 days ago)
to jmse

Dear All,

I am writing my Ph.D. dissertation and I have decided to put a great portion of the paper listed below in my dissertation. I was the corresponding author of this paper and I was wondering if I need to get permission from MDPI to reuse those materials. If so I would appreciate if you could provide me with a letter of permission. Thank you!

S. Zou, O. Abdelkhalik, "Control of Wave Energy Converters with Discrete Displacement Hydraulic Power Take-Off Units," Journal of Marine Science and Engineering, Vol 6, 2018.

Sincerely,

Shangyan

jmse@mdpi.com Jul 17 (3 days ago)
to me

English Burmese Translate message Turn off for: English

Dear Dr. Zou,

Thanks for your inquire. As the journal is an Open Access publication distributed under the terms and conditions of the Creative Commons by Attribution (CC-BY) license (http://creativecommons.org/licenses/by/4.0/) which permits unrestricted use, distribution, and reproduction in any medium, you may use/adapt the published paper, when the original work is properly cited. It is a benefit of open access for authors and readers.

Looking forward to publishing with you again in the near future.

Kind regards,
Ms. Esme Wang
Managing Editor
Email: esme.wang@mdpi.com
JMSE (http://www.mdpi.com/journal/jmse)

Figure B.7: The permission letter of reusing the paper [6].

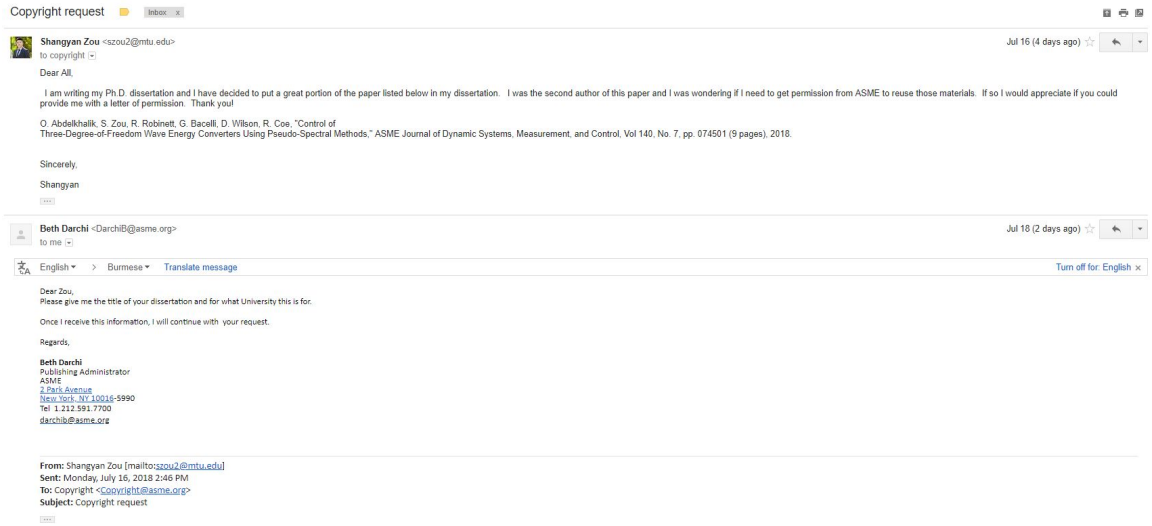
Copyright request Inbox x

Shangyan Zou <szou2@mtu.edu> Jul 16 (4 days ago)
to copyright

Dear All,

I am writing my Ph.D. dissertation and I have decided to put a great portion of the paper listed below in my dissertation. I was the second author of this paper and I was wondering if I need to get permission from ASME to reuse those materials. If so I would appreciate if you could provide me with a letter of permission. Thank you!

O. Abdelkhalik, S. Zou, R. Robinett, G. Bacelli, D. Wilson, R. Coe, "Control of
Three-Degree-of-Freedom Wave Energy Converters Using Pseudo-Spectral Methods," ASME Journal of Dynamic Systems, Measurement, and Control, Vol 140, No. 7, pp. 074501 (9 pages), 2018.

Sincerely,

Shangyan

Beth Darchi <DarchiB@asme.org> Jul 18 (2 days ago)
to me

English Burmese Translate message Turn off for: English

Dear Zou,
Please give me the title of your dissertation and for what University this is for.

Once I receive this information, I will continue with your request.

Regards,

Beth Darchi
Publishing Administrator
ASME
2 Park Avenue
New York, NY 10016-5990
Tel 1.212.591.7700
darchib@asme.org

From: Shangyan Zou [mailto:szou2@mtu.edu]
Sent: Monday, July 16, 2018 2:46 PM
To: Copyright <Copyright@asme.org>
Subject: Copyright request

Figure B.8: The permission letter of reusing the paper [1]. (1)

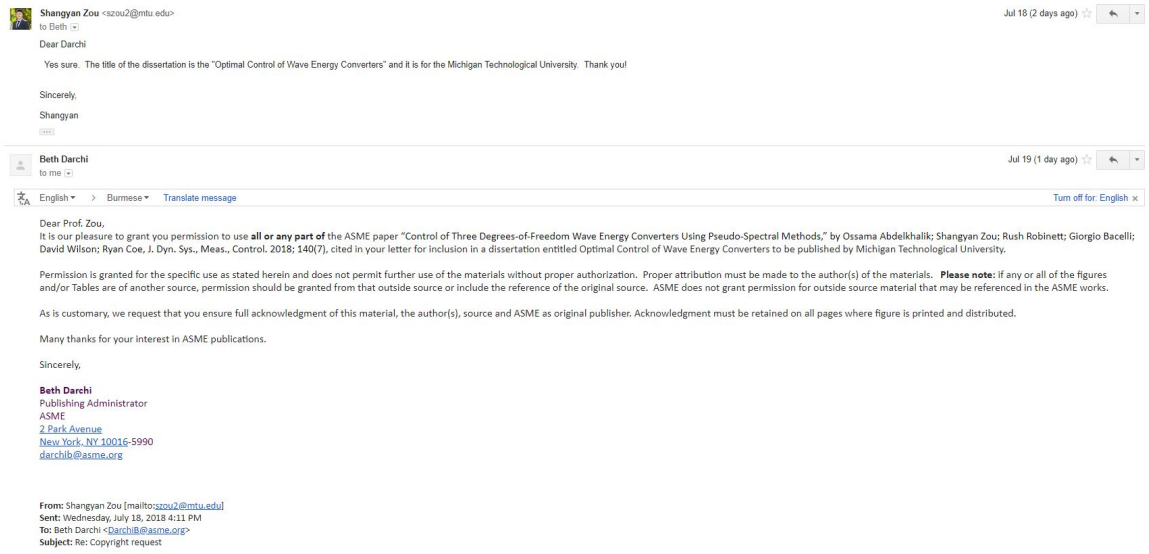

Shangyan Zou <szou2@mtu.edu> Jul 18 (2 days ago)
to Beth

Dear Darchi

Yes sure. The title of the dissertation is the "Optimal Control of Wave Energy Converters" and it is for the Michigan Technological University. Thank you!

Sincerely,

Shangyan

Beth Darchi Jul 19 (1 day ago)
to me

English › Burmese Translate message Turn off for: English

Dear Prof. Zou,
It is our pleasure to grant you permission to use **all or any part of** the ASME paper "Control of Three Degrees-of-Freedom Wave Energy Converters Using Pseudo-Spectral Methods," by Ossama Abdelkhalik; Shangyan Zou; Rush Robinett; Giorgio Bacelli; David Wilson; Ryan Coe, J. Dyn. Sys., Meas., Control. 2018; 140(7), cited in your letter for inclusion in a dissertation entitled Optimal Control of Wave Energy Converters to be published by Michigan Technological University.

Permission is granted for the specific use as stated herein and does not permit further use of the materials without proper authorization. Proper attribution must be made to the author(s) of the materials. **Please note:** If any or all of the figures and/or Tables are of another source, permission should be granted from that outside source or include the reference of the original source. ASME does not grant permission for outside source material that may be referenced in the ASME works.

As is customary, we request that you ensure full acknowledgment of this material, the author(s), source and ASME as original publisher. Acknowledgment must be retained on all pages where figure is printed and distributed.

Many thanks for your interest in ASME publications.

Sincerely,

Beth Darchi
Publishing Administrator
ASME
2 Park Avenue
New York, NY 10016-5990
darchib@asme.org

From: Shangyan Zou [mailto:szou2@mtu.edu]
Sent: Wednesday, July 18, 2018 4:11 PM
To: Beth Darchi <DarchiB@asme.org>
Subject: Re: Copyright request

Figure B.9: The permission letter of reusing the paper [1]. (2)

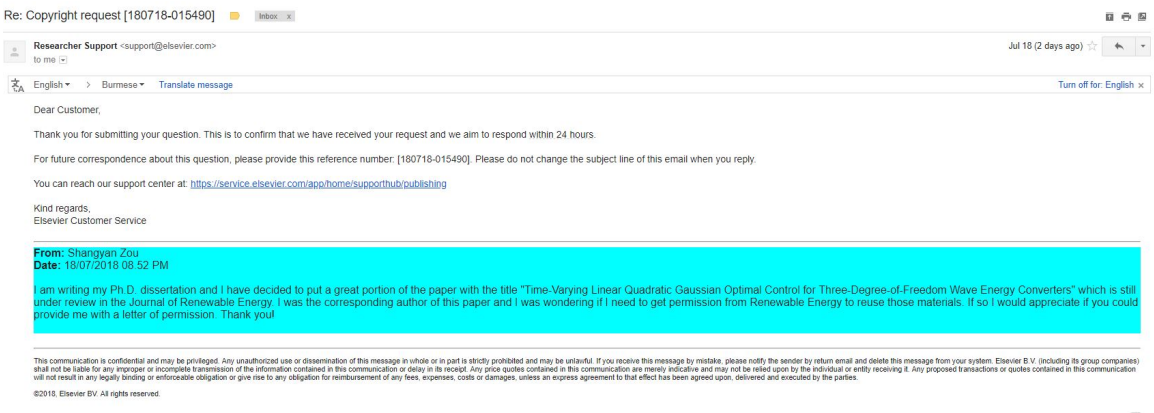

Re: Copyright request [180718-015490] Inbox

Researcher Support <support@elsevier.com> Jul 18 (2 days ago)
to me

English › Burmese Translate message Turn off for: English

Dear Customer,

Thank you for submitting your question. This is to confirm that we have received your request and we aim to respond within 24 hours.

For future correspondence about this question, please provide this reference number: [180718-015490]. Please do not change the subject line of this email when you reply.

You can reach our support center at: https://service.elsevier.com/app/home/supporthub/publishing

Kind regards,
Elsevier Customer Service

From: Shangyan Zou
Date: 18/07/2018 08:52 PM

I am writing my Ph.D. dissertation and I have decided to put a great portion of the paper with the title "Time-Varying Linear Quadratic Gaussian Optimal Control for Three-Degree-of-Freedom Wave Energy Converters" which is still under review in the Journal of Renewable Energy. I was the corresponding author of this paper and I was wondering if I need to get permission from Renewable Energy to reuse those materials. If so I would appreciate if you could provide me with a letter of permission. Thank you!

Figure B.10: The permission letter of reusing the paper [7]. (1)

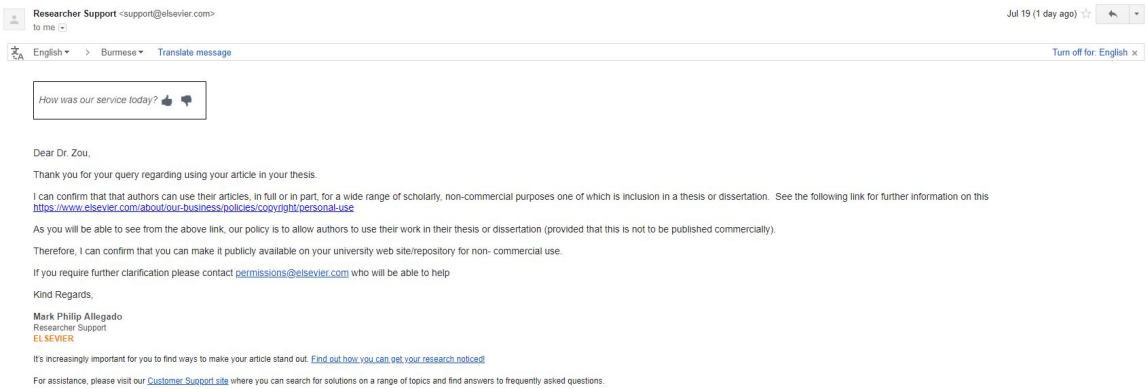

Researcher Support <support@elsevier.com>
to me

Jul 19 (1 day ago)

English > Burmese Translate message

Turn off for: English

How was our service today?

Dear Dr. Zou,

Thank you for your query regarding using your article in your thesis.

I can confirm that that authors can use their articles, in full or in part, for a wide range of scholarly, non-commercial purposes one of which is inclusion in a thesis or dissertation. See the following link for further information on this https://www.elsevier.com/about/our-business/policies/copyright/personal-use

As you will be able to see from the above link, our policy is to allow authors to use their work in their thesis or dissertation (provided that this is not to be published commercially).

Therefore, I can confirm that you can make it publicly available on your university web site/repository for non- commercial use.

If you require further clarification please contact permissions@elsevier.com who will be able to help

Kind Regards,

Mark Philip Allegado
Researcher Support
ELSEVIER

It's increasingly important for you to find ways to make your article stand out. Find out how you can get your research noticed!

For assistance, please visit our Customer Support site where you can search for solutions on a range of topics and find answers to frequently asked questions.

Figure B.11: The permission letter of reusing the paper [7]. (2)

7/16/2018 Rightslink® by Copyright Clearance Center

Copyright Clearance Center RightsLink®

Home | Account Info | Help

IEEE Requesting permission to reuse content from an IEEE publication

Title: Consensus Estimation in Arrays of Wave Energy Converters
Author: Shangyan Zou
Publication: Sustainable Energy, IEEE Transactions on
Publisher: IEEE
Date: Dec 31, 1969
Copyright © 1969, IEEE

Logged in as:
Shangyan Zou
MICHIGAN TECHNOLOGICAL UNIVERSITY
LOGOUT

Thesis / Dissertation Reuse

The IEEE does not require individuals working on a thesis to obtain a formal reuse license, however, you may print out this statement to be used as a permission grant:

Requirements to be followed when using any portion (e.g., figure, graph, table, or textual material) of an IEEE copyrighted paper in a thesis:

1) In the case of textual material (e.g., using short quotes or referring to the work within these papers) users must give full credit to the original source (author, paper, publication) followed by the IEEE copyright line © 2011 IEEE.
2) In the case of illustrations or tabular material, we require that the copyright line © [Year of original publication] IEEE appear prominently with each reprinted figure and/or table.
3) If a substantial portion of the original paper is to be used, and if you are not the senior author, also obtain the senior author's approval.

Requirements to be followed when using an entire IEEE copyrighted paper in a thesis:

1) The following IEEE copyright/ credit notice should be placed prominently in the references: © [year of original publication] IEEE. Reprinted, with permission, from [author names, paper title, IEEE publication title, and month/year of publication]
2) Only the accepted version of an IEEE copyrighted paper can be used when posting the paper or your thesis on-line.
3) In placing the thesis on the author's university website, please display the following message in a prominent place on the website: In reference to IEEE copyrighted material which is used with permission in this thesis, the IEEE does not endorse any of [university/educational entity's name goes here]'s products or services. Internal or personal use of this material is permitted. If interested in reprinting/republishing IEEE copyrighted material for advertising or promotional purposes or for creating new collective works for resale or redistribution, please go to http://www.ieee.org/publications_standards/publications/rights/rights_link.html to learn how to obtain a License from RightsLink.

If applicable, University Microfilms and/or ProQuest Library, or the Archives of Canada may supply single copies of the dissertation.

BACK | CLOSE WINDOW

https://s100.copyright.com/AppDispatchServlet#formTop 1/1

Figure B.12: The permission letter of reusing the paper [8]